ASTEROID RENDEZVOUS MISSIONS USING INDIRECT METHODS OF OPTIMAL CONTROL

A DISSERTATION SUBMITTED TO THE GRADUATE DIVISION OF THE UNIVERSITY OF HAWAIʻI AT MĀNOA IN PARTIAL FULFILLMENT OF THE REQUIREMENTS FOR THE DEGREE OF

DOCTOR OF PHILOSOPHY

IN

MATHEMATICS

AUGUST 2015

By

Geoff Patterson

Dissertation Committee:

Monique Chyba, Chairperson
Dilmurat Azimov
Thomas Hangelbroek
Robert Jedicke
George Wilkens

ACKNOWLEDGMENTS

I would first like to thank my advisor Monique Chyba, without whose time, advice, and guidance this dissertation would not have been possible.

I'd also like to thank my brother Austin Salisbury, for the donation of his time and computing resources to help with the millions of calculations.

Finally, I owe an enormous amount of gratitude to my wife Tonia, for her unyielding patience, support, and love. She and our daughter Avril are my whole world and I'd be lost without them.

ABSTRACT

The main contribution of this dissertation is the development of techniques to overcome the difficulty in initializing algorithms based on indirect methods of optimal control and the Pontryagin maximum principle. Moreover, the developed techniques efficiently solve an enormous set of time-minimal and fuel-minimal spacecraft trajectory optimization problems, demonstrating the large scale applicability of the techniques as well as presenting a new approach to trajectory optimization. Using the techniques developed within, a main objective of this dissertation is to assess the feasibility of space missions to a new population of near Earth asteroids which temporarily orbit Earth, called minimoons. We design rendezvous missions to a database of over 16,000 simulated minimoons.

As a first approach, the time-minimization rendezvous problem is investigated. The Circular restricted three-body problem is used to model the gravitational effects of the Earth and Moon on the spacecraft. Continuation-based techniques which rely on the knowledge of an existing solution are used to initialize the algorithms. For a spacecraft with 1 Newton maximum thrust, our methods successfully compute locally time-minimal transfers to over 96% of the 16,923 simulated minimoons, with transfer times on the order of one month. For a sample of 250 minimoons, continuation techniques further reduce the maximum thrust as low as 0.1 Newtons with transfer times less than four months.

The time-minimal results give some understanding of a lower bound for the transfer times, but have high fuel requirements. To improve the results and investigate fuel constraints, the fuel-minimization problem is investigated. The spacecraft is assumed to start on a Halo orbit around the Earth-Moon L2 Lagrangian point. The Circular Restricted Four-Body Problem is used to model the gravitational effects of the Earth, Moon, and Sun, and the mass variation of the spacecraft is modeled. The structure of the control is fixed to three boosts, and the transfer times are constrained to be less than six months. Again indirect methods are employed to identify fuel-minimal transfers, and a continuation-based "cloud" technique is developed to overcome the initialization difficulty. For a spacecraft with 22 Newton maximum thrust and 230 second specific impulse, our methods produce rendezvous missions with delta-v values under 500 meters per second for over 30% of the simulated asteroids, and for some transfers delta-v values less than 100 meters per second.

Most importantly, the work presented in this dissertation strongly suggests that minimoons are accessible via spacecraft at low cost and should continue to be investigated.

CONTENTS

LIST OF TABLES

LIST OF FIGURES

CHAPTER 1
INTRODUCTION

The primary contribution of this dissertation is to develop techniques to overcome the well-known initialization difficulty associated with algorithms based on indirect methods of optimal control and the Pontryagin maximum principle. A main objective of this dissertation is to study the feasibility of space missions to a new population of near Earth orbiters, the so-called *minimoons*. To this end, we use the techniques developed within to efficiently solve an enormous set of time-minimal and fuel-minimal spacecraft trajectory optimization problems to design rendezvous transfers to simulated minimoons. Simulatenously, our results demonstrate the large scale applicability of our techniques and present a new approach to trajectory optimization with indirect methods.

In the continued pursuit of knowledge regarding the origins of our solar system, scientists have been looking toward the minor bodies – asteroids and comets. These small yet abundant objects are distributed throughout the solar system and are pristine representatives of the history of our planet and the universe. Moreover, it has been recently suggested that missions to near Earth asteroids could be the key stepping stones for interplanetary human flight. The opportunity for research is huge, and potentially affordable, when considering those near Earth asteroids that come close to home. Indeed, interest in asteroids has been increasing greatly in recent years.

Based on the asteroids humans have already visited (Table 1.2), the target asteroids have been characteristically large, far away from Earth, and on elliptic, heliocentric orbits. Minimoons are different: they are temporarily captured near Earth asteroids and present intuitively many advantages for a space mission. There is, however, a trade-off since their capture time is on average only nine months and their orbits display a challenging complexity for an orbital transfer. Moreover, only one minimoon has been officially detected as of now. The primary objective of this dissertation is to answer whether or not minimoons are suitable targets for spacecraft missions, and in so doing provide a strong push to develop detection programs for this new population of asteroids. More specifically, we assess the rendezvous suitability of a large sample of simulated minimoons in order to determine and characterize those that are better suited from those that are worse. We use indirect methods of optimal control theory and develop a foliation technique in order to successfully initialize the algorithms.

The work presented here demonstrates that a large percentage of minimoons are theoretically

reachable with mission times less than three months and delta-v requirements less than 500 meters per second. In a broader scope, our results provide evidence that the well-known initialization problem for indirect methods can be overcome using the techniques described in this dissertation.

Background on missions to minor bodies. Numerous actual missions to asteroids and comets have been successfully executed, and several more are planned. Actual missions to minor bodies of the solar system began as early as 1978 when the *ISEE-3* spacecraft was launched to inevitably be the first spacecraft to flyby a comet – namely, Comet Giacobini-Zinner. The mission was operated by the United States National Aeronautics and Space Administration (NASA) and the European Space Agency (ESA). After launch, *ISEE-3* was parked on a halo orbit about the Earth-Sun L_1 libration point, which was a first and proved that the theoretical suspension between gravitational fields was indeed realizable. It would later fire its thrusters to depart the halo orbit and begin a trajectory to enter a Lissajous orbit around the Earth-Sun L_2 libration point – another first. By 1984, *ISEE-3* had departed for its encounter with Comet Giacobini-Zinner, and on September 11, 1985, the craft passed through the comet's plasma tail. In 1986 the craft continued on to be one of several spacecraft (*Vega 1, Vega 2, Sakigake, Giotto, Suisei* – the "Halley Armada") destined to encounter Comet Halley. A status check of the craft in 2008 revealed that it is still functional, and since then there has been discussion of reusing the probe to observe more comets in coming years.

Efficiency is critical when designing space mission, and it is determined by the overall cost which is correlated to the amount of fuel necessary for the spacecraft to execute the designed mission. A standard measure for the amount of velocity to be generated by the spacecraft's propulsion system in order to perform a set of maneuvers is known as *delta-v* (Δv). Some Δv estimates along with other data for several realized missions involving asteroids and comets, including *ISEE-3*, are given in Table 1.1. In Table 1.2 some data is given regarding the size of some of the asteroids or comets observed by the missions in Table 1.1, as well as the minor body's proximity to Earth (perigee, measured in Lunar Distances (LD), where 1 LD = 384,400 km, an approximate average distance between the Earth and Moon).

Since then, numerous other missions have also involved minor bodies, some of which are summarized next.

- In 1989, NASA launched *Galileo* which performed the first ever asteroid flyby on its way to study Jupiter. On October 29, 1991, *Galileo* flew by the asteroid Gaspra, and on August

Launch	Mission	Minor body	Rdvz/Flyby	Propulsion	Time (yrs)	Δv (m/s)
1978	*ISEE-3*	comet	flyby	chemical	7.08	430
1989	*Galileo*	asteroid	flyby	chemical	2.03	1,300
1996	*NEAR Shoemaker*	asteroid	rdvz	chemical	1.36	1,450
1997	*Cassini*	asteroid	flyby	chemical	2.21	500
1998	*Deep Space 1*	both	flyby	ion	2.91	1,300
1999	*Stardust*	both	flyby	chemical	5.34	230
2003	*Hayabusa*	asteroid	rdvz	ion	2.32	1,400
2004	*Rosetta*	comet	rdvz	chemical	4.51	2,200
2005	*DIXI*	comet	rdvz	chemical	5.63	190
2007	*Dawn*	asteroid	rdvz	ion	3.76	10,000
2010	*Chang'e 2*	asteroid	flyby	chemical	2.20	200
2014	*Hayabusa 2*	asteroid*	rdvz*	ion	4.00*	-
2016*	*Osiris-Rex**	asteroid*	rdvz*	-	-	-
2020*	*ARM**	asteroid*	rdvz*	-	-	-
2025*	*Castalia**	comet*	rdvz*	-	-	-

Table 1.1: Some realized missions involving asteroids and comets. (* = planned). The "Time" column indicates how long after launch the craft first interacted with a minor body.

28, 1993, it flew by the asteroid Ida. The craft found Ida had a natural satellite (Dactyl), which was the first discovery of a moon orbiting an asteroid. In 2003, after completing its mission objectives, *Galileo* was intentionally crashed into Jupiter to eliminate the possibility of impacting one of Jupiter's moons and contaminating it with bacteria.

- As recent as 1996, NASA launched the *NEAR Shoemaker* mission which would set several asteroid milestones. In 1997 *NEAR* became the first spacecraft to perform a flyby of a near Earth asteroid, namely 253 Mathlide. The spacecraft flew within 1200 km of Mathilde and captured images and gravitational data. A year later *NEAR* flew by its main target, another near Earth asteroid 433 Eros. In 2000 *NEAR* went into orbit around 433 Eros and in 2001 the craft landed on the asteroid – both of which were firsts. The *NEAR* spacecraft conducted the first long-term study of an asteroid at close quarters, taking observations and measurements regarding Eros' mass, structure, composition, and gravity. Likely due to the extreme conditions on Eros, contact with the craft was eventually lost and the mission was shut down.

- Several other spacecraft have since taken observations of asteroids – either as the mission's primary objective, or while the craft was en route to another destination. In 1997 the spacecraft

Minor Body	Encounter year	Perigee (LD)	Diameter (km)
Ida	1993	680.3	31
Mathilde	1997	369.7	53
Gaspra	1991	326.1	18
Borrelly	2001	188.1	8
Halley	1986	164.7	11
Churyumov	2014	153.4	4
Braille	1999	123.3	2
Eros	2000	59.0	17
Itokawa	2005	13.6	0.54

Table 1.2: Some asteroids and comets which have been targets of actual missions.

Cassini-Huygens was launched as a joint effort by NASA, ESA, and the Italian Space Agency (ASI), designed primarily to study Saturn and its moon Titan. In January of 2000, while passing through the asteroid belt, the spacecraft performed a flyby of asteroid Masursky, taking photographs and estimating the asteroid's size. Another NASA spacecraft *Deep Space 1*, launched on October 24, 1998 and designed to test several advanced space technologies, flew by the asteroid Braille at an impressively close distance of only 26 km. The mission was later extended to include an encounter with Comet Borrelly. Both flybys added substantially to what was already known about asteroids and comets.

- Launched in 1999, the NASA spacecraft *Stardust* would return to Earth in 2006 with the first ever comet sample. On its way to Comet Wild 2, *Stardust* also flew by asteroid Annefrank. After successfully achieving its primary objective in 2006 when the sample return capsule landed on Earth, the mission was extended (*Stardust-NExT*) and a flyby of Comet Tempel 1 was completed in 2011. The craft has since expended all of its fuel and is no longer in communication with Earth.

- Similarly, launched in 2003, the Japanese Aerospace Exploration Agency (JAXA) spacecraft *Hayabusa* would return to Earth in 2010 with the first ever asteroid sample. During the two years it took to get from Earth to the asteroid Itokawa, the ion engine system generated 1,400 m/s Δv while only consuming 22 kg of propellant. In November of 2005 the craft landed on the asteroid and collected tiny grains of asteroid samples, which were returned to Earth (aboard the craft) five years later.

- The *Deep Impact Extended Investigation (DIXI)* spacecraft and impactor combo was launched in 2005 by NASA, with the purpose of collecting data on Comet Tempel 1. The impactor was propelled into the comet in order for the main spacecraft to study the excavated debris. The successful mission was extended (and renamed *EPOXI*) and eventually flew by three other comets. In 2013 communications with the spacecraft were lost.

- Very recently the *Rosetta* and *Philae* mission has made headlines. In 2014, the ESA mission (which launched in 2004) arrived at its comet destination 67P/Churyumov-Gerasimenko, and *Rosetta* became the first spacecraft to orbit a comet. A 90 kg robotic lander *Philae* was deployed from *Rosetta* which became the first ever comet lander. The craft continues to observe the comet, and specifically will monitor changes in the comet as it goes through perihelion in August 2015.

- The *Dawn* spacecraft was launched by NASA in 2007 to study the two largest bodies in the main asteroid belt: Vesta and Ceres. The ion propulsion system has the capability to perform more than 10,000 m/s Δv, far more than any previous mission, by applying very low thrust over a long period of time. *Dawn* entered orbit around Vesta in 2011, where it stayed for 14 months to survey the body. On March 6, 2015 *Dawn* entered orbit around Ceres, where it is predicted to remain perpetually after the conclusion of its mission. *Dawn* was the first craft to visit either of these bodies, and moreover, the first craft to visit a dwarf planet.

- Originally launched in 2010 by the Chinese National Space Agency (CNSA), *Chang'e 2* flew by the asteroid Toutatis in 2012 as part of an extended mission after successfully completing other objectives. This made the CNSA the fourth space agency to have directly explored an asteroid. The spacecraft is still active and being used to verify CNSA's deep space tracking and control systems.

- *Hayabusa 2* was just launched in December of 2014 and is scheduled to reach its asteroid destination in 2018. Like its predecessor, *Hayabusa 2* is an asteroid sample return mission operated by JAXA. The mission plans have learned from and addressed the weaknesses of the first *Hayabusa* mission, and hopes to collect a larger sample from the asteroid 1999 JU_3. It is expected to arrive at its target by 2018, and then return to Earth by 2020.

- NASA's *Osiris-Rex* mission plans to be the first U.S. mission to return samples from an

asteroid to Earth. While still in development, it is scheduled to launch in September of 2016, rendezvous with asteroid Bennu in 2018, and return to Earth by 2023.

- Another current NASA initiative is the *Asteroid Redirect Mission (ARM)*, which (as of 2014) has the goal of being the first-ever mission to identify, capture and redirect a near Earth asteroid to a stable orbit around the moon. The mission hopes to launch by the end of this decade.

- The *Castalia* space mission is planning to launch in the mid-2020s, to explore Comet 133P/Elst-Pizarro, a Main Belt Comet. The mission is gaining support as Main Belt Comets are a new solar system population with stable asteroid-like orbits but comet-like appearances.

Background on minimoons, and asteroid 2006 RH$_{120}$ Clearly there is an increasing interest in asteroid exploration and many missions have taken place already, but it remains an important question to find the best targets. A claim supported by this dissertation is that there is a population of near Earth orbiters that has been neglected until now, but that has the potential to accelerate exploration of asteroids and discoveries. Table 1.3 provides data for the asteroid 2006 RH$_{120}$ (from now on just referred to as RH$_{120}$) and we can see that it is a tiny asteroid (3 meters in diameter) that comes very close to Earth (closer than our Moon). Furthermore, in Figure 1.1 we see the exotic trajectory of RH$_{120}$ from 2006 to 2007 (data obtained from the Jet Propulsion Laboratory's Horizons database).

RH$_{120}$, a near Earth asteroid discovered by the Catalina Sky Survey in September of 2006, is the only documented asteroid to date to have been *temporarily captured* in orbit around the Earth (a formal definition of *temporarily captured* is given in Chapter 2). The asteroid was in orbit around Earth for about a year, starting in June of 2006, and came as close as 0.7 LD from the Earth while completing 3.6 revolutions about Earth in the Earth-Sun co-rotating frame.

It is a natural question to ask if there are more asteroids like this, waiting to be detected, and if so, would they make good targets for space missions. The first question is indeed answered by Granvik *et al.*, in [1], which gives numerical evidence that there is an abundance of these small asteroids in orbit around Earth (Chapter 2). The second question is the focus of this work – are these types of asteroids good targets for space missions, in terms of time and fuel requirements? More specifically, we design time-minimal and fuel-minimal spacecraft missions to rendezvous (match position and velocity) with simulated asteroids which are temporarily captured in orbit around Earth.

Minor Body	Perigee (LD)	Diameter (km)
2006 RH_{120}	0.7	0.003

Table 1.3: Data for asteroid 2006 RH_{120}

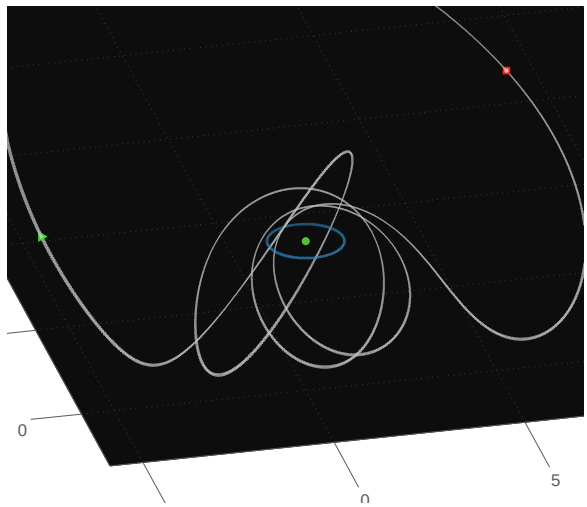

Figure 1.1: Trajectory of 2006 RH_{120}

Background on trajectory optimization A crucial first step to realizing an asteroid rendezvous mission is theoretical trajectory planning and optimization. Many well-developed tools exist for solving a variety of trajectory optimization scenarios, also known as *orbital transfer* problems. Formally, an orbital transfer is the use of propulsion systems to change the orbit of a spacecraft from some initial orbit to a desired final orbit. The main focus of this work is to design efficient rendezvous transfers between a chosen parking orbit for the spacecraft and a desired minimoon's orbit. It is a first step toward a round trip mission. A main objective when designing orbital transfers is to minimize the required amount of fuel necessary for the completion of the spacecraft journey. In addition, for our application we must take into account the fact that the minimoons are only temporarily captured for an average period of nine months, which necessitates a short transfer duration relative to typical orbital transfers. We are therefore facing an optimal control problem with a dual cost: time and fuel consumption.

The problem of trajectory optimization is a major component of designing and executing space missions. Tremendous progress has been made in the last fifty years developing mathematical and numerical tools for modeling accurate, feasible and efficient orbital transfers. In 1998, a survey of

existing methods for trajectory optimization was presented [2] which summarized and compared methods of optimal control versus nonlinear programming, as well as combinations of the two. Similarly, in 2006 [3] surveys noteworthy trajectory design techniques in the circular restricted three-body problem [4]. Since then tools have continued to be developed, and we briefly recount some recent work to motivate the methodology chosen for this dissertation.

Newton's laws of universal gravitation [5] are the foundation of classical celestial mechanics and they allow the generation of well-known Hohmann and bi-elliptic transfers [6], notably used during the Apollo program to bring spacecraft from a low-Earth circular orbit to a higher one while minimizing the change in velocity provided by the spacecraft's propulsion system – the so-called Δv. More recently new methods to compute low-energy transfers have been developed based on chaotic motion [7]. Belbruno in particular has continued to push the boundaries of low-energy trajectory planning [8, 9, 10, 11, 12]. An example [13] utilizes ballistic trajectories of the elliptic restricted three-body [4] problem to design low-energy interplanetary capture trajectories, which yield lower delta-v values than typical Hohmann transfers.

Other techniques, like in [14, 15], utilize invariant manifolds of equilibrium points and periodic orbits for the restricted three-body problem [4]. For instance, the design of the Genesis discovery mission [16] relies on such methods. Transfer methods are also designed using heteroclinic orbits [17]. Other notable works taking advantage of trajectories within the circular restricted three-body problem include [3, 18]. Finally, numerous softwares have been developed to compute low-energy transfers based on the above techniques, including a software suite by NASA known as *Copernicus* [19].

In a broader context than trajectory optimization, a lot of work as been done in developing numerical methods for optimal control and they can be divided into two categories: the deterministic class and the stochastic class. The survey paper [20] provides a very good overview of numerical methods for space transfers and in particular includes a detailed comparison of both.

The indirect and direct methods compose the class of deterministic approaches. Both methods have advantages and disadvantages, and typically the problem setting dictates which method is better suited. The direct methods are based on rewriting the optimal control problem as a nonlinear parametric optimization problem ([21] for example). The main idea is to discretize the control and possibly the state to transform the dynamics of the system into a set of finite number of nonlinear constraints. To solve this finite dimensional optimization problem many programs using standard

optimization techniques have been developed. Those methods can be used in a hybrid way, see for instance [22, 23] where the authors combine invariant manifold theory with a direct method. Actually, many spacecraft transfers are designed using invariant manifolds but those transfers are usually very long and in our case no invariant manifold is associated to the rendezvous point on the minimoon's orbit since the data is received as discretized ephemerides. The direct methods are known to be very robust with respect to the initial conditions, however they are very expensive in terms of computational time, especially to guarantee the solution reaches a desired accuracy. On the other hand, the idea of the indirect methods, also called shooting methods, is to transform the initial optimal control problem into a multiple points boundary value problem. This is done by using the necessary conditions for optimality provided by the Pontryagin Maximum Principle, [24]. To solve this boundary value problem, Newton-like methods are coupled with high precision ODE integrators. Clearly, the main challenge with indirect methods is the initialization for the shooting function but once this issue is solved they are very accurate and fast. To overcome this major challenge some authors have introduced hybrid direct/indirect methods ([25, 26] for instance).

The stochastic methods are the evolutionary algorithms and meta-heuristics, based on the concept of survival of the fittest ([27] for instance). Similar to the direct method, the first step is to discretize the control and state to obtain a finite dimensional optimization problem but the dimension is kept small (in the hundreds of variables compared to thousands for a deterministic direct method). Equality constraints in this setting are more difficult to address, but it can be done using a penalization approach. Once a small number of decision variables describe the problem, several random sets of those variables are generated. Then a sequence of evolution, combination, and selection of the best sets iteratively leads eventually to a set of decision variables which decreases the cost to a minimum. The heuristic method stops once the criterion to minimize is stationary. The main advantage is the simplicity of implementation of the method, and since it is not a gradient based method it tends to avoid local minima. However, by construction the method does not provide any necessary or sufficient conditions to be verified by the solution and it can be computationally expensive in case a large number of decision variables are to be optimized.

Numerous and various kinds of optimal transfers have been computed by means of both direct and indirect methods, for two, three, and even four-body trajectory optimization problems [28, 29, 30, 31, 32, 33]. The most significant differences between the problem we investigate here and those investigated by previous works are the enormous target population and the complexity of the target

orbits. Indeed, we design transfers to a database of over 16,000 asteroid orbits, each of which consists of several hundred to several thousand sampled points which are the candidate targets for the orbital transfers we design.

While any method could be applied for our application, our approach uses an indirect method. The main reasons for our choice are as follows. Indirect methods have proved to be very efficient for orbital transfers [30, 34], and the results obtained in [33] provided good initial guesses to develop a general algorithm for our specific application. This is because in [33] the author solves the initialization issue to design time optimal orbital transfers from the geostationary orbit to the Earth-Moon L_1 point, providing us with knowledge of an existing solutions. Moreover, a quick analysis of the minimoons' orbits show that many of them pass close to this libration point during their capture time, which suggested we should first design rendezvous transfers to the minimoons at their closest approach to L_1 as a stepping stone toward a more general analysis (note the minimoons collectively come close to other locations as well, and we do not presume that near L_1 is necessarily the best choice). Moreover, our main objective is to study the large population of simulated minimoons (more than 16,000) as targets for rendezvous transfers and computationally expensive methods are therefore ill-suited.

A main step forward toward a solution to the main goal of this dissertation was the construction of a *global initialization scheme* based on an indirect method to determine rendezvous transfers that satisfy the necessary conditions of the maximum principle. The computations carried out in this dissertation have been done using the software Hampath [35] that computes solutions of indirect methods in optimal control and checks the second order optimality condition when smooth optimal control problems are considered . Hampath relies on Fortran's MINPACK package, Tapenade's auto differentiation [36], and optionally Matlab, to carry out the calculations. The user supplies Hampath with a Fortran routine for each of the shooting function and real Hamiltonian. Hampath produces the state and costate dynamics using Tapenade and computes the shooting function value by numerically integrating using the `DOPRI5` routine [37]. Rather than the classical finite differences technique, variational equations derived and subsequently integrated in order to compute the Jacobian of the shooting function, again thanks to Tapenade and `DOPRI5`. Hampath then calls the Fortran solver `HYBRJ` from the MINPACK library to solve the shooting function. The software is an extension of an earlier version called `COTCOT` [38], and implements techniques based on [39, 40, 41, 42, 43].

Results and Outline The major contribution of this dissertation is to numerically identify time- and fuel-minimal spacecraft transfers to rendezvous with a new population of small near Earth asteroids which are temporarily in orbit around Earth. We consider the Circular Restricted Four-Body Problem (CR4BP) with the Sun as a perturbation of the Circular Restricted Three-Body Problem (CR3BP). This is different than prior results obtained using Hampath in orbital transfers, which were always based on the CR3BP. The main difficulty in utilizing so-called indirect methods to numerically solve optimal control problems is providing the algorithm with a close enough initial guess so that the algorithm converges. To overcome this difficulty, a technique is developed to create a database of known extremals, which are then used with a continuation method to solve the rendezvous problem for large population of asteroids. We provide analysis of the results in terms of the application and discussion of the effectiveness of our techniques. Our methods are applied to a large database of simulated asteroids and the results show that fuel efficient missions are indeed theoretically possible, while simultaneously taking into account the mission time constraints. In a broader context, the results suggest that the algorithm initialization problem may feasibly be overcome for a general optimal control problem following the techniques developed within this dissertation.

This dissertation is organized as follows. In Chapter 2 we summarize the development of the database of simulated minimoons from [1] which serve as the rendezvous targets. In Chapter 3 the general tools associated with indirect methods of optimal control and namely the Pontryagin maximum principle are summarized. In Chapter 4 the methodology specific to the time-minimization rendezvous problem is presented, along analysis of the associated results. Similarly, in Chapter 5 the methodology specific to the fuel-minimization problem is presented as well as results analysis.

CHAPTER 2
MINIMOONS

In this chapter, we briefly recall how the database of simulated minimoons was created, as well as some defining characteristics of minimoons which motivate our methods and support the analysis of our results. Our work is centered around the database of over sixteen-thousand simulated minimoons, developed by Granvik et al. *in [1], and one of our primary objectives is to numerically assess the accessibility of these minimoons. To that end, we use the minimoons from the database as targets in the computation of time-optimal and fuel-optimal rendezvous transfers.*

The primary application of the methods presented in this dissertation is to design fuel efficient rendezvous missions to temporarily-captured *natural Earth satellites* (NES). By definition a NES is a celestial body that orbits the Earth, and moreover, a NES is defined as a *temporarily captured orbiter* (TCO) of the Earth if it simultaneously satisfies

(i) the geocentric Keplerian energy $E_{geo} < 0$,

(ii) the geocentric distance is less than three Hill radii $R_{H,\oplus}$, where $3R_{H,\oplus} \approx 0.03$ AU for the Earth.

(iii) the object makes at least one full revolution around the Earth in the co-rotating frame while satisfying the first two criteria

The number of revolutions is measured by recording the longitudinal angle traversed during capture in the co-rotating ecliptic coordinate system where the line connecting the Earth and the Sun is fixed, and forms a line of reference. This number is negative for retrograde orbits.

A few different names have been used to describe these sorts of objects, though there is yet to be a single accepted choice by the scientific community: natural Earth satellites (NES), temporarily captured orbiters (TCO), and finally, *minimoons*. As a convention for this paper, we choose to use *minimoons* rather than one of the acronyms, but the three are interchangeable.

Despite a large body of work on satellite capture by Saturn and Jupiter, there has been much less published about the natural satellites of the Earth other than the Moon. In [1] by Granvik

et al., a study and characterization of the population statistics of the Earth's natural satellites is calculated for the first time. By generating, pruning, and integrating an enormous random sample of "test-particles" from the Near Earth Object (NEO) population, the authors of [1] calculate the size-frequency distribution (among other statistics) of the minimoon population.

To do so, an original random sample of 9,346,396,100 test-particles was generated over the 19-year Metonic Cycle (the time it takes for the Earth-Moon-Sun to approximately return to the same solar system configuration), so that after pruning there were 10,000,000 test-particles remaining for integration [1]. The test particles were originally generated based on existing population statistics for near Earth objects, and the pruning was done according to the fundamental assumption that test particles which can get captured are those with heliocentric orbital elements similar to Earth's orbit. Using a high-precision n-body model, each test-particle was integrated over time, and classified as a minimoon if for some portion of the integration the definition given above was satisfied. Of the 10 million integrated test-particles, the authors of [1] found that over 16,000 became minimoons. It is from this database of integrated minimoons that we select our targets for rendezvous missions.

As a convention for the rest of this dissertation we will refer to the 16,923 simulated minimoons as the *minimoon database* or simply the *database*, and when we say *minimoon* we are referring to an element in that database (except when discussing RH_{120} or otherwise specified). To each minimoon in the database, we assign an index number 1-16,923 so that we can refer to a specific simulated minimoon by its index number. Each minimoon in the database consists of a discretized time-history of the position and velocity of the asteroid during its capture. The Sun, Earth, and Moon ephemerides are also known at each time step, for every minimoon. Occasionally in figures we will abbreviate minimoon as *MM*.

Figure 2.1 shows six minimoon trajectories from the database: minimoons #6890, #17, #16, #110, #23, and #39. The distance units are normalized so that 1 Lunar Distance (LD) = 384,400 kilometers, an approximate average distance between the Earth and Moon. The diversity of the minimoons' trajectories is striking. Indeed, these objects are very different than the types of asteroids humans have previously visited. Instead of large asteroids, on far away, elliptic, heliocentric orbits, minimoons are tiny asteroids and (during their capture) are on nearby, rapidly evolving, geocentric orbits. It certainly begs the question: are minimoons good targets for spacecraft missions? "Good targets" encompass the idea of low fuel consumption and time duration compatible with the fact that minimoons are typically captured for a period of on average nine months. A main objective

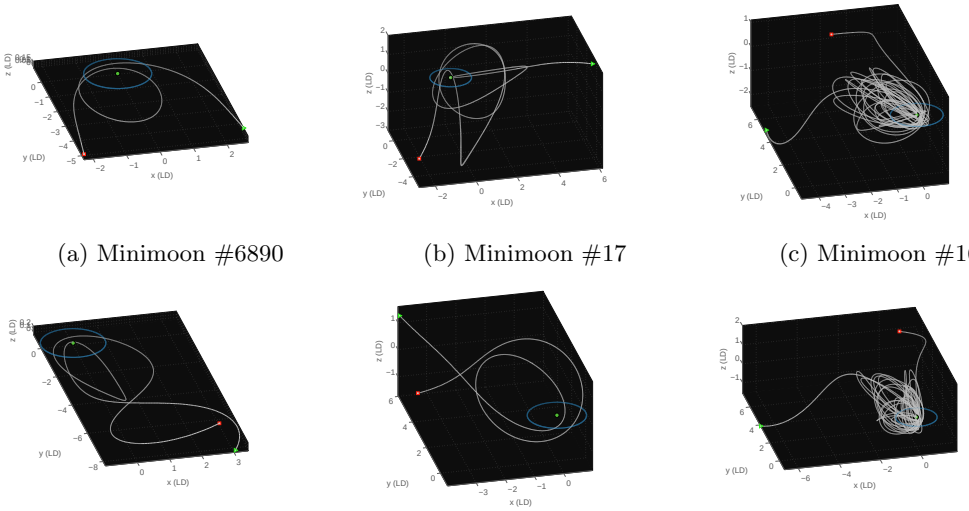

(a) Minimoon #6890 (b) Minimoon #17 (c) Minimoon #16

(d) Minimoon #110 (e) Minimoon #23 (f) Minimoon #39

Figure 2.1: Simulated minimoon trajectories from [1] database, plotted in the inertial Earth-Moon (EM)-barycentric reference frame.

is to characterize which minimoons are the best suited, since indeed it is expected that depending on their orbit characteristics some minimoons are good targets while others would require too much fuel to be able to achieve rendezvous before the minimoon escapes capture. Additionally, given a specific minimoon we would like to determine the best feasible rendezvous location for that precise orbiter.

The minimoon capture times vary from a few weeks to several years. The distribution of capture times less than three years for the database of 16,923 minimoons is shown in Figure 2.2.

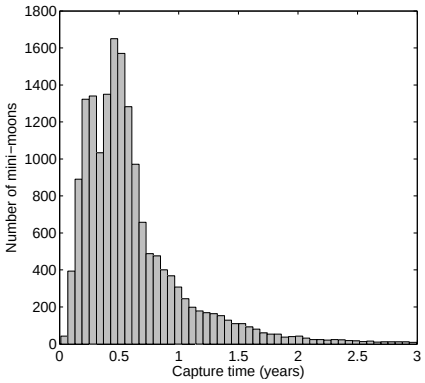

Figure 2.2: The distribution of minimoon capture times less than 3 years.

$\mathcal{MM}$ #	d_{L1} (LD)	T_{capt} (d)	n_{orbits}
1	1.46	452.16	-2.88
2	1.97	285.65	-1.84
3	0.85	139.96	-1.45
4	0.60	70.06	-1.11
5	0.37	85.94	-1.17
6	0.60	197.79	-1.41
7	1.06	168.07	-1.25
8	1.31	513.73	-2.74
9	0.36	182.29	1.31
10	1.15	359.72	-2.81
11	2.61	303.15	-1.93
12	0.90	206.05	-1.32
13	0.50	508.83	-1.12
14	0.45	153.16	-1.31
15	0.63	136.53	-1.33
16	0.16	1,506.92	16.82
17	0.42	448.26	-1.46
18	0.73	217.82	-1.32
19	0.23	517.89	-4.76
20	0.25	125.49	-1.32

Table 2.1: Capture statistics for 20 minimoons from the database [1]. Column 2 gives the Euclidean periapsis distance d_{L1} in LD for the minimoon at its closest approach to $L1$. Column 3 gives the total amount of time T_{capt} in days that the minimoon is captured, and column 4 gives the number of orbits n_{orbits} the minimoon makes around the Earth while captured (negative implies retrograde).

For your curiousity, capture statistics for a sample of 20 minimoons from the database [1] is given in Table 2.1.

Statistically, the results from [1] show that at any given time there is at least one 1-meter-diameter minimoon orbiting the Earth, although to date RH_{120} has been the only documented minimoon. The lack of more numerous discovery is likely due to the small size of the objects, which may go unnoticed or be dismissed as man-made debris, and due to the fact that the objects are only captured temporarily around Earth. In [44] theoretic work has been done to investigate the discoverability of minimoons by present or near-term ground-based and space-based facilities. The authors find that indeed, with current radar technology, there is a greater than 80% chance of detecting a minimoon of 10-centimeter-diameter or greater with about 40 hours of operation.

In addition to their statistical abundance and having been previously unexplored, minimoons have several characteristics which make them intuitively appealing targets for space missions. First, their closeness to Earth and the large amount of documentation already available regarding space

travel in the Earth-Moon vicinity. Second, an orbiting object allows for more time for detection, planning, and execution of a space mission than an object which just flies by (i.e., does not complete a revolution of the Earth). Note, the mean capture time for the simulated minimoons was 286 days, with the mean number of revolutions 2.88 [1]. In particular, it is reasonable to think that minimoons are excellent asteroids to be redirected on to a stable orbit in the Earth-Moon system. This has been demonstrated by the work in [45] on RH_{120}. A redirected minimoon would then be an ideal target for a manned mission. Third, the small size of the minimoons allows us to envision returning, not only a sample, but the entire asteroid to Earth which would provide a breakthrough in the geophysical study of asteroid. Finally, the chaotic trajectories (non-planar, non-elliptic) is actually appealing in the sense that spacecraft maneuvering capabilities and mission planning strategies can truly be put to the test – and right in our own backyard.

The minimoon data was provided to us as ephemerides with non-uniform time steps. The least number of time steps is 82 for MM #3373. The greatest number of time steps is 481,903 for MM #16216. The median number of time steps 686. For 15,620 of the 16,923 minimoons, the number of time steps is 2000 or less. For 16,679 the number of time steps is 5000 or less. Figure 2.3 shows the distribution for the number of time steps for those 16,679 minimoons, which shows the variety of ephemeris sizes. For your curiousity, Table 2.2 gives some data regarding the some of the minimoons with the largest filesizes, and similarly Table 2.3 gives data for the minimoons with the smallest filesizes.

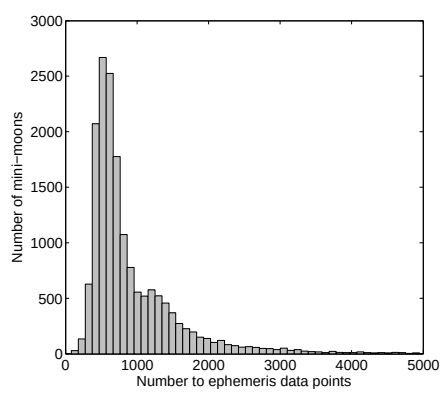

Figure 2.3: The distribution of the 16,679 ephemerides which have 5000 or less time steps.

Figure 2.4 shows the distribution of periapsis distances with respect to the Earth, Moon, L_1, and L_2. Recall that the definition of temporarily captured requires that the object be within 0.03

	# of time steps	capture duration (years)
MM #153	50996	21.7103
MM #209	323916	68.0910
MM #1117	63472	15.0049
MM #3419	124171	24.9698
MM #5172	401530	44.8553
MM #8308	60983	21.7000
MM #10439	76371	17.6731
MM #10476	54594	14.9753
MM #13026	70794	22.8599
MM #13212	65940	19.1732
MM #13468	92428	34.9166
MM #13730	97451	19.6025
MM #16216	481903	61.9912

Table 2.2: Data for minimoons with the largest filesize (> 50000)

	# of time steps
MM #1185	141
MM #3373	82
MM #3407	145
MM #4065	131
MM #6077	91
MM #6252	149
MM #13941	90
MM #13949	131
MM #14792	120
MM #15125	141

Table 2.3: Data for minimoons with the smallest filesize (< 150)

AU = 11.67 LD of the Earth, and in Figure 2.4 we see that all the minimoons come well-within this boundary. We mostly present this to observe that many minimoons come close to the Lagrangian points L_1 and L_2.

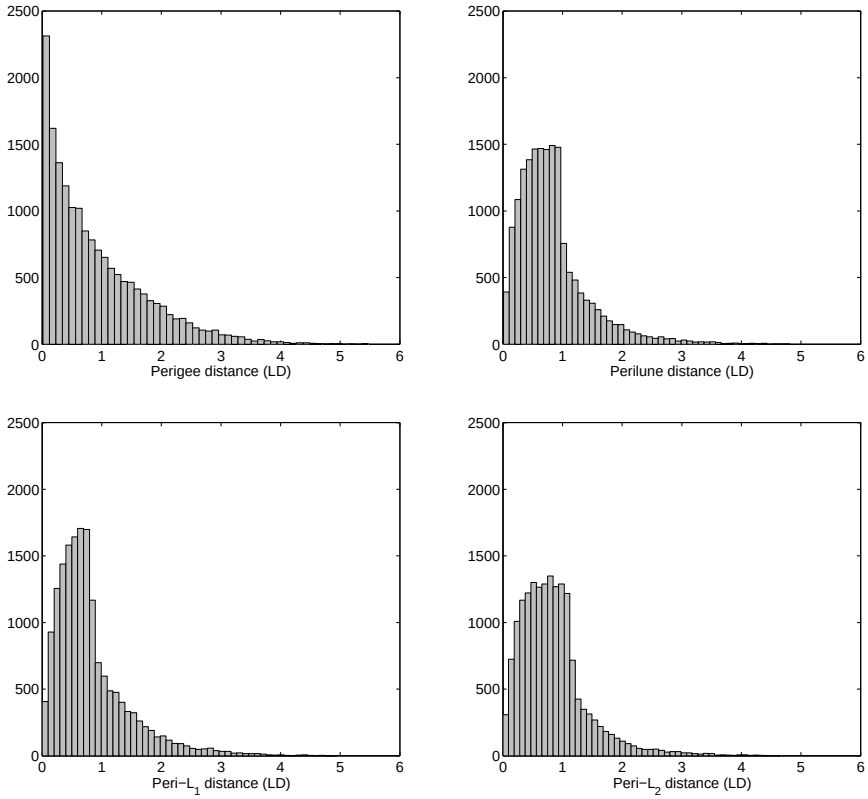

Figure 2.4: Distributions of the periapsis distances for all 16,923 minimoons, with respect to the Earth (perigee), Moon (perilune), L_1 (peri-L_1), and L_2 (peri-L_2).

CHAPTER 3
OPTIMAL CONTROL AND INDIRECT METHODS

Our work relies on indirect methods to numerically compute extremal solutions of an optimal control problem. Indirect methods are based on the Pontryagin maximum principle, which gives necessary conditions of first order for a solution to be optimal. In this chapter, we introduce a general version of the maximum principle and define the notion of extremals. Moreover, a primary objective of this dissertation is to develop strategies to overcome the initialization problem associated with such approach, and therefore we present in further detail the tools associated with indirect methods.

The methods used in this work are extensions of well-known methods of optimal control theory based primarily on the Pontryagin maximum principle (often just referred to as the "maximum principle"). We focus on an application to astrodynamics, but it is important to note that the tools we use and develop would be applicable to a broader set of problems. In that spirit, we first recall the basic formulation of a general optimal control problem and present the maximum principle and the associated tools. In the Chapters 4 and 5, we will formulate the specific optimal control problems solved in this dissertation as well as state explicitly the implications of the maximum principle for those problems.

3.1 A general optimal control problem

Let $\mathbf{x} = (x_1, \ldots, x_n)^{\mathrm{T}} \in \mathbb{R}^n$ be the *state variables*, for some integer n, the *state dimension*. Assume the state variables are changing over time t, so $\mathbf{x}(\cdot) : \mathbb{R} \to \mathbb{R}^n$, according to the ordinary differential equation

$$\dot{\mathbf{x}}(t) = \mathbf{f}\left(t, \mathbf{x}(t)\right),$$

where $\mathbf{f}(\cdot)$ is continuous in t and $\mathcal{C}^1$ with respect to $\mathbf{x}$.

If in addition the user is allowed some input to influence the behavior of the system, we instead have a *control system* of the form

$$\dot{\mathbf{x}}(t) = \mathbf{f}\left(t, \mathbf{x}(t), \mathbf{u}(t)\right), \tag{3.1}$$

where $\mathbf{u} = (u_1, \ldots, u_m)^{\mathrm{T}} \in \mathbb{U} \subseteq \mathbb{R}^m$ are the *control variables*, for some integer m, the *control dimension*. The control variables are also allowed to change over time, so $\mathbf{u}(\cdot) : \mathbb{R} \to \mathbb{U} \subseteq \mathbb{R}^m$. The set $\mathbb{U}$ is called the *control domain* which we assume is a smooth manifold. The class of *admissible* controls $\mathcal{U}$ is the collection of measurable functions $\mathbf{u}(\cdot)$ which take values in $\mathbb{U}$. These are the least regularity assumptions necessary to guarantee the existence of a unique solution to (3.1), and moreover given a convexity assumption on the control domain and regularity conditions on the cost to minimize they guarantee the existence of an optimal control.

An *optimal control problem* is then essentially to find the control function $\mathbf{u}(\cdot)$, and the corresponding *state trajectory* $\mathbf{x}(\cdot)$. that minimizes a given cost functional $J(\mathbf{u})$, while simultaneously satisfying some given initial and/or final constraints $\mathbf{x}(t_0) \in M_0$, $\mathbf{x}(t_f) \in M_f$ for some manifolds M_0 and M_f in $\mathbb{R}^n$, at initial and final times t_0 and t_f, respectively. A general cost function can be written

$$J(\mathbf{u}(\cdot)) = K\left(t_f, \mathbf{x}(t_f)\right) + \int_{t_0}^{t_f} L(t, \mathbf{x}(t), \mathbf{u}(t))dt, \tag{3.2}$$

where $K(\cdot)$ is a *terminal cost*, and $L(\cdot)$ is a so-called *running cost* or *integral cost*. When there is no terminal cost ($K = 0$) we have a so-called *Lagrange problem*, or when there is no running cost ($L = 0$) we have a so-called *Mayer problem*. It's worth noting that by augmenting the state variables a Lagrange problem can be transformed into a Mayer problem, and vice versa. So, concisely, we can write an optimal control problem $\mathcal{P}$ as:

$$\mathcal{P}\begin{cases} \min\limits_{\mathbf{u}\in\mathcal{U}} J(\mathbf{u}) = \displaystyle\int_{t_0}^{t_f} L(t, \mathbf{x}(t), \mathbf{u}(t))dt + K\left(t_f, \mathbf{x}(t_f)\right) \\ \text{subject to} \\ \dot{\mathbf{x}}(t) = \mathbf{f}\left(t, \mathbf{x}(t), \mathbf{u}(t)\right) \\ \mathbf{x}(t_0) \in M_0, \quad \mathbf{x}(t_f) \in M_f \end{cases} \tag{3.3}$$

3.2 Pontryagin maximum principle

The cornerstone result of geometric optimal control theory is the Pontryagin maximum principle (or simply, the "maximum principle") which gives first order necessary conditions for a solution pair $(\mathbf{u}(\cdot), \mathbf{x}(\cdot))$ of the problem (3.3) to be optimal.

Theorem 1 (Pontryagin maximum principle)**.** *Let $(\mathbf{u}(\cdot), \mathbf{x}(\cdot))$ be an optimal control and corresponding state trajectory for the problem (3.3). Then there exists an absolutely continuous func-*

tion $\mathbf{p}(\cdot) : [t_0, t_f] \to \mathbb{R}^n$*, called the adjoint vector or costate vector, and a constant* $p_0 \leq 0$*, with* $(p_0, \mathbf{p}) \neq (0, \mathbf{0})$ *such that for almost every time* $t \in [t_0, t_f]$ *we have:*

(i) ***Psuedo-Hamiltonian equations:***

$$\dot{\mathbf{p}}(t) = -\frac{\partial H}{\partial \mathbf{x}}(t, \mathbf{p}, \mathbf{x}, \mathbf{u}), \quad \dot{\mathbf{x}}(t) = \frac{\partial H}{\partial \mathbf{p}}(t, \mathbf{p}, \mathbf{x}, \mathbf{u})$$

where $H(t, \mathbf{p}, \mathbf{x}, \mathbf{u}) = \langle \mathbf{p}, \mathbf{f}(t, \mathbf{x}, \mathbf{u}) \rangle + p_0 L(t, \mathbf{x}, \mathbf{u})$.

(ii) ***Maximization condition:***

$$H(t, \mathbf{p}(t), \mathbf{x}(t), \mathbf{u}(t)) = \max_{\mathbf{v} \in \mathbb{U}} H(t, \mathbf{p}(t), \mathbf{x}(t), \mathbf{v})$$

(iii) ***Transversality condition:***

$$\mathbf{p}(t_0) \perp T_{\mathbf{x}(t_0)} M_0, \qquad \mathbf{p}(t_f) - p_0 \frac{\partial K}{\partial \mathbf{x}}(t_f, \mathbf{x}(t_f)) \perp T_{\mathbf{x}(t_f)} M_f$$

A tuple $(p_0, \mathbf{p}, \mathbf{x}, \mathbf{u})$ satisfying the conditions of the maximum principle is called an *extremal*. When p_0 and $\mathbf{u}$ are understood, we may omit them and just write $(\mathbf{p}, \mathbf{x})$. If $p_0 \neq 0$ the extremal is said to be *normal*, and *abnormal* otherwise. In our work, we assume $p_0 \neq 0$.

Notice that when $\mathbb{U}$ is a smooth manifold of $\mathbb{R}^m$, the maximization condition can be written $\frac{\partial H}{\partial \mathbf{u}} = \mathbf{0}$. Assuming then that $\frac{\partial^2 H}{\partial \mathbf{u}^2}$ is negative definite along the extremal, a straightforward application of the implicit function theorem shows that extremal controls are actually smooth feedback functions of the state and adjoint vectors in a neighborhood of $\mathbf{u}(\cdot) : \mathbf{u}_r(t) = \mathbf{u}_r(\mathbf{x}(t), \mathbf{p}(t))$. The pseudo-Hamiltonian H can thus be written as a real Hamiltonian function $H_r(t, \mathbf{p}, \mathbf{x}) = H(t, \mathbf{p}, \mathbf{x}, \mathbf{u}_r(\mathbf{x}, \mathbf{p}))$ and any extremal trajectory can be expressed as a solution $\mathbf{z} = (\mathbf{x}, \mathbf{p})^{\mathrm{T}}$ of the Hamiltonian system

$$\begin{cases} \dot{\mathbf{z}}(t) = \vec{H}_r(\mathbf{z}(t)) \\ \mathbf{z}_0 = (\mathbf{x}_0, \mathbf{p}_0)^{\mathrm{T}} = (\mathbf{x}(t_0), \mathbf{p}(t_0))^{\mathrm{T}} \end{cases} \tag{3.4}$$

where $\vec{H}_r = \left(\frac{\partial H_r}{\partial \mathbf{p}}, -\frac{\partial H_r}{\partial \mathbf{x}} \right)^{\mathrm{T}}$ is the Hamiltonian vector field associated with H_r.

The control domain for our applications are closed balls of $\mathbb{R}^2$ and $\mathbb{R}^3$ which are not manifolds. However, it turns out in both cases the extremal controls belong to the boundary of the balls and can still be written, almost everywhere, as feedback functions of the state and adjoint vectors, which

yields the formulation of a real Hamiltonian function H_r. This is described with more detail in Chapters 4 and 5.

In this context, any solution of the optimal control problem (3.3) is, consequently, necessarily the projection of an extremal curve solution of the Hamiltonian system (3.4). Thus, extremal curves provide candidate trajectories for being optimal solutions of (3.3).

Second order optimality conditions have been derived for both the constrained and unconstrained control and state, [46, 47, 48] and [49, 50, 51, 52] for instance, respectively. In the unconstrained case the conditions reduce to the analysis of conjugate points (as described in given references), and this is the case for the problems we investigate. Here we briefly recall the definition and results regarding conjugate points.

To the Hamiltonian system (3.4), let us associate the *Jacobi equation* equation on $\mathbb{R}^n$

$$\dot{\delta}\mathbf{z}(t) = d\vec{H}_r(\mathbf{z})\delta\mathbf{z}(t) \tag{3.5}$$

along an extremal $\mathbf{z}(\cdot) = (\mathbf{x}(\cdot), \mathbf{p}(\cdot))$, where $\delta\mathbf{z}(t)$ represents the first variation of $\mathbf{z}$. A *Jacobi field* is a nontrivial solution $J(t) = (\delta\mathbf{x}(t), \delta\mathbf{p}(t))$ of (3.5) along $\mathbf{z}(\cdot)$. A Jacobi field is said to be *vertical* at time t if $\delta\mathbf{x}(t) = 0$. A time t_c is said to be a *geometrically conjugate time* if there exists a Jacobi field which is vertical at 0 and at t_c. Then, $\mathbf{x}(t_c)$ is said to be *conjugate* to $\mathbf{x}(0)$. Conjugate times can be geometrically characterized by considering the *exponential mapping* which is defined, when the final time is free (such as in the time minimization problem) by

$$\exp_{\mathbf{x}_0,t} : \mathbf{p}_0 \longrightarrow \mathbf{x}(t, \mathbf{x}_0, \mathbf{p}_0) \tag{3.6}$$

where $\mathbf{x}(t, \mathbf{x}_0, \mathbf{p}_0)$ is the projection on the phase space of the solution of (3.4) evaluated at the time t. We denote $\exp_t(\frac{\partial H_r}{\partial p}, -\frac{\partial H_r}{\partial q})$ the flow of the vector field $(\frac{\partial H_r}{\partial p}, -\frac{\partial H_r}{\partial q})$. The following proposition results from a geometrical interpretation of the Jacobi equation, [50] for a detailed proof. Working in $\mathbb{R}^n$, the cotangent space at $\mathbf{x}_0$ is denoted $T^*_{\mathbf{x}_0}\mathbb{R}^n$.

Theorem 2. *Let $\mathbf{x}_0 \in \mathbb{R}^n$, $L_0 = T^*_{\mathbf{x}_0}\mathbb{R}^n$ and $L_t = \exp_t(\frac{\partial H_r}{\partial \mathbf{p}}, -\frac{\partial H_r}{\partial \mathbf{x}}))(L_0)$. Then L_t is a Lagrangian submanifold of $T^*\mathbb{R}^n$ whose tangent space is spanned by Jacobi fields starting from L_0. Moreover $\mathbf{x}(t_c)$ is geometrically conjugate to $\mathbf{x}_0$ if and only if $\exp_{\mathbf{x}_0,t_c}$ is not an immersion at $\mathbf{p}_0$.*

Under generic assumptions, the following theorem connects the notion of conjugate time and the

local optimality of extremals, for instance [49, 50, 51] for greater details.

Theorem 3. *Let t_c^1 be the first conjugate time along $\mathbf{z}(\cdot)$. The trajectory $\mathbf{x}(\cdot)$ is locally optimal on $[0, t_c^1)$ in L^∞ topology. If $t > t_c^1$ then $\mathbf{x}(\cdot)$ is not locally optimal on $[0, t]$.*

3.3 Indirect methods

Based on our assumptions on the control domain we determine extremal curves are solutions of a true Hamiltonian system, satisfying given boundary conditions and derived from the application of the Pontryagin maximum principle. They can be numerically computed by means of the so-called *indirect methods*. The main difficulty to overcome consists of determining the initial value of the adjoint vector $\mathbf{p}(0)$ such that the boundary conditions are satisfied. Rewriting the boundary and transversality conditions under the form $\mathbf{R}(\mathbf{z}(0), \mathbf{z}(t_f)) = \mathbf{0}$, admissible extremals can be expressed as solutions of

$$\begin{cases} \dot{\mathbf{z}}(t) = \vec{H}_r(\mathbf{z}(t)) \\ \mathbf{R}(\mathbf{z}(0), \mathbf{z}(t_f)) = \mathbf{0} \end{cases} \tag{3.7}$$

where $\mathbf{z} = (\mathbf{x}, \mathbf{p})^{\mathrm{T}}$.

Solving the boundary value problem is then equivalent to finding a zero of the so-called *shooting function* [53] S defined by

$$S : (\mathbf{z}_0) \longrightarrow \mathbf{R}(\mathbf{z}(0), \mathbf{z}(t_f)). \tag{3.8}$$

In the case of free final time, the variable t_f is also an input of the shooting function and the condition $H_r = 0$, deduced from the application of the maximum principle, is appended to the function $\mathbf{R}$. In other cases, such as when the structure of the control is defined by switching times t_i, other variables may also be included as inputs to the shooting function with corresponding constraints added to $\mathbf{R}$.

By construction S is a smooth function, and a Newton type algorithm can be used to determine its zeros. Newtonian methods, however, are very sensitive to the initial guess, which must be chosen accurately. To do so, we develop tools that rely on so-called *continuation methods* [39]. This technique is based on connecting the Hamiltonian H_r to a Hamiltonian H_0, whose corresponding shooting equation is easy to solve, via a parametrized family $(H_\lambda)_{\lambda \in [0,1]}$ of smooth Hamiltonians. The algorithm then is divided into the following steps:

(i) Solve the shooting equation associated with H_0.

(ii) Set up a discretization $0=\lambda_0, \lambda_1, \ldots, \lambda_N=1$ and solve iteratively the shooting equation associated with $H_{\lambda_{i+1}}$ by using as initial guess the solution of the shooting equation corresponding to H_{λ_i}.

(iii) The solution of the last shooting equation associated with H_{λ_N} is consequently a zero of the shooting function S.

The software Hampath, [35], relies on the Fortran MINPACK package and is designed along the method described above and allows one to check the second order optimality conditions.

CHAPTER 4
TIME-MINIMAL RENDEZVOUS PROBLEM

In this chapter, we present the time-minimization rendezvous problem. A spacecraft with characteristics comparable to an electric-propulsion spacecraft is assumed to start on a geostationary orbit and must achieve rendezvous with a minimoon at a preselected rendezvous point along the minimoon's trajectory, in as little time as possible. The Circular Restricted Three-Body Problem is used to model the effects of the Earth's and Moon's gravities on the spacecraft during the transfer, so we recall here some basic properties of the model. The selection of rendezvous points, application of the maximum principle, and homotopic methods are detailed within, followed by the numeric results we obtained. The main result of this chapter is that rendezvous is achievable with over 96% of the minimoon database, with thrusts as low as 0.1 Newtons and transfer times under three months.

In this chapter we apply the methods described in Chapter 3 to design time-minimal rendezvous missions to minimoons. The major goal of this dissertation is to assess the feasibility of space missions to minimoons by designing theoretical missions to a large sample of simulated minimoons. As a first approach toward this goal, we use indirect methods of optimal control paired with continuation techniques to identify two-dimensional and then three-dimensional time-minimal transfers to rendezvous with minimoons in the vicinity of the Earth-Moon L_1 point, when starting from a geostationary orbit using a maximum thrust of 1 Newton or less.

Our solution strategy is summarized by the flow chart in Figure 4.1. Labeled arrows are referred to throughout the discussion of the methodology and results.

4.1 Circular Restricted Three-Body Problem

The Circular Restricted Three-Body Problem (CR3BP) [4] is the classical model used to approximate the motion of a spacecraft subject to the respective gravitational fields of the Earth and Moon. It is a well-known case of the general three-body problem, which models the motion of three masses

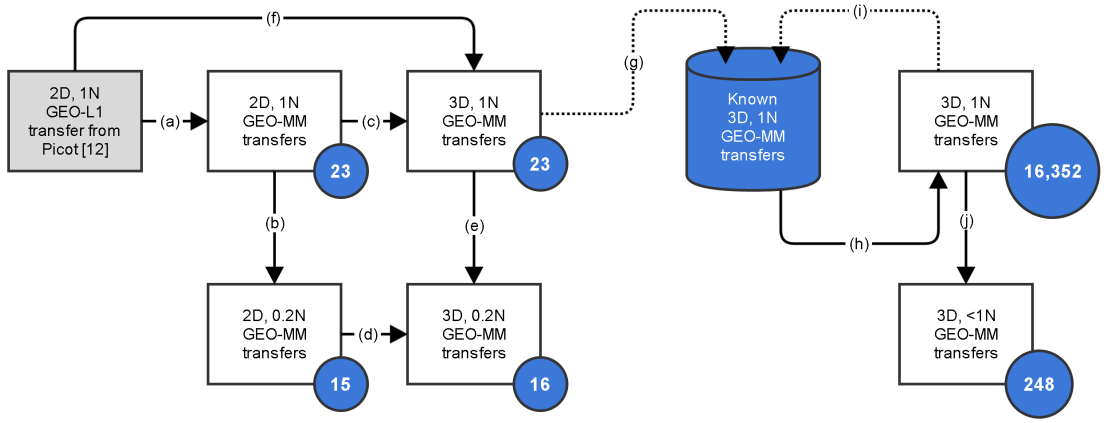

Figure 4.1: Work flow chart for the time-minimization rendezvous problem. A solid arrow from one element to another indicates that a continuation method was initialized by a solution from the first element in order to attempt to compute a solution to the other. Blue circles indicate how many total solutions were computed successfully for each corresponding element. A dashed arrow indicates new solutions being added to a database of known solutions which can be used to initialize continuation methods.

in space under the influence of their mutual gravitational attraction. In the restricted problem, the two main bodies are called *primaries* and are denoted by their masses M_1 and M_2 for the Earth and Moon, respectively. The two primaries are assumed to be on coplanar circular orbits around their mutual center of mass G under the influence of their mutual attraction. Units are normalized so that the total mass $M_1 + M_2 = 1$, the distance between the primaries is 1, and the primaries orbit uniformly with angular velocity 1. Note that this is a reasonable approximation of reality since the eccentricity of the Moon's orbit around the Earth is small (≈ 0.0549). The third mass (for us, the spacecraft) is assumed to be of negligible mass, so that it does not influence the primaries. Let us also note that the minimoons are also assumed to be of negligible mass so that they have no influence on the motion of any of the bodies, which is a reasonable assumption due to their small size.

We denote by $\mu = \frac{M_2}{M_1+M_2}$ the normalized mass of the smaller primary and use a coordinate system centered at G, rotating with angular velocity 1 so that the primaries M_1 and M_2 are fixed points at $(-\mu, 0, 0)$ and $(1-\mu, 0, 0)$ respectively. Then, the position of the spacecraft evolving under the influence of the Earth and Moon's gravities at time t is denoted $(x(t), y(t), z(t))$, and the

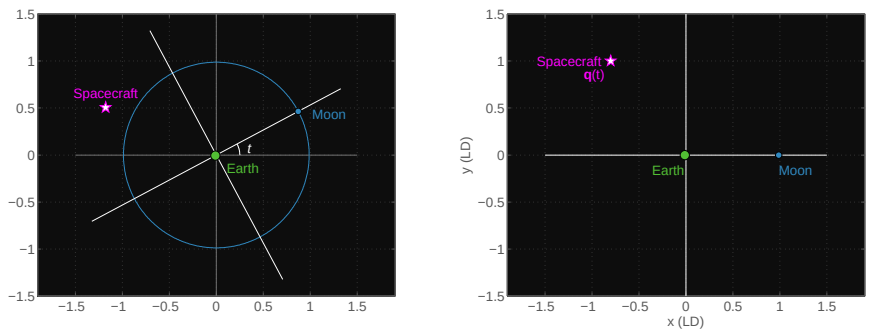

Figure 4.2: The Circular Restricted Three-Body Problem reference frame

uncontrolled equations of motion for the spacecraft can then be written:

$$\begin{cases} \ddot{x} = 2\dot{y} - \frac{\partial V}{\partial x} \\ \ddot{y} = -2\dot{x} - \frac{\partial V}{\partial y} \\ \ddot{z} = -\frac{\partial V}{\partial z} \end{cases} \tag{4.1}$$

where V is the potential energy function:

$$-V = \frac{x^2 + y^2}{2} + \frac{1-\mu}{\rho_1} + \frac{\mu}{\rho_2} + \frac{\mu(1-\mu)}{2} \tag{4.2}$$

and

$$\rho_1 = \sqrt{(x+\mu)^2 + y^2 + z^2}, \qquad \rho_2 = \sqrt{(x-1+\mu)^2 + y^2 + z^2},$$

are there distances from the spacecraft to the Earth and Moon, respectively.

This dynamical system has five well-known equilibrium points, denoted by L_i for $i = 1, \ldots, 5$, and defined as the critical points of the potential V. All five are in the (x, y) plane, and are shown in Figure 4.3. The first three are unstable and collinear along the x-axis; whereas L_4 and L_5 make two equilateral triangles with the two primaries and are both stable when $\mu < \frac{1}{2}\left(1 - \frac{\sqrt{69}}{9}\right) \approx 0.0385$, which is the case for the Earth-Moon system ($\mu \approx 0.01215361914$).

It is also well-known that the CR3BP is a conservative system, with the energy $E = K + V$ constant over trajectories, where $K = \frac{1}{2}\left(\dot{x}^2 + \dot{y}^2 + \dot{z}^2\right)$ is the kinetic energy. This implies that when the spacecraft is uncontrolled it is restricted to move within its current energy level set. Figure 4.3 also illustrates a few level sets by the different shaded regions.

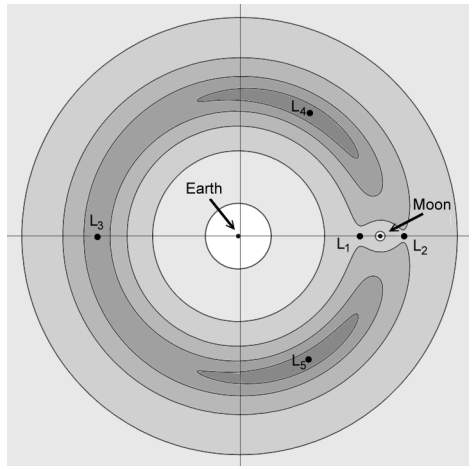

Figure 4.3: Equilibrium points and energy level sets for the CR3BP

The *controlled* CR3BP in the rotating frame is then formulated by adding control terms $\mathbf{u} = (u_1, u_2, u_3)^{\mathrm{T}}$, with $\|\mathbf{u}\| \leq 1$, representing the thrust of the spacecraft to the x, y, and z accelerations, giving

$$\begin{cases} \ddot{x} = 2\dot{y} - \frac{\partial V}{\partial x} + \frac{T_{max}}{m} u_1 \\ \ddot{y} = -2\dot{x} - \frac{\partial V}{\partial y} + \frac{T_{max}}{m} u_2 \\ \ddot{z} = -\frac{\partial V}{\partial z} + \frac{T_{max}}{m} u_3 \end{cases} \tag{4.3}$$

where T_{max} is a constant representing the maximum thrust of the spacecraft. The spacecraft mass variation $m(t)$ may be modelled by considering the equation $\dot{m} = -\beta T_{max} \|\mathbf{u}\|$, for a constant β, but will not be taken into account until the next chapter. Thus, for now, the mass m of a spacecraft is assumed constant over the trajectory.

In this chapter we design time-minimal transfers for a spacecraft starting on a geostationary orbit to rendezvous with minimoons when the maximum thrust is assumed to be low. The mathematical formulation of our problem is to compute solutions of the system (4.3) which minimize the transfer time, expressed as an integral cost:

$$\min_{\mathbf{u} \in \mathcal{U}} \int_0^{t_f} 1 \; dt \tag{4.4}$$

where $\mathcal{U} = \{\mathbf{u} : \mathbb{R} \to B_{\mathbb{R}^3}(0,1);\ \mathbf{u} \text{ measurable } \}$ is the set of so-called admissible controls. The times t_0 and t_f are the fixed initial time and free final time, respectively.

4.2 Methodology

In order to design low thrust time-minimal transfers to a large sample of minimoons we choose to use indirect methods which are known to be precise and computationally fast, however challenging to initialize. As a first approach to overcome the initialization difficulty, in this chapter we use continuation techniques from an existing planar time-optimal transfer to the Earth-Moon L_1 point computed in [33] to compute transfers to planar projections of minimoon trajectories passing in a neighborhood of the L_1 point. The solutions to the planar trajectories are then used to initialize computation of transfers to the actual spatial minimoon trajectories. Continuation techniques are then also used to decrease the maximum thrust bound in order to obtain very low thrust transfers. For the last round of calculations, found solutions are added to a database of known solutions and also serve as starting points for initializing the continuation method to other minimoons.

4.2.1 Two-dimensional transfers

As a step toward initializing the computation of three-dimensional time-minimal transfers, we first focus on the planar time-minimal problem, where motion is restricted to the (x, y)-plane ($z = 0$). In this case, $\mathbf{u} = (u_1, u_2)^{\mathrm{T}}$ and we let $\mathbf{q} := (q_1, q_2, q_3, q_4)^{\mathrm{T}} = (x, y, \dot{x}, \dot{y})^{\mathrm{T}}$ be the state variables, so that the equations of motion are rewritten as a first order bi-input system:

$$\dot{\mathbf{q}} = \mathbf{F}_0(\mathbf{q}) + \frac{T_{max}}{m}\left(\mathbf{F}_1(\mathbf{q})u_1 + \mathbf{F}_2(\mathbf{q})u_2\right), \tag{4.5}$$

where

$$\mathbf{F}_0(\mathbf{q}) = \begin{pmatrix} q_3 \\ q_4 \\ 2q_4 + q_1 - (1-\mu)\frac{q_1+\mu}{\left((q_1+\mu)^2+q_2^2\right)^{3/2}} - \mu\frac{q_1-1+\mu}{\left((q_1-1+\mu)^2+q_2^2\right)^{3/2}} \\ -2q_3 + q_2 - (1-\mu)\frac{q_2}{\left((q_1+\mu)^2+q_2^2\right)^{3/2}} - \mu\frac{q_2}{\left((q_1-1+\mu)^2+q_2^2\right)^{3/2}} \end{pmatrix}$$

$$\mathbf{F}_1(\mathbf{q}) = \begin{pmatrix} 0 \\ 0 \\ 1 \\ 0 \end{pmatrix}, \quad \mathbf{F}_2(\mathbf{q}) = \begin{pmatrix} 0 \\ 0 \\ 0 \\ 1 \end{pmatrix}$$

Our objective is to compute low-thrust time-minimal transfers from a specific point $\mathbf{q}_{dprt}$ on a

geostationary orbit $\mathcal{O}_g$ to rendezvous with minimoons at preselected points on their orbits $\mathcal{O}_{MM}$. In mathematical terms, we want to solve optimal control problems of the form

$$\begin{cases} \dot{\mathbf{q}} = \mathbf{F}_0(\mathbf{q}) + \epsilon\left(\mathbf{F}_1(\mathbf{q})u_1 + \mathbf{F}_2(\mathbf{q})u_2\right) \\ \min_{\mathbf{u}\in\mathcal{U}} \int_0^{t_f} dt \\ \mathbf{q}(0) = \mathbf{q}_{dprt} \in \mathcal{O}_g, \quad \mathbf{q}(t_f) = \mathbf{q}_{rdvz} \in \mathcal{O}_{MM} \end{cases} \tag{4.6}$$

where $\mathbf{q}_{rdvz}$ is the planar position and velocity of the rendezvous point. The final time t_f is free and is what we seek to minimize. The initial time is assumed to be $t_0 = 0$, and $\epsilon = \frac{T_{max}}{m}$ is a constant dependent on the maximum thrust T_{max} and mass m of the spacecraft. The control domain $\mathbb{U}$ is the unit disk, so the set of admissible controls is $\mathcal{U} = \{\mathbf{u} : \mathbb{R} \to B_{\mathbb{R}^2}(0,1) : \mathbf{u} \text{ measurable}\}$. Applying the Pontryagin maximum principle, we have the existence of p^0 a non-positive constant and $\mathbf{p}$ an absolutely continuous function with $(p^0, \mathbf{p}) \neq (0, \mathbf{0})$. We assume we are in the so-called normal case where $p^0 \neq 0$ and can be normalized to $p^0 = -1$. In this case, it comes that every solution $\mathbf{q}(t)$ of the optimal control problem (4.6) is necessarily the projection of an extremal curve $(\mathbf{q}(t), \mathbf{p}(t))$ solution of the system

$$\dot{\mathbf{q}}(t) = \frac{\partial H}{\partial \mathbf{p}}, \quad \dot{\mathbf{p}}(t) = -\frac{\partial H}{\partial \mathbf{q}} \tag{4.7}$$

where the pseudo-Hamiltonian function H is defined by

$$H(\mathbf{p}, \mathbf{q}, \mathbf{u}) = -1 + H_0(\mathbf{p}, \mathbf{q}) + \epsilon\left(u_1 H_1(\mathbf{p}, \mathbf{q}) + u_2 H_2(\mathbf{p}, \mathbf{q})\right)$$

with $H_i(\mathbf{p}, \mathbf{q}) = \langle \mathbf{p}, \mathbf{F}_i(\mathbf{q})\rangle, i = 0, 1, 2$. Moreover, from the maximization condition we can conclude that whenever $(H_1, H_2) \neq (0, 0)$ the control $\mathbf{u}$ is given by

$$u_i = \frac{H_1}{\sqrt{H_1^2 + H_2^2}}, \quad i = 1, 2.$$

Substituting this definition of $\mathbf{u}$ into H gives the expression of the real Hamiltonian H_r as

$$H_r(\mathbf{p}, \mathbf{q}) = -1 + H_0(\mathbf{p}, \mathbf{q}) + \epsilon\sqrt{H_1^2(\mathbf{p}, \mathbf{q}) + H_2^2(\mathbf{p}, \mathbf{q})}$$

which no longer depends on $\mathbf{u}$. Since the final time is free, the maximum principle also implies that H_r is identically zero on $[0, t_f]$.

We can define the so-called switching surface $\Sigma = \{(H_1, H_2) = (0, 0)\}$; then any point in $\mathbb{R}^8 \backslash \Sigma$ is said to be of order 0. In [54] the authors prove that every normal time-minimal extremal trajectory is a concatenation of a finite number of arcs of order 0. More details about the structure of the extremals can be found in [54] – here we focus on the practical application of the theory. Therefore, to compute time-minimal extremal trajectories we must find a zero to the shooting function

$$\begin{aligned} E &: \mathbb{R}^5 \to \mathbb{R}^5 \\ (\mathbf{p}(0), t_f) &\to \begin{pmatrix} \mathbf{q}(t_f) - \mathbf{q}_{rdvz} \\ H_r\left(\mathbf{p}(t_f), \mathbf{q}(t_f)\right) \end{pmatrix}. \end{aligned}$$

In [33], the parameters $T_{max} = 1$ Newton and $m = 350$ kilograms are chosen and are approximately consistent with a small electric propulsion spacecraft. For the first calculations we adopt the same parameter values, and then using a homotopy method compute transfers for even lower maximum thrust values. Also as in [33], as an initial approach we depart from a geostationary orbit, denoted $\mathcal{O}_g$, where specifically $\mathbf{q}_{dprt} = (0.0947,\ 0,\ 0,\ 2.8792)$, expressed in the rotating frame units, is the point on $\mathcal{O}_g$ exactly between the Earth and Moon.

We first compute planar time-minimal transfers to a sample of 100 rendezvous points projected from 100 different minimoons trajectories. In the database, 343 simulated minimoons come within 0.1 LD of the Earth-Moon L_1 point. Of these 343 minimoons, we choose the 100 with the smallest absolute z-coordinate so that the projections onto the plane are reasonable approximations of the actual rendezvous points. For reference, the largest absolute z-coordinate for any of the 100 selected rendezvous points is $|z| = 0.0166$ LD. Note that all projections onto the plane have taken into account the position of the Moon and its inclination, and are transformed into the CR3BP reference frame.

The algorithm initialization is indeed less sensitive for higher max thrust boundaries (which correspond to shorter transfer times), so for all 100 rendezvous points we first attempt to compute 1 N transfers using the reference solution from [33] as an initial guess for the algorithm (Figure 4.1(a)). A discrete homotopic continuation method on the parameter ϵ is then used to determine solutions for smaller maximum thrust bounds (Figure 4.1(b)). The continuation method iteratively uses known solutions for ϵ_n to initialize the algorithm for smaller values $\epsilon_{n+1} < \epsilon_n$ (Chapter 3). The local optimality of each solution is then verified using second order conditions based on the notion of conjugate times as described in Chapter 3. All computations are carried out using the software

Hampath [35].

4.2.2 Three-dimensional transfers

To compute three-dimensional transfers the methodology from the two-dimensional case has to be adjusted to account for the vertical coordinate z. Now let $\mathbf{q} = (x, y, z, \dot{x}, \dot{y}, \dot{z})^{\mathrm{T}}$, and then the controlled equations of motion are given by

$$\dot{\mathbf{q}} = \mathbf{F}_0(\mathbf{q}) + \frac{T_{max}}{m} \sum_{i=1}^{3} \mathbf{F}_i(\mathbf{q}) u_i \tag{4.8}$$

where

$$\mathbf{F}_0(\mathbf{q}) = \begin{pmatrix} q_4 \\ q_5 \\ q_6 \\ 2q_5 + q_1 - (1-\mu)\frac{q_1+\mu}{\left((q_1+\mu)^2+q_2^2+q_3^2\right)^{3/2}} - \mu\frac{q_1-1+\mu}{\left((q_1-1+\mu)^2+q_2^2+q_3^2\right)^{3/2}} \\ -2q_4 + q_2 - (1-\mu)\frac{q_2}{\left((q_1+\mu)^2+q_2^2+q_3^2\right)^{3/2}} - \mu\frac{q_2}{\left((q_1-1+\mu)^2+q_2^2+q_3^2\right)^{3/2}} \\ -(1-\mu)\frac{q_3}{\left((q_1+\mu)^2+q_2^2+q_3^2\right)^{3/2}} - \mu\frac{q_3}{\left((q_1-1+\mu)^2+q_2^2+q_3^2\right)^{3/2}} \end{pmatrix}$$

$$\mathbf{F}_1(\mathbf{q}) = \begin{pmatrix} 0 \\ 0 \\ 0 \\ 1 \\ 0 \\ 0 \end{pmatrix}, \quad \mathbf{F}_2(\mathbf{q}) = \begin{pmatrix} 0 \\ 0 \\ 0 \\ 0 \\ 1 \\ 0 \end{pmatrix}, \quad \mathbf{F}_3(\mathbf{q}) = \begin{pmatrix} 0 \\ 0 \\ 0 \\ 0 \\ 0 \\ 1 \end{pmatrix}$$

and the optimal control problem we seek to solve is

$$\begin{cases} \dot{\mathbf{q}} = \mathbf{F}_0(\mathbf{q}) + \epsilon \sum_{i=1}^{3} \mathbf{F}_i(\mathbf{q}) u_i \\ \min_{\mathbf{u}\in\mathcal{U}} \int_0^{t_f} dt \\ \mathbf{q}(0) = \mathbf{q}_{dprt} \in \mathcal{O}_g, \quad \mathbf{q}(t_f) = \mathbf{q}_{rdvz} \in \mathcal{O}_{MM} \end{cases} \tag{4.9}$$

where, as before, $\mathbf{q}_{dprt}$ is a selected departure point on a geostationary orbit, $\mathbf{q}_{rdvz}$ is a selected rendezvous point along a minimoon's orbit (now a three-dimensional position and velocity), and the final time t_f is free and is what we seek to minimize. The control domain $\mathbb{U}$ is the unit sphere, so

the set of admissible controls is $\mathcal{U} = \{\mathbf{u} : \mathbb{R} \to B_{\mathbb{R}^3}(0,1) : \mathbf{u} \text{ measurable}\}$. The constant $\epsilon = \frac{T_{max}}{m}$ is as before. Applying the Pontryagin maximum principle gives similar results to those obtained in the two-dimensional case. In particular, we assume we are in the normal case $p^0 \neq 0$, so every solution $\mathbf{q}(t)$ of (4.9) is the projection of an extremal curve $(\mathbf{q}(t), \mathbf{p}(t))$ solution of the Hamiltonian system

$$\dot{\mathbf{q}}(t) = \frac{\partial H_r}{\partial \mathbf{p}}, \quad \dot{\mathbf{p}}(t) = -\frac{\partial H_r}{\partial \mathbf{q}}$$

where the Hamiltonian function H_r is given by

$$H_r(\mathbf{p}, \mathbf{q}) = -1 + H_0(\mathbf{p}, \mathbf{q}) + \epsilon \sqrt{\sum_{i=1}^{3} H_i^2(\mathbf{p}, \mathbf{q})}$$

with $H_i(\mathbf{p}, \mathbf{q}) = \langle \mathbf{p}, \mathbf{F}_i(\mathbf{q}) \rangle,\ i = 0, \ldots, 3$. As in the two-dimensional case, H_r is identically zero on $[0, t_f]$ since the final time is free. Therefore, computing three-dimensional time-minimal extremals is equivalent to solving the shooting equation

$$\begin{aligned} &E : \mathbb{R}^7 \to \mathbb{R}^7 \\ &(\mathbf{p}(0), t_f) \to \begin{pmatrix} \mathbf{q}(t_f) - \mathbf{q}_{rdvz} \\ H_r\left(\mathbf{p}(t_f), \mathbf{q}(t_f)\right) \end{pmatrix}. \end{aligned}$$

Again, the spacecraft mass is assumed to be constant 350 kg and the initial condition on the geostationary orbit is given at $\mathbf{q}_{dprt} = (0.0947,\ 0,\ 0,\ 0,\ 2.8792,\ 0)$. The selected rendezvous points are the 100 associated spatial points corresponding to the two-dimensional problem, the 100 minimoons within 0.1 LD of L_1 with the lowest absolute z coordinate. The two-dimensional 1 N time-optimal transfers to (x, y)-projections of these rendezvous points are used as the initial guess to solve the shooting method (Figure 4.1(c)). Note that the two-dimensional solutions do not provide initial guesses for the z and $\dot{z}$ components of $\mathbf{p}(0)$, so as a convention we set them equal to zero. For the selected 100 minimoons, we attempt to compute both 1 N and 0.2 N time-minimal transfers. Three continuation strategies are tried: 1) using the 0.2 N planar transfers to initialize a continuation method to the 0.2 N spatial transfers (Figure 4.1(d)); 2) using the 1 N spatial transfers to initialize a continuation method to the 0.2 N spatial transfers (Figure 4.1(e)); 3) directly using the 1 N transfer from [33] to initialize 1 N spatial transfers (Figure 4.1(f)) then performing a continuation to 0.2 N transfers (Figure 4.1(e)).

Finally, the collection of successful 1 N three-dimensional time-minimal transfers is then used to set up a database of initial guesses to compute 1 N time-minimal transfers to all remaining minimoons in the simulated database (Figure 4.1(g)). The remaining transfers are initialized as follows: for a given minimoon denoted $\mathcal{MM}_i$, we define the rendezvous location $\mathbf{q}^i_{rdvz}$ to be the point at which $\mathcal{MM}_i$ is nearest to L_1. Then among the database of known 1 N time-minimal transfers, we select that transfer which realizes a rendezvous with minimoon $\mathcal{MM}_j$ at the location $\mathbf{q}^j_{rdvz}$ such that the Euclidean norm $\|\mathbf{q}^j_{rdvz} - \mathbf{q}^i_{rdvz}\|$ is minimized. This transfer is used as the initial guess (Figure 4.1(h)) for ths shooting equation to compute a time-minimal extremal curve to rendezvous with $\mathcal{MM}_i$, and the first conjugate point along this extremal is computed to guarantee its local time-optimality. If the algorithm converges to a solution, and thus a rendezvous with $\mathcal{MM}_i$ is computed, we update the database of known solutions to include the new solution (Figure 4.1(i)). If either the shooting method or the second order condition fails, $\mathcal{MM}_i$ is placed back in the set of minimoons for which no transfer has been computed. We continue to attempt computing time-minimal transfers to the remaining minimoons, and eventually loop back to retry with the expanded database of initializations any computations that have failed.

Finally, for a sample of 250 minimoons we again investigate lower thrust transfers, by performing continuations on the maximum thrust bound ϵ and recording the lowest value ϵ_{min} for which a transfer is found (Figure 4.1(j)).

4.3 Results

4.3.1 Two-dimensional transfers

Applying the methodology described in Section 4.2 for the 100 selected minimoons, we first obtain a collection of 23 two-dimensional extremal transfers with maximum thrust of $T_{max} = 1$ N, when using the 1 N L_1 transfer from [33] to initialize the algorithm (Figure 4.1(a)). For 15 of the 23, the continuation to a maximum thrust of 0.2 N is successful (Figure 4.1(b)). Data regarding the 15 transfers is given in Table 4.1.

The transfer times for the computed two-dimensional 1 N minimoon rendezvous are all between 10.01 and 19.39 days, and the 0.2 N transfer times are all between 47.23 and 73.00 days. For 13 of the 15 low-thrust transfers, the transfer time $t_f^{0.2}$ is less than the time it takes the corresponding minimoon to evolve from its capture point to the rendezvous point (t_{rdvz}). This remark is crucial

$\mathcal{MM}$ #	t_f^1	t_c^1	$t_{rdvz} - t_f^1$	$t_f^{0.2}$	$t_c^{0.2}$	$t_{rdvz} - t_f^{0.2}$
57	11.1	12.5	189.7	47.2	49.8	153.6
651	19.4	∞	13.5	73.0	∞	-40.1
3813	10.1	14.0	123.2	56.0	∞	77.3
3867	10.2	16.6	55.0	55.1	61.8	10.2
4980	11.4	∞	67.4	58.0	62.3	20.9
5481	11.0	26.0	315.7	59.4	101.2	267.2
7548	12.2	17.7	66.5	59.3	420.4	19.3
8962	11.8	∞	72.4	60.0	76.9	24.2
10585	10.1	30.8	54.1	55.6	121.0	8.5
10979	10.1	∞	49.1	59.0	∞	0.3
11249	10.0	13.9	65.7	58.3	∞	17.5
12028	13.4	22.7	425.0	61.5	149.2	376.9
13933	10.7	14.1	14.4	59.4	65.1	-34.3
14487	10.1	22.6	121.8	58.5	∞	73.4
16803	10.7	15.0	234.1	66.5	91.8	178.3

Table 4.1: Data for the successful two-dimensional transfers (units are days). The second column gives the 1 N transfer times t_f^1 and similarly column 5 gives the 0.2 N transfer times $t_f^{0.2}$. The conjugate times t_c^1 and $t_c^{0.2}$ for all transfers are calculated and given in columns 3 and 6, which are all greater than the transfer times thus guaranteeing local optimality of the transfers. Note a conjugate time of ∞ indicates that no conjugate times were found with 100 times the transfer time. Columns 4 and 7 give the differences between the transfer time and the minimoon's time since capture, $t_{rdvz} - t_f$. Note that a negative value in these columns implies the transfer would be impractical, since we'd have to start the transfer before the minimoon was even captured (which is likely before it was detected).

from a practical stand point since it suggests that the mission could be feasible if the minimoons are able to be detected at or near their capture time.

Figure 4.4 gives examples of 1 N and 0.2 N transfers to four minimoons, shown in the rotating frame.

4.3.2 Three-dimensional transfers

Next, continuation techniques described in Section 4.2 are used to compute three-dimensional 1 N and 0.2 N transfers. Using the 15 planar 0.2 N transfers to initialize the continuation method, we obtain 5 successful spatial 0.2 N transfers (Figure 4.1(d)). Using the 23 planar 1 N transfers to initialize the continuation method, we obtain 17 successful spatial 0.2 N transfers (Figure 4.1(c)(e)). Finally, using the original planar 1 N L_1 transfer computed in [33] to initialize the continuation method, we obtain 12 spatial 0.2 N transfers (Figure 4.1(f)(e)). Note that some of the successful spatial transfers overlapped between the different attempted continuations strategies. In total from the first round of computations, we have 23 distinct spatial 1 N transfers and 16 distinct spatial 0.2 N transfers. The durations of the spatial 1 N transfers were all between 10.01 and 19.46 days, and the 0.2 N spatial transfers were all between 55.31 and 81.46 days. Data for the successful three-dimensional transfers is given in Table 4.2.

In Figure 4.5, locally time-minimal three-dimensional transfers to four distinct minimoons for 1 N and 0.2 N maximum thrusts are shown in the rotating reference frame.

The solutions for the minimoon rendezvous above populate a database of known solutions that is referred to when computing new spatial time-minimal transfers (Figure 4.1(g)). Therefore, for those 16,923 minimoons which we haven't already found a transfer to, the database of known solutions is used to initialize a transfer as described in Section 4.2 (Figure 4.1(h)). Our techniques provided 1 N spatial transfers to 16,352 of the 16,923 minimoons – over 96% of the database. The shortest computed transfer was 9.11 days and the longest was 32.10 days. The mean transfer time was 20.12 days, and the median 19.92 days. Figure 4.6 shows the distribution of computed 1 N transfer times for the 16,352 transfers.

A preliminary analysis of the 571 minimoons for which we did not identify a transfer suggests that those rendezvous points were too close to Earth or had too high velocities for a transfer to be found. Indeed, Figure 4.7 demonstrates that the rendezvous points for which we did not obtain transfers to (represented as black dots) were typically close to Earth with high velocities. Figure

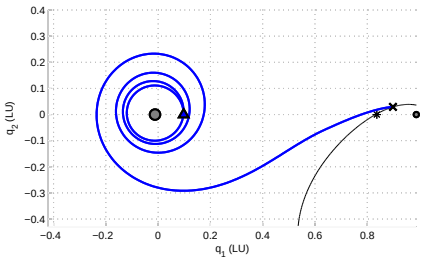

(a) $\mathcal{MM}$ 57, 1N, t_f=11.1 days

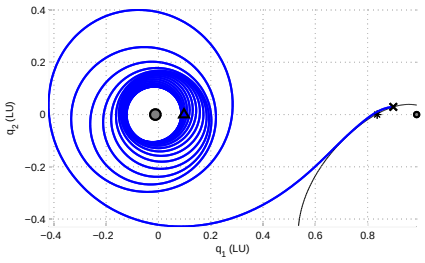

(b) $\mathcal{MM}$ 57, 0.2N, t_f=47.2 days

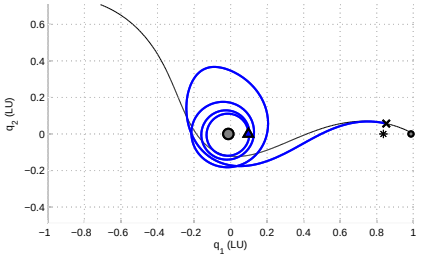

(c) $\mathcal{MM}$ 5481, 1N, t_f=11.0 days

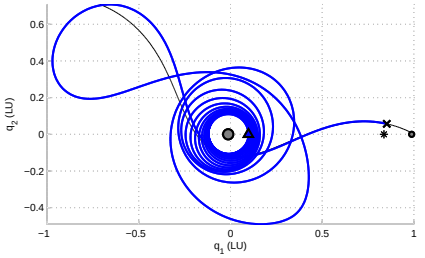

(d) $\mathcal{MM}$ 5481, 0.2N, t_f=59.4 days

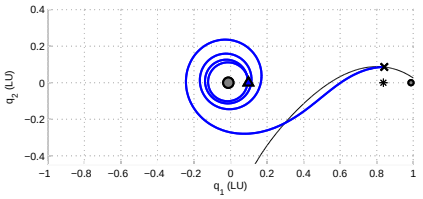

(e) $\mathcal{MM}$ 10585, 1N, t_f=10.1 days

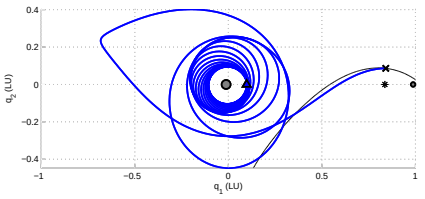

(f) $\mathcal{MM}$ 10585, 0.2N, t_f=55.6 days

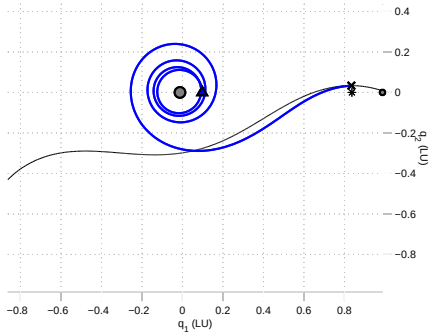

(g) $\mathcal{MM}$ 11249, 1N, t_f=10.0 days

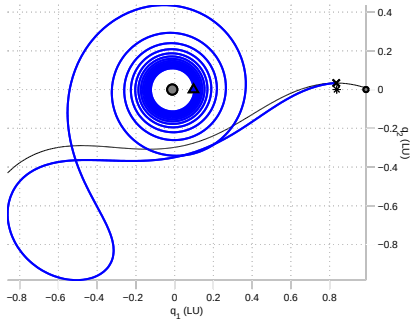

(h) $\mathcal{MM}$ 11249, 0.2N, t_f=58.3 days

Figure 4.4: Two-dimensional time-minimal transfers to four minimoons.
$T_{max} = 1$ N (left), $T_{max} = 0.2$ N (right) The Earth (left) and Moon (right) are shown as circles and the asterisk marks the point L_1, in each. The thin black curve shows a portion of the projection of the minimoon's trajectory, and the thick blue curve is the spacecraft's trajectory from the geostationary orbit (marked as a triangle) to minimoon rendezvous (marked as an X).

$\mathcal{MM}$ #	t_f^1	t_c^1 ()	$t_{rdvz} - t_f^1$	$t_f^{0.2}$	$t_c^{0.2}$	$t_{rdvz} - t_f^{0.2}$
57	13.1	15.6	187.6	62.3	67.3	138.5
651	19.5	28.4	13.4	81.5	91.2	-48.6
2778	18.6	20.2	100.2	77.7	80.1	41.1
3813	13.5	21.4	119.8	62.0	69.5	71.3
3955	19.3	26.9	27.5	80.6	89.4	-33.8
4227	10.1	68.4	56.8	55.3	∞	11.6
5481	11.1	13.2	315.6	59.9	107.0	266.8
7628	18.5	20.5	123.1	76.2	79.0	65.3
8962	11.9	19.2	72.4	65.1	82.8	19.1
10585	12.6	16.9	51.5	64.2	67.8	-0.1
10747	19.2	23.9	43.3	81.4	87.4	-18.8
10979	12.8	15.5	46.4	73.5	78.6	-14.3
11249	10.0	19.6	65.7	57.3	63.1	18.4
14487	12.8	16.5	119.1	62.9	66.8	69.0
16519	15.8	18.3	905.5	78.8	83.2	842.4
16803	10.8	14.6	234.0	67.1	70.7	177.7

Table 4.2: Data for the successful three-dimensional transfers (units are days). Column 2 gives the transfer times for the 1N transfers t_f^1, and column 3 gives the corresponding conjugate times t_c^1. Similarly, column 5 gives the transfer times for the 0.2N transfers $t_f^{0.2}$, and column 6 gives the corresponding conjugate times $t_c^{0.2}$. Note that a conjugate time marked ∞ means that no conjugate times were found within 100 times the transfer time. Columns 4 and 7 give the differences between the minimoon rendezvous time t_{rdvz} and the transfer times t_f. Note that a negative value in these columns means the transfer would be impractical, since we'd have to start the transfer before the minimoon was captured (which would likely be before it was detected). Also note that t_{rdvz} is known from the original ephemeris data.

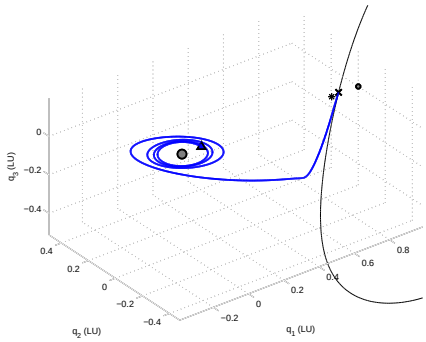

(a) $\mathcal{MM}$ 57, 1N, t_f=13.1 days

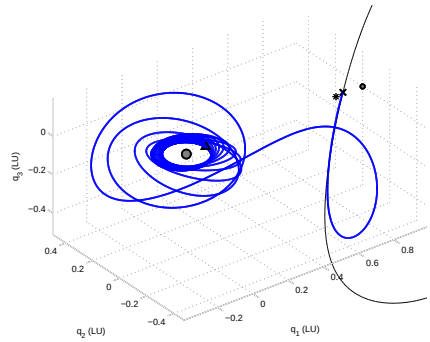

(b) $\mathcal{MM}$ 57, 0.2N, t_f=62.3 days

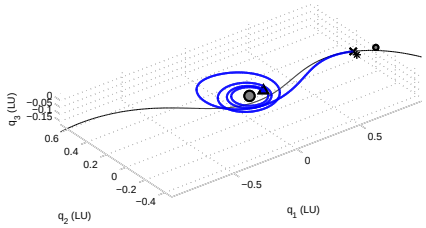

(c) $\mathcal{MM}$ 5481, 1N, t_f=11.1 days

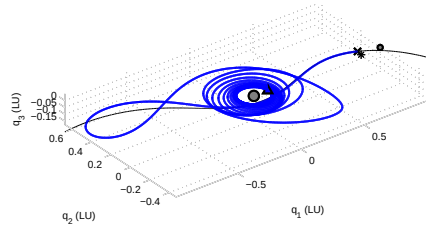

(d) $\mathcal{MM}$ 5481, 0.2N, t_f=59.9 days

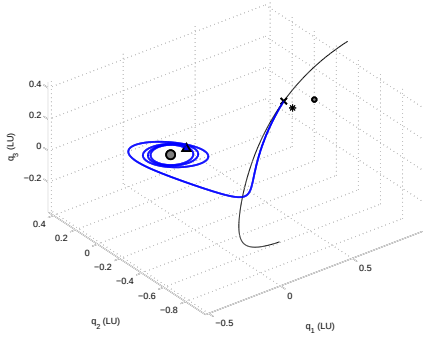

(e) $\mathcal{MM}$ 10585, 1N, t_f=12.6 days

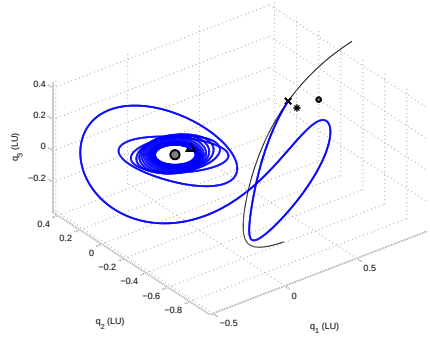

(f) $\mathcal{MM}$ 10585, 0.2N, t_f=64.2 days

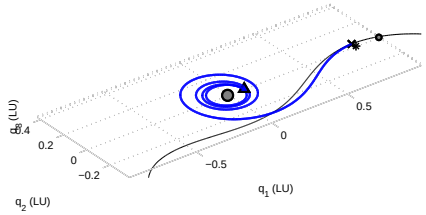

(g) $\mathcal{MM}$ 11249, 1N, t_f=10.0 days

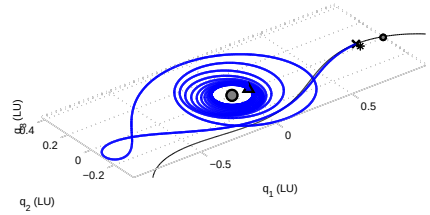

(h) $\mathcal{MM}$ 11249, 0.2N, t_f=57.3 days

Figure 4.5: Three-dimensional time-minimal transfers to four minimoons.
T_{max} = 1 N (left), T_{max} = 0.2 N (right). In each, the Earth (left) and the Moon (right) are shown as circles and the point L_1 by an asterisk. The thin black curves represent portions of the minimoon trajectories. The thick blue curves represent the extremal transfer for the spacecraft from the geostationary orbit (marked as a triangle) to the minimoon rendezvous (marked as an X).

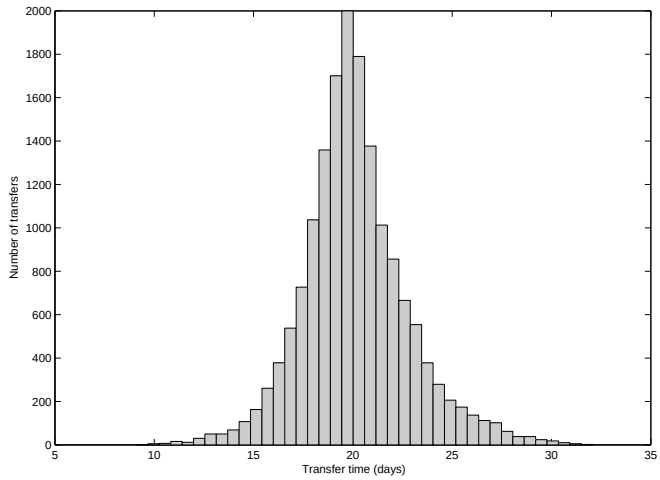

Figure 4.6: Distribution of 1N transfer times in days.

4.8 gives a histogram of the number of rendezvous points with respect to their distance from Earth, sorted by rendezvous points we did and did not find transfers for. It is clear from the figures that most of the rendezvous points that we did not find transfers to are within 0.2 LD of Earth, with velocities upwards of 0.6 LD/d.

For a random sample of 250 of the 1 N transfers, continuations techniques are used to compute transfers with thrusts less than 1 N by initializing the algorithm with the corresponding successful 1 N transfer (Figure 4.1(j)). For each of the selected 250 minimoons, the lowest maximum thrust bound ϵ_{min} for which a successful transfer was found was recorded. The lowest value of ϵ_{min} was 0.1316 N for $\mathcal{MM}$ # 16, with a transfer time of 103.3 days. For two of the 250 minimoons, a transfer could not be found with thrust less than 1 N (i.e. $\epsilon_{min} = 1$ N for those two minimoons). The mean value was $\epsilon_{min} = 0.4441$ N, and the median value was $\epsilon_{min} = 0.4101$ N. In case it is of interest to the reader, for $\mathcal{MM}$ #16 we provide some specific details of our numerical results: All values are given in the rotating reference frame, including the time units for the final time $t_f = 23.75782$.

$$\mathbf{q}_{rdvz} = \begin{pmatrix} 0.7692503 & -0.05583765 & 0.1354263 & 1.0486000 & -0.2893604 & 0.3826522 \end{pmatrix}^{\mathrm{T}}$$

$$\mathbf{p}(0) = \begin{pmatrix} -52.524900 & -12.281740 & 21.225210 & -0.475141 & -2.105559 & -0.449771 \end{pmatrix}^{\mathrm{T}}$$

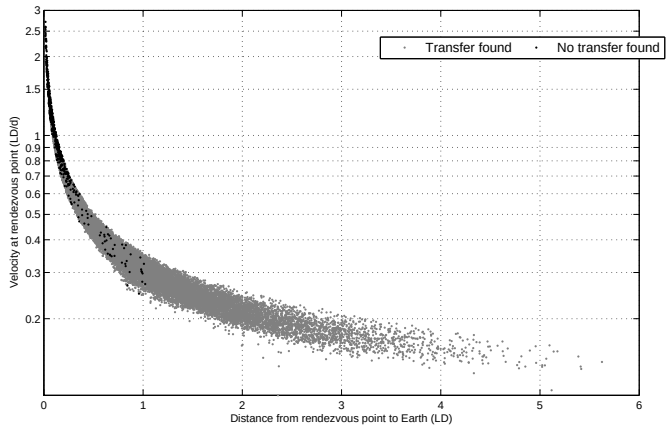

Figure 4.7: A scatter plot representing the rendezvous points which we did (gray) and did not (black) obtain transfers to.

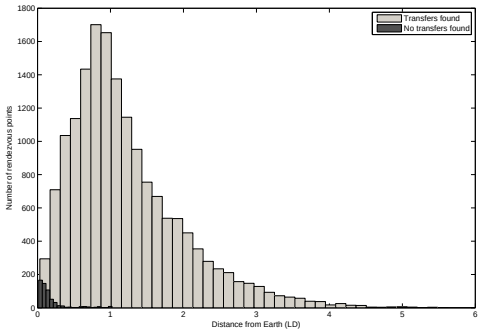

(a) Wide view of histogram

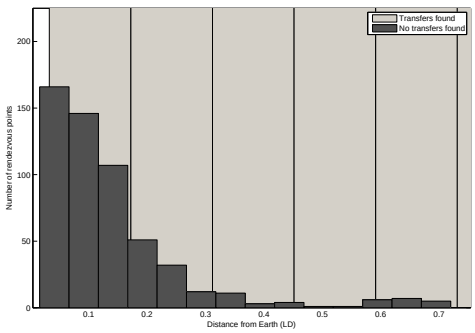

(b) Zoomed view of histogram

Figure 4.8: Histogram showing the distances from rendezvous points to Earth (transfers found = light gray, not found = dark gray).

CHAPTER 5
FUEL-MINIMAL RENDEZVOUS PROBLEM

In this chapter we present the time-constrained fuel-minimization rendezvous problem. The influence of the Sun and the mass variation of the spacecraft are added to the model. First, the general problem is presented with the new mission assumptions, new model, and the application of the maximum principle. In order to overcome the major difficulty of algorithm initialization, we present a restricted version of the general problem and develop a methodology to solve the restricted problem for large sample of minimoons. The methodology relies on the construction of a large database of so-called *cloud extremals*, which do not necessarily rendezvous with minimoons but are used to initialize continuation methods to compute minimoon rendezvous extremals. The construction of the *cloud* is detailed within.

Next, the application of the cloud methodology on the minimoon database is done in three stages. First, continuations are attempted for a random selection of 100 minimoons, for which our methods successfully compute rendezvous transfers for 93 of the 100. Second, we search the entire database of minimoons and attempt continuations to those minimoons with characteristics similar to the characteristics of those 93 minimoons for which low delta-v transfers were found. This provides transfers to over 1,000 minimoons. Finally, the general problem is solved for the original 93 minimoon transfers using the computed solutions to the restricted problems as initial guesses.

Analysis of the computed rendezvous missions is given, and we extract some properties of the rendezvous points and of the minimoons which may characterize low delta-v transfers.

New mission scenario In order to assess the delta-v requirements necessary for a minimoon rendezvous mission, fuel-minimal rendezvous transfers are computed for a chemical propulsion spacecraft with maximum thrust $T_{max} = 22$ Newtons, specific impulse $I_{sp} = 230$ seconds, and initial mass $m_0 = 350$ kilograms (summarized in Table 5.1). Indeed, the electric-propulsion time-minimal transfers computed in Chapter 4 had very low transfer times, but their corresponding delta-v requirements were too high (over 2,000 m/s). The spacecraft starts on a Halo orbit, with period 14.8 days and z-excursion of 5,000 kilometers, around the Earth-Moon L_2 point – which we denote by $\mathcal{O}_H$. Figure 2.4 shows that a majority of the minimoons come within 1 LD of L_2, and moreover, the Artemis mission [55] among others has demonstrated that such an orbit can be maintained for very

T_{max} (N)	I_{sp} (s)	m_0 (kg)
22	230	350

Table 5.1: Spacecraft parameter values.

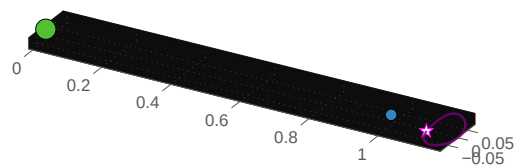

Figure 5.1: Halo orbit around L_2 in the rotating frame. The Earth (left) and Moon (right) are shown for reference.

low delta-v. Figure 5.1 depicts $\mathcal{O}_H$ in the rotating frame, with the Earth and Moon plotted for reference. The influence of the Sun is added to perturb the CR3BP, which gives the *circular restricted four-body problem* (CR4BP). The mass variation of the spacecraft is also included. Although we no longer seek to minimize time, we are still constrained by the capture time of the minimoons. Therefore, we verify that the computed transfers take place entirely while their associated minimoons are in capture, meaning our optimization problem has a dual cost: the minimization of fuel while simultaneously keeping the transfer time low.

5.1 Circular restricted four-body problem

We briefly present the new drift dynamics – the circular restricted four-body problem – which are a perturbation of the CR3BP [4, 56, 57, 58]. We begin with the same assumptions as in the CR3BP (4.1) and then assume that a fourth body – the Sun – with mass μ_s (in normalized CR3BP units) influences the motion of the spacecraft but not the Earth and Moon. The Sun is assumed to move uniformly on a circular orbit around the origin with angular momentum ω_s, so that at time t its normalized position is $(r_s \cos(\theta(t)), r_s \sin(\theta(t)))$, where r_s is a constant representing the radial distance from the origin and $\theta(t)$ is the true anomaly of the Sun at time t with respect to the x-axis

μ_s	ω_s	r_s
329012.512	-0.925	389.17

Table 5.2: Sun parameter values, normalized units.

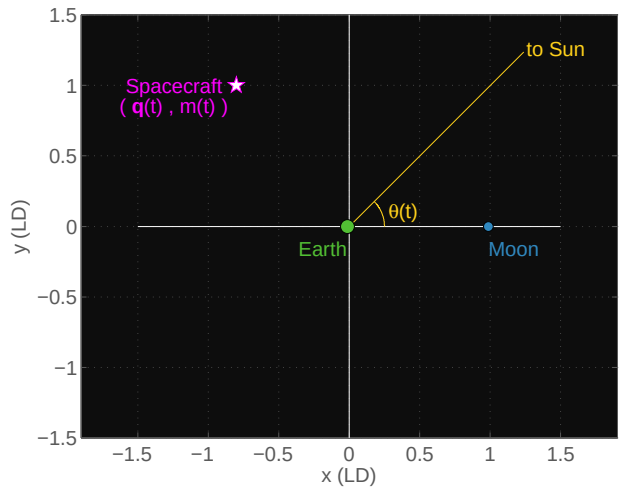

Figure 5.2: The circular restricted four-body problem

of the CR3BP. The specific parameter values for the Earth, Moon, Sun system are given in Table 5.2. An illustration of the model is given in Figure 5.2.

Under these assumptions the uncontrolled equations of motion from the CR3BP are augmented to give the equations of motion for the CR4BP:

$$\begin{cases} \ddot{x} = 2\dot{y} - \frac{\partial V_4}{\partial x} \\ \ddot{y} = -2\dot{x} - \frac{\partial V_4}{\partial y} \\ \ddot{z} = -\frac{\partial V_4}{\partial z} \end{cases} \tag{5.1}$$

where the potential energy $V_4 = V + V_s$ is the CR3BP potential energy function V plus the additional terms V_s from the Sun's influence:

$$-V_s = \frac{\mu_s}{\rho_s} - \frac{\mu_s}{r_s^2}\left(x\cos\theta + y\sin\theta\right) \tag{5.2}$$

and

$$\rho_s = \sqrt{(x - r_s \cos\theta)^2 + (y - r_s \sin\theta)^2 + z^2}$$

is the distance from the spacecraft to the Sun. Recall that the Earth and Moon are fixed points at $(-\mu, 0, 0)$ and $(1-\mu, 0, 0)$ respectively; however, the system is nonautonomous since the Sun's position changes with time according to

$$\theta(t) = \theta_0 + \omega_s t, \tag{5.3}$$

where θ_0 represents the initial Sun's true anomaly. Note that the system can be rewritten autonomously by considering $\theta(t)$ as a state variable which evolves according to $\dot{\theta} = \omega_s$.

The new system has no equilibrium points and no first integrals of motion. We assume the spacecraft starts on a Halo orbit around L_2 despite the fact that it is a periodic solution of the circular restricted *three* body problem, not four. Indeed Halo orbits have been utilized in actual missions including the Artemis mission [55], and since our computations have the spacecraft immediately departing from the Halo orbit, this is a reasonable approximation.

The *controlled* CR4BP is formulated by adding control terms $\mathbf{u} = (u_1, u_2, u_3)^{\mathrm{T}}$, $\|\mathbf{u}\| \leq 1$, to the x, y, and z accelerations, giving

$$\begin{cases} \ddot{x} = 2\dot{y} - \frac{\partial V_4}{\partial x} + \frac{T_{max}}{m} u_1 \\ \ddot{y} = -2\dot{x} - \frac{\partial V_4}{\partial y} + \frac{T_{max}}{m} u_2 \\ \ddot{z} = -\frac{\partial V_4}{\partial z} + \frac{T_{max}}{m} u_3 \\ \dot{m} = -\beta T_{max} \|\mathbf{u}\| \end{cases} \tag{5.4}$$

where as before T_{max} is the constant representing the maximum thrust of the spacecraft. The mass depletion is now included in the model, so that $m(t)$ decreases as the thrusters are fired according to the last equation of (5.4). The constant $\beta = (g_0 I_{sp})^{-1}$ is related to the Earth's gravity at sea level $g_0 \approx 9.81$ m/s^2 and the spacecraft's specific impulse I_{sp} which measures how quickly a spacecraft expends fuel.

The mathematical formulation of our problem is to compute solutions of the system (5.4) which minimize the expended fuel, which is equivalent to minimizing the *delta-v*. Delta-v, denoted Δv, is a standard measure of the acceleration generated by the spacecraft in order to perform maneuvers,

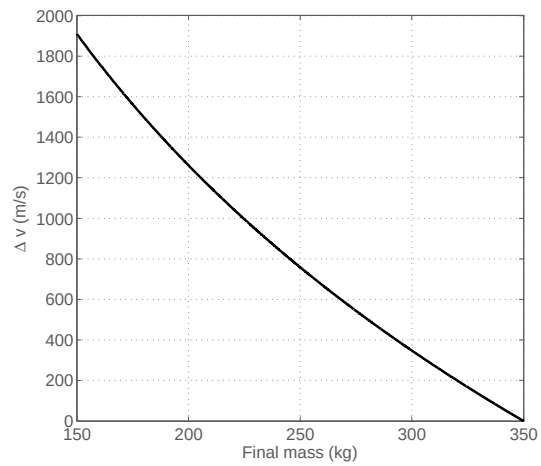

Figure 5.3: Delta-v versus final mass

and is defined as

$$\Delta v := \int_0^{t_f} \frac{T_{max}\|\mathbf{u}(t)\|}{m(t)} dt = -\frac{1}{\beta}\int_0^{t_f} \frac{\dot{m}(t)}{m(t)} dt = -\frac{1}{\beta}\left(\ln(m(t_f)) - \ln(m(0))\right) \tag{5.5}$$

The Δv budgets for actual space missions can vary greatly depending on the specific mission objectives. For our purposes, we consider Δv values less than 1,000 m/s as good, and below 500 m/s as great. From Equation (5.5) it's obvious that minimizing Δv is also equivalent to maximizing the final mass $m(t_f)$. As a convention, we will say "fuel-minimization" and "Δv-minimization" interchangeably. Figure 5.3 shows the relationship between $m(t_f)$ and Δv for the specific parameter values we use.

The relationship between Δv and $m(t)$ allows our cost functional to be stated as:

$$\min_{\mathbf{u}\in\mathcal{U}} \int_0^{t_f} \|\mathbf{u}(t)\| dt \tag{5.6}$$

where the control domain $\mathbb{U} = B_{\mathbb{R}^3}(0,1)$ is the unit ball in $\mathbb{R}^3$ and the set of admissible functions is $\mathcal{U} = \{\mathbf{u} : \mathbb{R} \to B_{\mathbb{R}^3}(0,1);\ \mathbf{u} \text{ measurable }\}$. The initial time is assumed to be $t_0 = 0$, and the transfer time t_f is free for the general problem, though is later considered fixed.

5.2 Problem statements and the maximum principle

We present the general fuel-minimization problem and the corresponding application of the maximum principle. In order to overcome the difficulties inherent in initializing the indirect algorithms, we also present a restricted version of the problem which is computationally less sensitive to the initialization, and is a vital step toward computing solutions to the general problem.

5.2.1 General problem

Let the control variables be given by $\mathbf{u} = (u_1, u_2, u_3)^{\mathrm{T}}$ and the state variables by $\mathbf{X} = (x, y, z, \dot{x}, \dot{y}, \dot{z}, m)^{\mathrm{T}}$. It will sometimes be convenient to refer to the position $\mathbf{s} = (x, y, z)^{\mathrm{T}}$ and velocity $\mathbf{v} = (\dot{x}, \dot{y}, \dot{z})^{\mathrm{T}}$ separately, or concatenated as $\mathbf{q} = (x, y, z, \dot{x}, \dot{y}, \dot{z})^{\mathrm{T}}$. With this notation the equations of motion can be written as the first order control system:

$$\dot{\mathbf{X}} = \mathbf{F}_0(\mathbf{X}) + \frac{T_{max}}{m} \sum_{i=1}^{3} u_i \mathbf{F}_i - T_{max}\beta \|\mathbf{u}\| \mathbf{F}_4 \tag{5.7}$$

where

$$\mathbf{F}_0(\mathbf{X}) = \begin{pmatrix} \dot{x} \\ \dot{y} \\ \dot{z} \\ 2\dot{y} + x - (1-\mu)\frac{x+\mu}{\rho_1^3} - \mu\frac{x-1+\mu}{\rho_2^3} & -\mu_s \frac{x - r_s\cos\theta}{\rho_s^3} - \frac{\mu_s}{r_s^2}\cos\theta \\ -2\dot{x} + y - (1-\mu)\frac{y}{\rho_1^3} - \mu\frac{y}{\rho_2^3} & -\mu_s \frac{y - r_s\sin\theta}{\rho_s^3} - \frac{\mu_s}{r_s^2}\sin\theta \\ -(1-\mu)\frac{z}{\rho_1^3} - \mu\frac{z}{\rho_2^3} & -\mu_s \frac{z}{\rho_s^3} \\ 0 & \end{pmatrix}$$

$$\mathbf{F}_1 = \begin{pmatrix} 0,0,0,1,0,0,0 \end{pmatrix}^{\mathrm{T}}, \quad \mathbf{F}_2 = \begin{pmatrix} 0,0,0,0,1,0,0 \end{pmatrix}^{\mathrm{T}}$$

$$\mathbf{F}_3 = \begin{pmatrix} 0,0,0,0,0,1,0 \end{pmatrix}^{\mathrm{T}}, \quad \mathbf{F}_4 = \begin{pmatrix} 0,0,0,0,0,0,1 \end{pmatrix}^{\mathrm{T}}$$

Let $\mathbf{q}_{rdvz}$ be the position and velocity of a point along a chosen minimoon's orbit, and let θ_{rdvz} be the corresponding true anomaly of the Sun when the minimoon is at $\mathbf{q}_{rdvz}$. Computing Δv-minimal

transfer from $\mathcal{O}_H$ to $\mathbf{q}_{rdvz}$ amounts to solving the optimal control problem

$$\begin{cases} \dot{\mathbf{X}} = \mathbf{F}_0(\mathbf{X}) + \frac{T_{max}}{m}\sum_{i=1}^{3} u_i \mathbf{F}_i - T_{max}\beta\|\mathbf{u}\|\mathbf{F}_4 \\ \min_{\mathbf{u}\in\mathcal{U}} \int_0^{t_f} \|\mathbf{u}(t)\| dt \\ \mathbf{q}(0) \in \mathcal{O}_H, \quad m(0) = m_0 \\ \mathbf{q}(t_f) = \mathbf{q}_{rdvz}, \quad \theta(t_f) = \theta_{rdvz} \end{cases} \tag{5.8}$$

Note the difference in expressing the initial and final position and velocity constraints: the minimoon data is discretized and cannot be expressed as a manifold, hence a specific rendezvous location is chosen, namely $\mathbf{q}(t_f) = \mathbf{q}_{rdvz}$. On the other hand, the Halo orbit $\mathcal{O}_H$ is a continuous curve and so the depature point can be any point along that curve, i.e. $\mathbf{q}(0) \in \mathcal{O}_H$.

Applying the Pontryagin maximum principle to (5.8), we have the existence of a non-positive constant p_0 and an absolutely continuous function $\mathbf{P} : [t_0, t_f] \to \mathbb{R}^8$, with $(p_0, \mathbf{P}) \neq (0, \mathbf{0})$, which is a solution of th pseudo-Hamiltonian equations (5.9). We denote the so-called costate variables by $\mathbf{P} = (p_x, p_y, p_z, p_{\dot{x}}, p_{\dot{y}}, p_{\dot{z}}, p_m, p_\theta)^{\mathrm{T}}$, the components of $\mathbf{P}$ which correspond to the state variables of $\mathbf{X}$. We assume we are in the so-called normal case with $p_0 \neq 0$ so we can normalize $p_0 = -1$. We know that every solution $\mathbf{X}(t)$ to (5.8) is necessarily a projection of an extremal curve $(\mathbf{X}(t), \mathbf{P}(t))$ solution of the system

$$\dot{\mathbf{X}} = \frac{\partial H}{\partial \mathbf{P}}, \quad \dot{\mathbf{P}} = -\frac{\partial H}{\partial \mathbf{X}} \tag{5.9}$$

where the pseudo-Hamiltonian function H is defined as

$$H(\mathbf{P}, \mathbf{X}, \mathbf{u}) = -\|\mathbf{u}\| + H_0(\mathbf{P}, \mathbf{X}) + T_{max}\left(\frac{1}{m}\sum_{i=1}^{3} u_i H_i(\mathbf{P}, \mathbf{X}) - \beta\|\mathbf{u}\| H_4(\mathbf{P}, \mathbf{X})\right)$$

with $H_i(\mathbf{P}, \mathbf{X}) = \langle \mathbf{P}, \mathbf{F}_i(\mathbf{X})\rangle, i = 0, ..., 4$. Note in particular that $H_4(\mathbf{P}, \mathbf{X}) = p_m$, and also that

$$\sum_{i=1}^{3} u_i H_i(\mathbf{P}, \mathbf{X}) = \langle \mathbf{u}, \mathbf{p}_v \rangle$$

where $\mathbf{p}_v = (p_{\dot{x}}, p_{\dot{y}}, p_{\dot{z}})^{\mathrm{T}}$. The term $\langle \mathbf{u}, \mathbf{p}_v \rangle$ is the only part of H which depends on the direction of $\mathbf{u}$, and so by the maximization condition and from the Cauchy-Schwarz inequality we can determine that

$$\mathbf{u} = \alpha \frac{\mathbf{p}_v}{\|\mathbf{p}_v\|} \tag{5.10}$$

where α now denotes the yet to be determined magnitude of the control. Substituting and rewriting, we have the so called *real Hamiltonian* H_r where

$$H_r(\mathbf{P}, \mathbf{X}, \mathbf{u}) = H_0(\mathbf{P}, \mathbf{X}) + \alpha \left(-1 + T_{max} \left(\frac{\|\mathbf{p}_v\|}{m} - \beta p_m \right) \right).$$

Letting $\Phi = -1 + T_{max} \left(\frac{\|\mathbf{p}_v\|}{m} - \beta p_m \right)$ denote the so-called *switching function*, the maximization condition further implies that

$$\alpha(t) = \begin{cases} 1, & \Phi(t) > 0 \\ 0, & \Phi(t) < 0 \\ \in [0,1] & \Phi(t) = 0 \end{cases}$$

The case when $\Phi(t) \neq 0$ corresponds to a so-called *bang* arc where the control norm is either maximized or minimized. Isolated times where $\Phi(t) = 0$ are the so-called *switching times* where the control switches between bang arcs. When $\Phi(t) \equiv 0$ on a non-trivial time interval $t \in (t_1, t_2)$ we have a so-called *singular arc*, where more work must be done to determine the norm of the control. It is not in the scope of this work to analyze the singular arcs since we are focused primarily on the application. Moreover, in the next section restrictions will be made on the control structure which eliminate the possibility of singular arcs.

The transversality conditions of the maximum principle also give constraints on some components of the costate vector at the initial time and final times. Since $m(t_f)$ is free, the maximum principle implies

$$p_m(t_f) = 0. \tag{5.11}$$

Inspection of $\dot{p}_m = -\frac{\partial H_r}{\partial m}$ shows that $\dot{p}_m \geq 0$ for all $t \in [0, t_f]$. So since $p_m(t_f) = 0$ we know $p_m(t) \leq 0$ for all $t \in [0, t_f]$.

Since the departure point from $\mathcal{O}_H$ is free, we also get that

$$\mathbf{p_q}(0) \perp T_{\mathbf{q}(0)}\mathcal{O}_H \tag{5.12}$$

where $\mathbf{p_q}$ are the components of $\mathbf{P}$ corresponding to the $\mathbf{q}$ components of $\mathbf{X}$.

Furthermore, as in [24], if the final time is free, the maximum principle implies that the real

Hamiltonian is identically zero on $[0, t_f]$, so we also have the constraint

$$H_r(\mathbf{P}(t_f), \mathbf{X}(t_f)) = 0. \tag{5.13}$$

Denoting the pair $\mathbf{Z} = (\mathbf{X}, \mathbf{P})^{\mathrm{T}}$, the computation of solutions to (5.8) can be carried out by solving the shooting equation associated with the function

$$S : \mathbb{R}^{15} \to \mathbb{R}^9$$

$$(t_f, \mathbf{Z}(0)) \to \begin{pmatrix} \mathbf{q}(t_f) - \mathbf{q}_{rdvz} \\ p_m(t_f) \\ \mathbf{p_q}(0) \perp T_{\mathbf{q}(0)}\mathcal{O}_H \\ H_r(\mathbf{P}(t_f), \mathbf{X}(t_f)) \end{pmatrix} \tag{5.14}$$

Although $m(0) = m_0$ and $\theta(t_f) = \theta_{rdvz}$ are also boundary conditions, they can always be satisfied by construction and therefore are omitted from the shooting function. Note, equation (5.3) is equivalently rewritten $\theta(t) = \theta_{rdvz} + \omega_s(t - t_f)$.

A Newton-like algorithm, provided by the software Hampath [35], attempts to compute a zero of the shooting function. If successful, the corresponding triple $(t_f, \mathbf{X}(t), \mathbf{P}(t))$ is an extremal and a candidate local minima. Second order optimality conditions are checked, also thanks to Hampath, which can verify the local optimality. The difficulty of course is providing the solver with a good enough initial guess so that the algorithm converges.

5.2.2 Restricted problem

We want to solve optimal control problems of the form (5.8) for a large variety of $(\mathbf{q}_{rdvz}, \theta_{rdvz})$ from multiple points along over 16,000 minimoons, so there is a major need for computational efficiency. As a first approach we instead compute solutions to a restricted version of the problem $(\star)$. The main restriction we make is to reduce the set of admissible controls $\mathcal{U}$ by fixing the control structure. Additionally, to reduce the number of constraints in the shooting function we do not verify the transversality conditions associated with the transfer time $(H_r(\mathbf{P}(t_f), \mathbf{X}(t_f)) = 0)$ or with the departure point on from the Halo orbit $(\mathbf{p_q} \perp T_{\mathbf{q}(0)}\mathcal{O}_H)$. Some explanation and justification for each choice is given below, followed by the statement of the restricted problem.

We fix the control structure by assuming that the spacecraft performs three or less maximum-

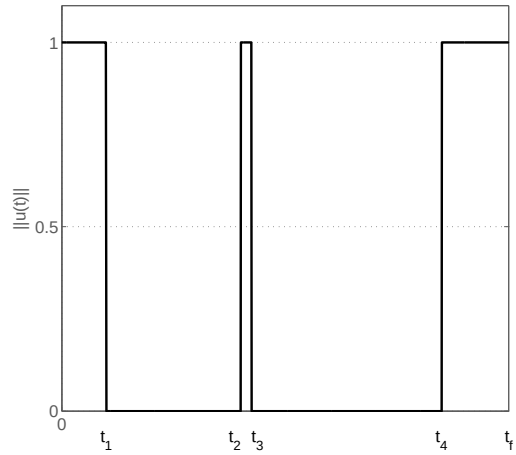

Figure 5.4: Fixed control structure

thrust boosts, so that the restricted control norm $\bar{\alpha}(t)$ is given by

$$\bar{\alpha}(t) = \begin{cases} 1, & t \in [0, t_1] \cup [t_2, t_3] \cup [t_4, t_f] \\ 0, & \text{else} \end{cases}$$

with $0 \leq t_1 \leq t_2 \leq t_3 \leq t_4 \leq t_f$. The times t_i, $i = 1, \ldots, 4$ are now called the *switching times*, and we will omit writing "$i = 1, \ldots, 4$" whenever it is understood. The possible equalities allow for only one or two boosts instead of three. This choice is motivated by the physical application since utilizing less maneuvers is less risky in terms of the success of the mission. There is also some intuitive theoretical motivation: the first boost allows us to depart the initial orbit onto the orbit's unstable invariant manifold, the second boost puts us on course for rendezvous, and the third boost is used at arrival to actually achieve rendezvous. Moreover, tests showed that adding more boosts increases the computation time significantly without lowering the resulting delta-v values very much. Figure 5.4 illustrates an example of the control norm for the fixed control structure.

In [30], the authors overcome the general fuel-minimal initialization for a specific mission scenario using a homotopic method which related the problem of minimizing the L^1-norm ($\min \int_0^{t_f} \|\mathbf{u}\| dt$) to the problem of minimizing the L^2-norm ($\min \int_0^{t_f} \|\mathbf{u}\|^2 dt$), rather than fixing the structure of the control. We explored this approach applied to the minimoon rendezvous scenario, however determined it was too computationally demanding and therefore ill-suited for the large scale analysis we are aiming to conduct. It's worth mentioning however that the few solutions we did compute

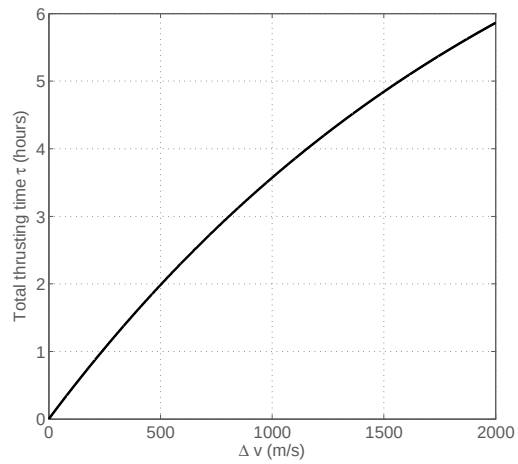

Figure 5.5: Δv (m/s) vs. total thrusting time τ (hours)

using this method consisted of either two or three boosts, which further supports the choice of restriction we make here.

Additionally, we now consider the transfer time t_f to be fixed and therefore do not verify the transversality condition $H_r(\mathbf{X}(t_f), \mathbf{P}(t_f))$, and therefore the transfer times for computed transfers are not necessarily optimal. Similarly, the departure point from $\mathcal{O}_H$ is now considered fixed, and denoted $\mathbf{q}_{dprt}$. We do not verify the transversality condition $\mathbf{p_q}(0) \perp T_{\mathbf{q}(0)}\mathcal{O}_H$, so the $\mathcal{O}_H$ departure point $\mathbf{q}_{dprt}$ for computed transfers is not necessarily optimal.

We remark that with the fixed control structure, Δv can be calculated from the switching times t_i and final time t_f. Recall $\Delta v = \int_0^{t_f} \frac{T_{max}\|\mathbf{u}(t)\|}{m(t)} dt$. Since $\|\mathbf{u}\|$ is now assumed to always be either 0 or 1, let τ be the total thrusting time (i.e. $\tau = t_1 + (t_3 - t_2) + (t_f - t_4)$), then

$$\Delta v = \int_0^{\tau} \frac{T_{max}}{m(t)} dt = -\frac{1}{\beta} \int_0^{\tau} \frac{\dot{m}(t)}{m(t)} dt = -\frac{1}{\beta} \left(\ln(m(\tau)) - \ln(m_0) \right).$$

Solving for τ, we get $\tau = \frac{m_0}{\beta T_{max}} \left(1 - \exp(-\beta \Delta v)\right)$. Therefore, for a fixed Δv value, we know exactly the total thrusting time τ. The relationship between Δv and τ is graphed in Figure 5.5 for the specific parameter values we use.

Note that these three restrictions only serve to make the restricted problem a special case of the general problem, and therefore solutions to the general problem will perform *at least* as well as solutions to the restricted problem. That is, the delta-v values we compute for the restricted

problem are upperbounds for those of the general problem.

Let $\overline{\mathcal{U}} = \{\mathbf{u} : \mathbb{R} \to B_{\mathbb{R}^3}(0,1) : \mathbf{u} \text{ measurable}, \|\mathbf{u}(t)\| = \bar{\alpha}(t) \text{ for a sequence of times } 0 \leq t_1 \leq t_2 \leq t_3 \leq t_4 \leq t_f\}$. Then the restricted optimal control problem is written

$$(\star) \begin{cases} \dot{\mathbf{X}} = \mathbf{F}_0(\mathbf{X}) + \frac{T_{max}}{m} \sum_{i=1}^{3} u_i \mathbf{F}_i - T_{max}\beta\|\mathbf{u}\|\mathbf{F}_4 \\ \min_{\mathbf{u}\in\overline{\mathcal{U}}} \int_0^{t_f} \|\mathbf{u}(t)\| dt \\ \mathbf{q}(0) = \mathbf{q}_{dprt}, \quad m(0) = m_0 \\ \mathbf{q}(t_f) = \mathbf{q}_{rdvz}, \quad \theta(t_f) = \theta_{rdvz} \end{cases} \tag{$\star$}$$

We will attempt to solve $(\star)$ for a variety of transfer times, departure points, and rendezvous points. As such, the parameters that define a specific instance of the problem $(\star)$ are t_f, $\mathbf{q}_{dprt}$, $\mathbf{q}_{rdvz}$ and θ_{rdvz} (m_0 is always assumed to be 350). For convenience we will refer to a tuple $D = (t_f, \mathbf{q}_{dprt}, \mathbf{q}_{rdvz}, \theta_{rdvz})$ as the *problem data* and the associated instance of the optimal control problem as $(\star)_D$.

The derivation and expression of the real Hamiltonian from the maximum principle is the same as in the general case, except that the control norm is now fixed, yielding:

$$\mathbf{u} = \bar{\alpha}\frac{\mathbf{p_v}}{\|\mathbf{p_v}\|}. \tag{5.15}$$

The mass variation is then given by

$$\dot{m} = -\beta T_{max}\bar{\alpha}. \tag{5.16}$$

That is, the mass is only depleting when the engines are firing ($\bar{\alpha} = 1$).

Substituting (5.15) into H yields the expression of the real Hamiltonian H_r:

$$H_r(\mathbf{P}, \mathbf{X}) = H_0(\mathbf{P}, \mathbf{X}) + \bar{\alpha}\left(-1 + T_{max}\left(\frac{\|\mathbf{p}_v\|}{m} - \beta p_m\right)\right).$$

and we have the flow of the real Hamiltonian:

$$\dot{\mathbf{X}}(t) = \frac{\partial H_r}{\partial \mathbf{P}}, \quad \dot{\mathbf{P}} = -\frac{\partial H_r}{\partial \mathbf{X}} \tag{5.17}$$

By continuity of the Hamiltonian, we must have that the so-called *switching conditions* $\Phi(t_i) = 0$ must hold at each switching time, as is shown in [59].

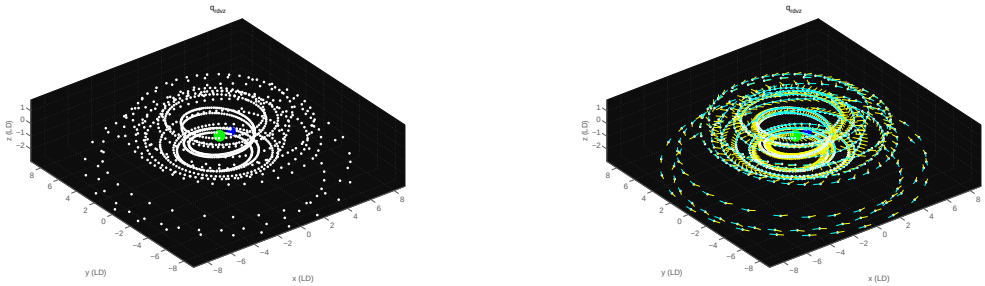

Figure 5.6: Rendezvous points (in white) for minimoon #1. The right plot also shows vectors indicating the direction of the velocity (cyan) and direction of the Sun (yellow) for each rendezvous point.

Again denoting the pair $\mathbf{Z} = (\mathbf{X}, \mathbf{P})^{\mathrm{T}}$, the computation of solutions to $(\star)$ can be carried out by solving the shooting equation associated with the function

$$S : \mathbb{R}^{11} \to \mathbb{R}^{11}$$

$$(t_i, \mathbf{P}(0)) \to \begin{pmatrix} \mathbf{q}(t_f) - \mathbf{q}_{rdvz} \\ p_m(t_f) \\ \Phi(t_i) \end{pmatrix} \tag{5.18}$$

As before, the software Hampath [35] attempts to compute a zero of the shooting function. If successful, the corresponding tuple $(t_f, t_i, \mathbf{X}(t), \mathbf{P}(t))$ is an extremal and a candidate local minima for $(\star)$. We now address the major difficulty of algorithm initialization.

5.3 Cloud construction

The problem $(\star)_D$, for $D = (t_f, \mathbf{q}_{dprt}, \mathbf{q}_{rdvz}, \theta_{rdvz})$, asks: what is the fuel-optimal way to get from $\mathbf{q}_{dprt}$ to $\mathbf{q}_{rdvz}$ in exactly t_f units of time, and so that the Sun's true anomaly at arrival is θ_{rdvz}? We seek to answer this question for thousands of choices of $(\mathbf{q}_{rdvz}, \theta_{rdvz})$ on minimoon orbits, and a variety of choices for $\mathbf{q}_{dprt}$ and t_f. Figures 5.6 and 5.7 give depictions of $(\mathbf{q}_{rdvz}, \theta_{rdvz})$. Solving $(\star)_D$ for any choice of problem data D amounts to properly initializing the (very sensitive) shooting algorithm. The so-called *cloud* we construct here provides an intuitive and effective way to initialize the shooting algorithm so that it converges to a solution for a large variety of problem data D.

Let t_f be a fixed transfer time and let $\mathbf{q}_{dprt}$ be a departure position and velocity on the halo

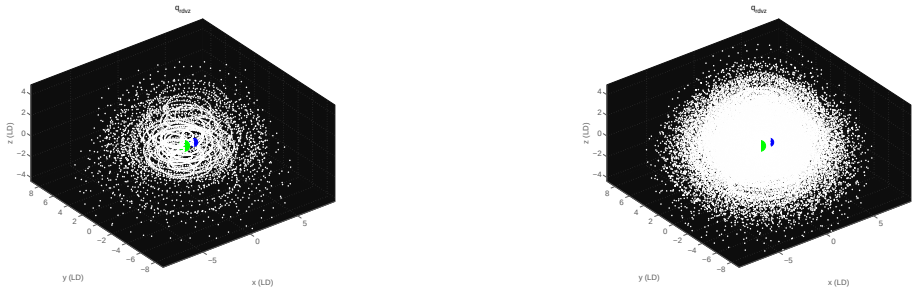

Figure 5.7: Rendezvous points (in white) for minimoons #1-10 (left) and minimoons #1-100 (right). These are still only a small portion of all the rendezvous points $\mathbf{q}_{rdvz}$ we consider for the 16,923 minimoons.

orbit. If $\mathbf{q}_{rdvz}$ represents a point along a minimoon's orbit with associated Sun true anomaly θ_{rdvz}, then we will call $\mathbf{q}_{rdvz}$ a *rendezvous point*, and call an extremal for problem $(\star)_D$, with $D = (t_f, \mathbf{q}_{dprt}, \mathbf{q}_{rdvz}, \theta_{rdvz})$, a *rendezvous extremal*.

If $(t_f, t_i, \mathbf{X}(0), \mathbf{P}(0))$ is an extremal for a problem $(\star)_D$ with $D = (t_f, \mathbf{q}_{dprt}, \mathbf{q}_1, \theta_1)$, but $\mathbf{q}_1$ is *not* on a minimoon orbit, we will call $\mathbf{q}_1$ a *cloud point* and $(t_f, t_i, \mathbf{X}(0), \mathbf{P}(0))$ a *cloud extremal*. These are locally optimal trajectories that go *somewhere* in space, not necessarily to a minimoon. The idea is to compute rendezvous extremals by performing a continuation method from a nearby cloud extremal. We describe next how we can construct cloud extremals. We will refer to the collection of constructed cloud extremals as, simply, the *cloud*. With enough cloud extremals, we expect (and will show that indeed) rendezvous points will be very near cloud points, ensuring that the continuation method will have a high success rate. Thus, the first task is to construct a large pool of cloud extremals.

The construction of a cloud extremal relies on the fact that a random choice of $(t_i, \mathbf{P}(0))$ and of $(t_f, \mathbf{q}(0), \theta(0))$ completely determines a trajectory $(\mathbf{X}(t), \mathbf{P}(t))$, thanks to (5.17). In particular, $\mathbf{q}(t_f)$ and $\theta(t_f)$ are determined. Note that $(\mathbf{X}(t), \mathbf{P}(t))$ is a trajectory from $\mathbf{q}(0)$ to $\mathbf{q}(t_f)$, but it is not necessarily optimal since the transversality condition $p_m(t_f) = 0$ and switching conditions $\Phi(t_i) = 0$ are not neccessarily satisfied. In other words $(t_f, t_i, \mathbf{X}(t), \mathbf{P}(t))$ is not necessarily an extremal of problem $(\star)_D$, $D = (t_f, \mathbf{q}(0), \mathbf{q}(t_f), \theta(t_f))$. By attempting to solve the shooting function $S_D(\cdot) = \mathbf{0}$ for $D = (t_f, \mathbf{q}_{dprt}, \mathbf{q}(t_f), \theta(t_f))$ with initial guess $(t_i, \mathbf{P}(0))$, the first six components of $S_D(\cdot)$ are by construction zero, allowing the algorithm to converge more easily.

The flow charts in Figures 5.8 and 5.9 summarize our process. Random, sub-optimal trajectories

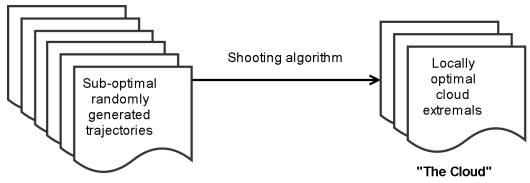

Figure 5.8: Constructing cloud extremals from random sub-optimal trajectories

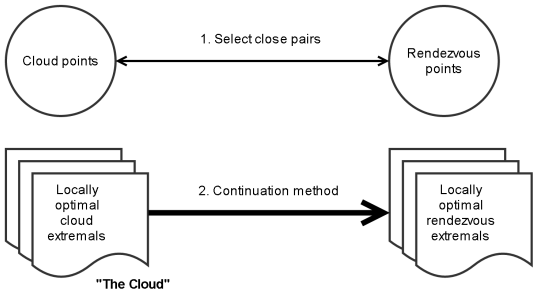

Figure 5.9: Performing continuations from cloud extremals to compute rendezvous extremals

are generated and the shooting method is applied to find optimal trajectories – those that converge are the cloud extremals. The cloud points corresponding to those cloud extremals are compared to the rendezvous points, and pairs which are close to each other are chosen. For each chosen pair, a continuation method is attempted from the cloud point to the rendezvous point. If successful, we've found a rendezvous extremal.

Without any *a priori* knowledge of solutions, we can construct a large database of cloud extremals. The process is summarized:

(i) Choose values for $(t_f, t_i, \mathbf{q}_{dprt}, \theta_0, \mathbf{P}(0))$.

(ii) Integrate according to (5.17) to determine $\mathbf{q}(t_f)$ and $\theta(t_f)$.

(iii) Define the problem $(\star)_D$ with problem data $D = (t_f, \mathbf{q}_{dprt}, \mathbf{q}(t_f), \theta(t_f))$

(iv) Attempt to solve the shooting function (5.18) associated with $(\star)_D$ using the chosen values of $(t_i, \mathbf{P}(0))$ as the initial guess.

(v) If successful, we have computed a *cloud extremal*, which is added as an element to the cloud.

Notice in step (iv) that the first six components of the shooting function S are initially zero by

construction. Intuitively then, it should be easier for the algorithm to converge since it is in some sense already close to a solution.

By repeating this process for varying choices of $(t_f, t_i, \mathbf{q}_{dprt}, \theta_0, \mathbf{P}(0))$, we populate the desired large database of extremals. Although it is unlikely that any of these extremals achieve rendezvous with any of the minimoons, by developing a dense enough cloud we expect that at least some of the extremals end near some of the minimoon orbits, and that from there continuation techniques will prove successful.

5.3.1 Example

(i) Choose $t_f = 20$ days ($\frac{480}{24}$ hours) and $\{t_i\} = \left\{\frac{1}{24}, \frac{240}{24}, \frac{241}{24}, \frac{479}{24}\right\}$ days, so that all three boosts are one hour, and the second boost occurs 10 days after the mission start. Choose $\mathbf{q}_{dprt} = (1.12,\ 0,\ 0.01,\ 0,\ 0.18,\ 0)^{\mathrm{T}}$, the point of positive z-excusion on $\mathcal{O}_H$. Choose $\theta_0 = \pi/2$. Choose random values for $\mathbf{P}(0) = (5.85,\ -2.24,\ -7.51,\ -2.55,\ 5.06,\ -6.99, -0.0089)^{\mathrm{T}} \times 10^{-3}$ (choices discussed more below).

(ii) Integrate $(\mathbf{q}_{dprt}, 350, \mathbf{P}(0))^{\mathrm{T}}$ according to (5.17) with the selected final and switching times and initial Sun true anomaly. This gives

$$\mathbf{q}(t_f) = (-2.25,\ -2.45,\ 0.29,\ -2.71,\ 1.78,\ 0.42)^{\mathrm{T}},$$

$$m(t_f) = 244.7, \quad \theta(t_f) = -2.69 = (\theta_0 + \omega_s t_f)$$

A two-dimensional projection of the complete trajectory is shown as the solid blue path in Figure 5.10, with $\mathbf{q}_{dprt}$ marked as a triangle and $\mathbf{q}(t_f)$ marked as a square. The second boost after 10 days at $\mathbf{q}(t_2)$ is marked as a circle. By construction, all three boosts are one hour, so the total thrusting time $\tau = 3$ hours which corresponds to $\Delta v = 807.6$ m/s.

(iii) Use the choices for t_f and $\mathbf{q}_{dprt}$ with the integrated values for $\mathbf{q}(t_f)$ and $\theta(t_f)$ to define the problem data $D = (t_f, \mathbf{q}_{dprt}, \mathbf{q}(t_f), \theta(t_f))$ and corresponding optimal control problem $(\star)_D$.

(iv) Attempt to solve $(\star)_D$ using $(t_i, \mathbf{P}(0))$ as the initial guess for the shooting method. Again, note that by construction now the first six component of $S(t_i, \mathbf{P}(0))$ are zero, and so our initial guess is in some sense close to a solution. The algorithm iteratively adjusts the values of $(t_i, \mathbf{P}(0))$ to satisfy the transversality and switching conditions. For this example, the algorithm

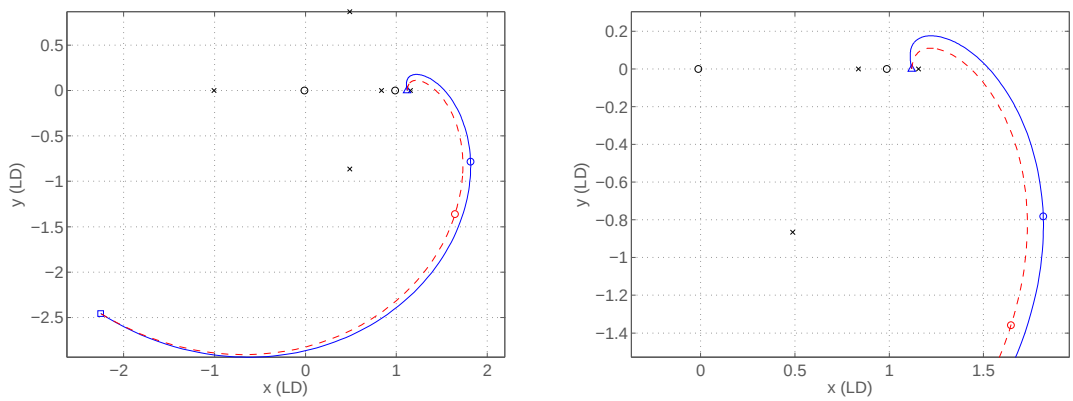

Figure 5.10: Example of cloud extremal construction. In blue, our constructed trajectory. In red, the resulting cloud extremal.

converges to a solution, though convergence is in general not guaranteed. Our initial choices for the switching times t_i and costate variables $\mathbf{P}(0)$ are compared to the the solution values $(t_i^*, \mathbf{P}(0)^*)$ in Tables 5.3 and 5.4 respectively.

(v) The computed solution $(t_f^*, t_i^*, \mathbf{X}^*(t), \mathbf{P}^*(t))$ is an extremal to $(\star)_D$. We call extremals $(t_f^*, t_i^*, \mathbf{X}^*(t), \mathbf{P}^*(t))$ created in this fashion *cloud extremals*, which are added to a database of known extremals which we call the *cloud*. A two-dimensional projection of the cloud extremal trajectory is shown as the dashed red path in Figure 5.10, along with the initial guess trajectory in solid blue. The Earth (left) and Moon (right) are shown as black circles, and the CR3BP equilibrium points L_i are plotted for reference as x's. Note that both transfers take the same amount of time: $t_f = 20$ days. Also notice that the two trajectories depart from and arrive at the same locations, but otherwise are different. The cloud extremal has a total thrusting time of $\tau^* = 2.58$ hours and $\Delta v = 674.8$ m/s. We reiterate that $\mathbf{q}(t_f)$ is probably not on a minimoon orbit, but hope that some minimoon orbits come near $\mathbf{q}(t_f)$ so that a continuation method may succeed in computing a rendezvous transfer.

5.3.2 Populating the cloud

We repeat the above process 1,000,000 times, generating random initial values according to the following:

t_1	t_2	t_3	t_4
1.00	240.00	241.00	479.00
t_1^*	t_2^*	t_3^*	t_4^*
0.42	265.64	266.43	478.62

Table 5.3: Comparison of chosen values t_i versus solution values t_i^*. Units are in hours.

$p_x(0)$	$p_y(0)$	$p_z(0)$	$p_{\dot{x}}(0)$	$p_{\dot{y}}(0)$	$p_{\dot{z}}(0)$	$p_m(0)$
0.0059	-0.0022	-0.0075	-0.0026	0.0051	-0.0070	-0.0000089
$p_x^*(0)$	$p_y^*(0)$	$p_z^*(0)$	$p_{\dot{x}}^*(0)$	$p_{\dot{y}}^*(0)$	$p_{\dot{z}}^*(0)$	$p_m^*(0)$
0.1029	-0.0144	-0.0323	0.0116	0.0301	0.0015	-0.000071

Table 5.4: Comparison of chosen values $\mathbf{P}(0)$ versus solution values $\mathbf{P}(0)^*$.

- $0 \leq t_f \leq 182.5$ days. Recall that our transfer times are constrained by the capture time of the target minimoon. The average minimoon capture time is nine months, so as a first approach we'd like to have extremals taking between 0-6 months.

- $0 \leq \tau \leq 1.98$ hours, which implies $0 \leq \Delta v \leq 500$ m/s. This should give us extremals with low delta-v values. As in the example, we always assume three equal boosts of length $\tau/3$ for the initial guess, with one boost at the start ($t_1 = \tau/3$) and one boost at the end ($t_4 = t_f - \tau/3$). The middle boost from t_2 to $t_2 + \tau/3$ is randomaly placed between boost one and boost three. Figure 5.12 illustrates the constructed initial guess control norm. Note, as in the example, the solver adjusts the values of t_i so the resulting cloud extremals will not necessarily have three equal length boosts.

- $\mathbf{q}_{dprt} \in \mathcal{O}_H$. We discretize the Halo orbit $\mathcal{O}_H$ into 100 equally spaced (in terms of time, 3.55 hour steps) points, and randomally select one (Figure 5.11).

- $0 \leq \theta_0 \leq 2\pi$. The initial Sun true anomaly is randomly selected.

- $\mathbf{P_q}(0) \in [-0.01, 0.01]^6, \quad -0.001 \leq p_m(0) < 0$. These choices are made based on exploration which seem to give a higher rate of convergence to cloud extremals. We do not claim that these are the best choices, and admit that some extremals may be missed by not considering initial guesses outside of this range. To that remark, we reiterate that this is a first approach to generate a large pool of extremals and that it is not our intent to analyze the costate space.

On a standard personal laptop, the 1,000,000 cloud construction iterations took approximately two weeks to run. Of the 1,000,000 attempts, the algorithm converged 12,558, yielding 12,558 cloud

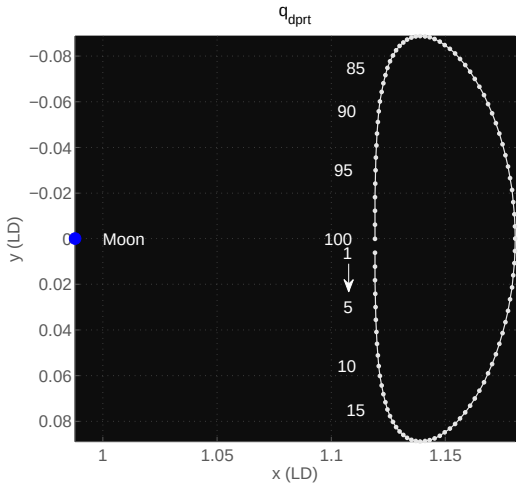

Figure 5.11: The Halo orbit discretized into 100 equally spaced (in terms of time) points.

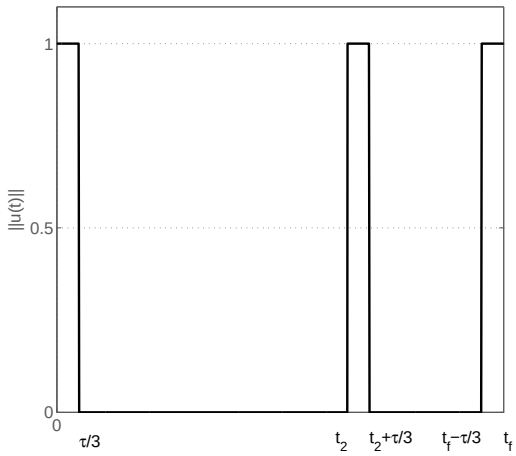

Figure 5.12: Control structure for constructing cloud extremals

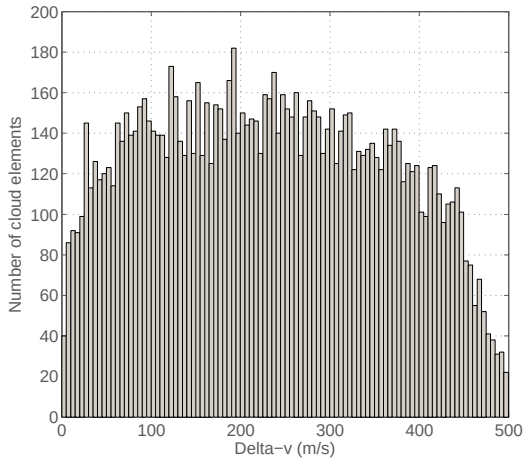

Figure 5.13: Delta-v distribution for the 12,558 cloud elements

extremals. The initialization parameters were taken from uniform random distributions, but we may expect that the algorithm converges more easily for certain parameter values. The distribution of delta-v, transfer times t_f, and initial Sun anomalies θ_0 for the 12,558 cloud elements are shown in Figures 5.13, 5.14, and 5.15, respectively. We observe a slight bell shaped distribution, with small tails for delta-v less than 100 m/s and also between 400 and 500 m/s. For the initial Sun true anomalies we see a fairly uniform distribution. The distribution is not uniform for transfer times, suggesting that the algorithm was more likely to converge for transfer times between approximately 10 and 30 days.

Twelve-thousand out of one million is a small percentage, which attests to the sensitivity of the shooting method. Albeit small, we are satisfied using the 12,558 cloud extremals as our reference database to initialize continuation methods to compute rendezvous transfers. As justification, we provide the following statistics to quantify the density of the cloud and its relationship to the minimoon orbits.

For each cloud extremal $(t_f^*, t_i^*, \mathbf{X}^*(t), \mathbf{P}^*(t))$ in the database, let $\mathbf{q}_{cloud} := \mathbf{q}(t_f)$ be the associated *cloud point* and let $\theta_{cloud} := \theta(t_f)$ be the associated final Sun true anomaly. Of the 12,558 cloud extremals, 11,128 of the cloud points are within 5 LD of the origin (Euclidean distance). For each of these cloud points, we compute the distance to the closest neighboring cloud point in terms of the spatial Euclidean distance. The maximum of this value over all 11,128 cloud points is 0.64 LD, and the mean and median distances are 0.05 LD and 0.03 LD respectively. Focusing closer to the

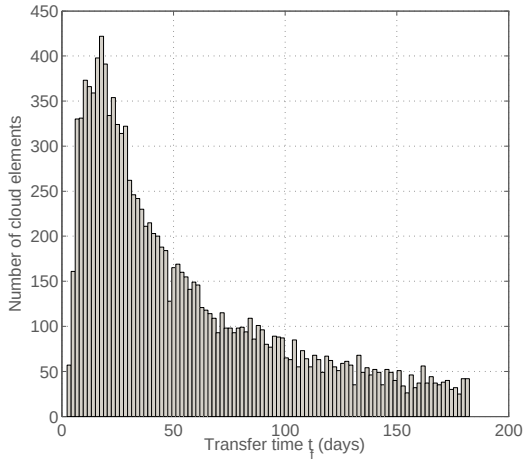

Figure 5.14: Transfer time distribution for the 12,558 cloud elements

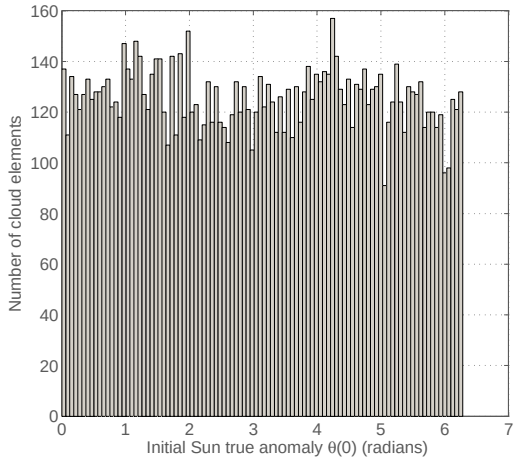

Figure 5.15: Initial Sun true anomaly distribution for the 12,558 cloud elements

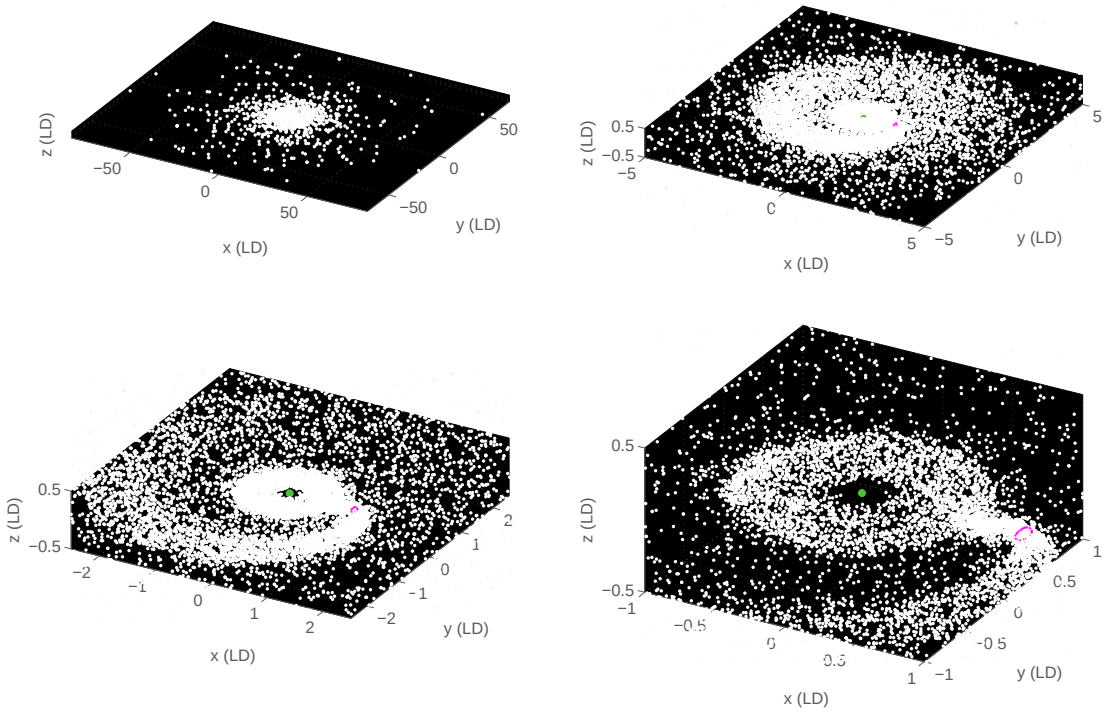

Figure 5.16: Cloud points $\mathbf{q}_{cloud}$ for the 12,558 cloud elements, shown at different zoom levels.

origin, 6,771 cloud points are within 2 LD of the origin. The same maximum-minimum distance for these points is 0.37 LD, and the mean and median distances are 0.03 LD and 0.02 LD respectively. The small mean and median values indicate that our cloud is dense in the the space within 5 LD of the origin. In Figure 5.16 the set of all $\mathbf{q}_{cloud}$ points are plotted, and the density closer to the origin is observable, and further away points begin to spread out.

To some degree the set of cloud points represents the accessibility set from the halo orbit (shown as magenta in Figure 5.16) for less than 500 m/s delta-v. The Earth is shown in green and the Moon in blue. Note for different zoom levels, the halo orbit, Earth and Moon are not always visible. From the closer of the zoomed images, we see the "ghosts" of the energy level sets from the three-body problem, even though we are in the four-body problem.

We now briefly compare the cloud points to the minimoon orbits. For every minimoon in the database, we compare every point $\mathbf{q}_{rdvz}$ along its orbit to every cloud point $\mathbf{q}_{cloud}$, and compute the

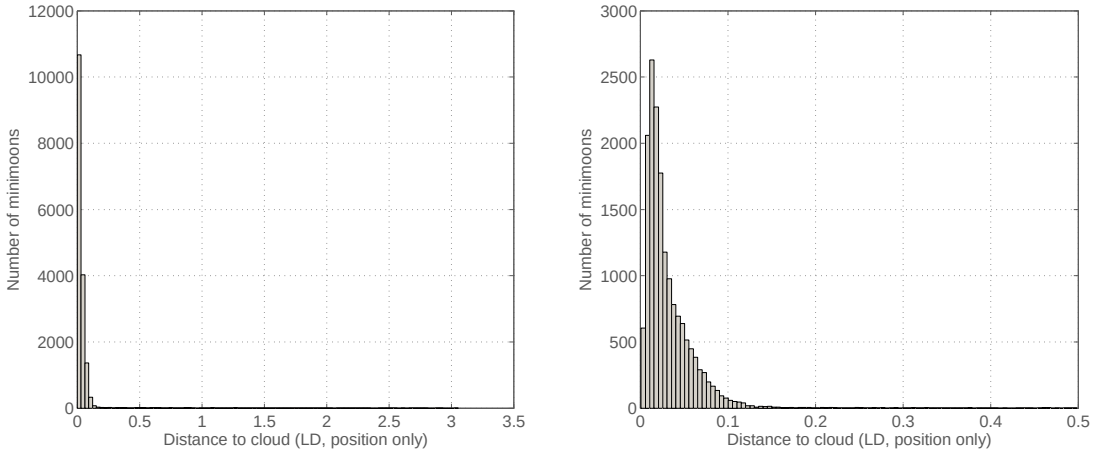

Figure 5.17: Distribution of minimoon cloud distances (LD, position only). Left: all minimoons, Right: truncated for distances less than 0.5 LD only.

minimum Euclidean distance between any pair. In this sense, the furthest minimoon from the cloud is minimoon 13313 at 3.056 LD away, and the closest is minimoon 12752 at 0.00088 LD away. The mean distance over all minimoons is 0.055 LD and the median distance is 0.023 LD. The histogram in Figure 5.17 shows the distribution of Euclidean distances from every minimoon to the cloud.

It is important to consider the velocity components as well when discussing rendezvous. So, for a selected rendezvous point $\mathbf{q}_{rdvz}$ on a minimoon's orbit and a selected cloud point $\mathbf{q}_{cloud}$, we now define the distance between them to be the non-dimensional Euclidean norm of the difference of the position-velocity vectors: $\|\mathbf{q}_{cloud} - \mathbf{q}_{rdvz}\|$. For each minimoon, we compute the minimum distance between any $\mathbf{q}_{rdvz}$ on the minimoon orbit and any cloud point $\mathbf{q}_{cloud}$. In this sense, the furthest minimoon from the cloud is minimoon # 3187, which is 3.196 units at its closest. The closest minimoon to the cloud is minimoon # 10425 which is 0.0279 units away. The mean value over all minimoons is 0.613 units, and the median is 0.546 units. The histogram in Figure 5.18 shows the distribution of non-dimensional distances from every minimoon to the cloud.

5.4 Continuation methodology and results

With a database of cloud extremals established, we now attempt continuations to finally compute rendezvous transfers to minimoons. We present three different rounds of calculations. For the first initial results, we attempt 50 continuations to each of 100 minimoons in order to get a preliminary

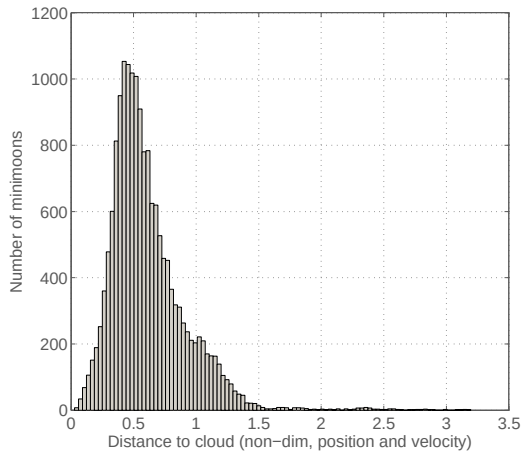

Figure 5.18: Distribution of minimoon cloud distances (non-dimensional, position and velocity)

assessment of our methodology and to guide the forthcoming large scale analysis.

5.4.1 Initial results

In order to gage the suitability of continuation methods from the cloud of extremals, we first attempt 50 continuations to the first 100 minimoons. For each minimoon, we select the 50 pairs $(\mathbf{q}_{rdvz}, \mathbf{q}_{cloud})$ with the smallest distance $\|\mathbf{q}_{cloud} - \mathbf{q}_{rdvz}\|$. Note in particular that the same $\mathbf{q}_{cloud}$ may be paired with more than one $\mathbf{q}_{rdvz}$ in the top 50, and similarly, the same $\mathbf{q}_{rdvz}$ may be paired with multiple $\mathbf{q}_{cloud}$ points. For each continuation, the cloud extremal associated with $\mathbf{q}_{cloud}$ is used to initialize the continuation method. The continuation method, as described in Chapter 3, iteratively solves problems $(\star)_{D_\lambda}$ for $\lambda = 0, ..., 1$, where the problem data is given by

$$D_\lambda = (t_f,\ \mathbf{q}_{dprt},\ (1-\lambda)\mathbf{q}_{cloud} + \lambda\mathbf{q}_{rdvz},\ (1-\lambda)\theta_{cloud} + \lambda\theta_{rdvz}) \tag{5.19}$$

When $\lambda = 0$ we have the problem $(\star)_{D_0}$ for which the cloud extremal associated with $\mathbf{q}_{cloud}$ is a solution. If the algorithm converges for $\lambda = 1$, we have successfully computed a rendezvous transfer to the minimoon, and an extremal to problem $(\star)_{D_1}$.

For the 5,000 total attempted continuations, the algorithm succeeded for 1,338. Figure 5.19 gives the Δv distribution for all 1,338 found transfers. The mean and median Δv values for these initial transfers were 1,020.3 and 911.1 m/s, respectively. The lowest computed Δv was 195.6 m/s

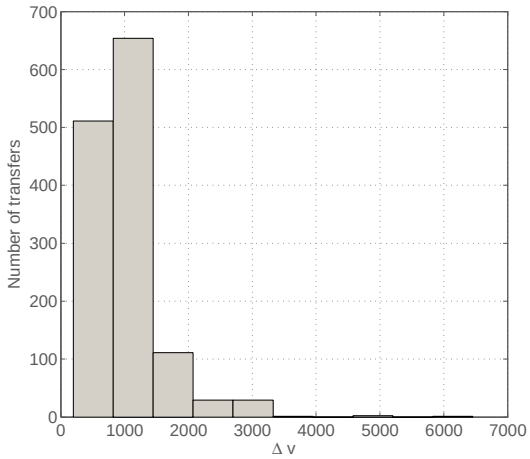

Figure 5.19: Initial results: Distribution of Δv for 1,338 computed transfers.

for minimoon #9, with a transfer time of 58.4 days. The highest computed Δv was 6,455.7 m/s for minimoon #13 with a transfer time of 163.5 days. Figures 5.20 and 5.21 show the respectively trajectories in the non-rotating reference frame. Notice the complexity of the spacecraft's trajectory for the bad Δv compared to the best one. Moreover, note the larger minimoon z-coordinate variation for the bad transfer.

For all transfer figures, the Moon's orbit is shown as the (blue) ellipse around the (green) Earth. The thin grey path is the orbit of the minimoon, starting from its capture point (green triangle) to its escape point (red square). The blue circle on the minimoon orbit marks where the minimoon was when the craft departed, and the yellow star is the point of rendezvous. The magenta path is the spacecraft's trajectory. It's three boosts are marked as yellow dots (including the final rendezvous boost).

At least one transfer was found for 93 of the 100 minimoons. Looking at the best computed transfer for each of the 93 minimoons, we get the mean and median Δv values were 764.3 and 666.3 m/s, respectively. The highest computed best Δv for a minimoon was 3,086.2 m/s for minimoon #14 with a transfer time of 59.2 days. The transfer is shown in Figure 5.22, and again notice the complexity of the spacecraft's trajectory and high z-variation of the minimoon. Figure 5.23 gives the Δv distribution for best transfers for the 93 minimoons where transfers were found.

We analyze characteristics of the cloud and rendezvous points which guides our forthcoming calculations.

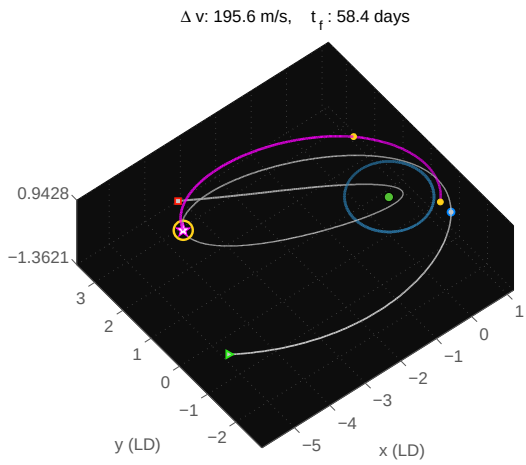

Figure 5.20: Initial results: Rendezvous with minimoon #9

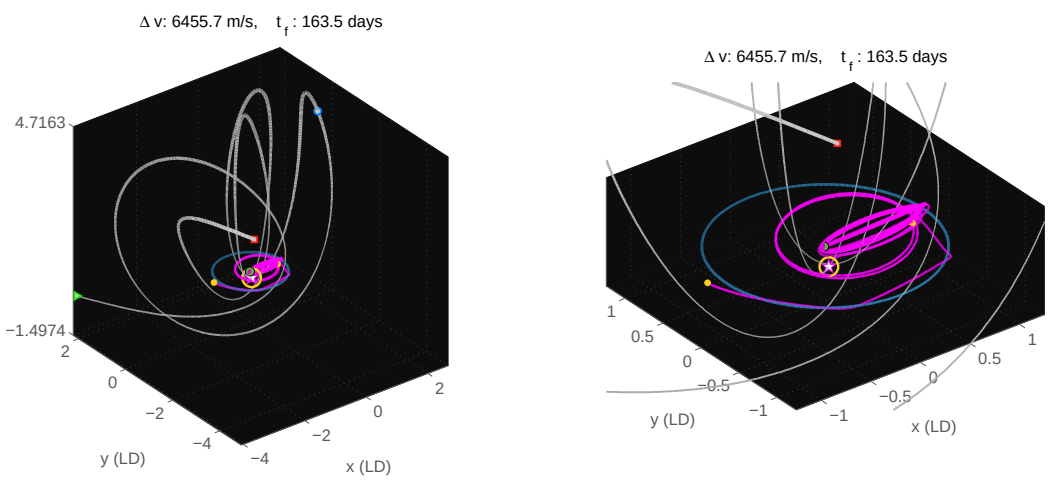

Figure 5.21: Initial results: Rendezvous with minimoon #13

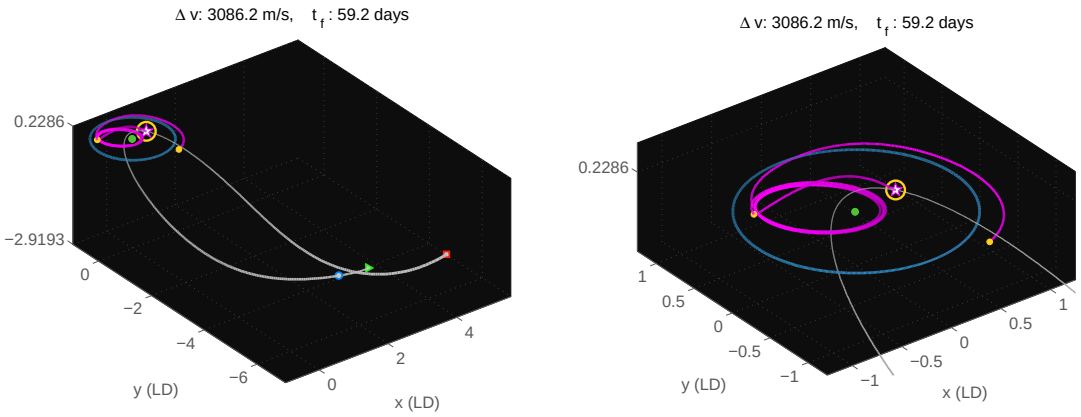

Figure 5.22: Initial results: Rendezvous with minimoon #14

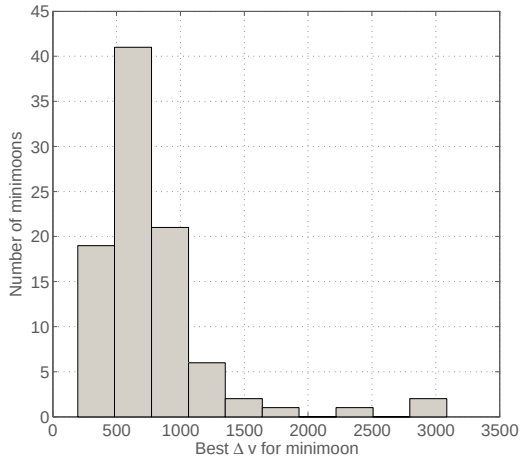

Figure 5.23: Initial results: Distribution of Δv for the best computed transfers for 93 minimoons.

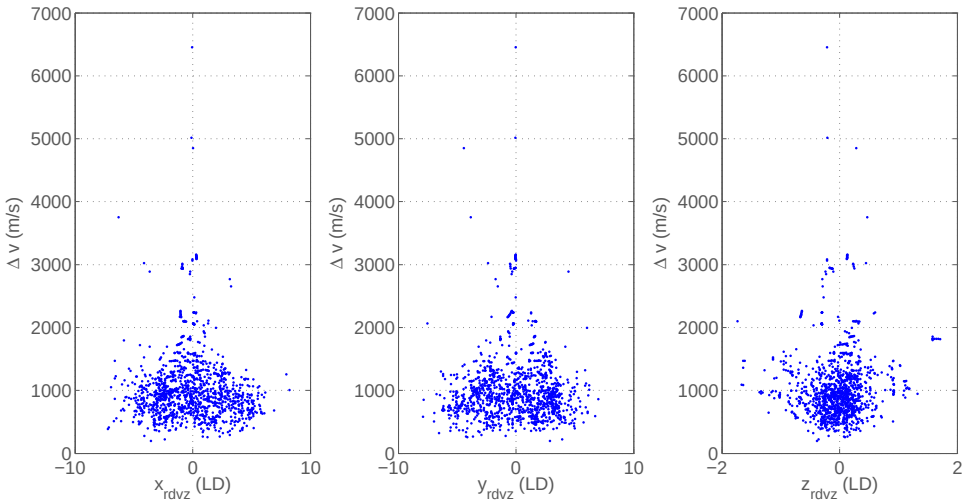

Figure 5.24: Initial results: Position components of $\mathbf{q}_{rdvz}$ versus Δv

Figure 5.24 compares the position components of the $\mathbf{q}_{rdvz}$ points versus Δv. From the z_{rdvz} plot, it is clear that $\mathbf{q}_{rdvz}$ with low absolute z-coordinates gave lower Δv values. Similarly, Figure 5.25 compares the velocity components of the $\mathbf{q}_{rdvz}$ points versus Δv which shows that $\mathbf{q}_{rdvz}$ with low absolute $\dot{z}$-coordinates gave lower Δv values.

Computing the CR3BP energy value E at each $\mathbf{q}_{rdvz}$ and comparing it to the Δv values, we get Figure 5.26 and see a positive trend as the rendezvous energy moves away from the departure energy (dashed red line). Similarly, we can compare the CR3BP energy values of the $\mathbf{q}_{cloud}$ points to their corresponding rendezvous extremal Δv values, as shown in Figure 5.27.

We suggest one way to quantify the interaction of the spacecraft with the Earth and Moon, by computing the winding numbers of the spacecraft's trajectory around the Earth and Moon. More specifically, we look at the planar projection of $\mathbf{q}(t)$ and compute the winding numbers (w_e, w_m) around the Earth at $(-\mu, 0)$ and Moon at $(1-\mu, 0)$ respectively. Note that in order to have closed curves we connect $\mathbf{q}(0)$ to $\mathbf{q}(t_f)$ with a straight line. Table 5.5 lists all the unique pairs of winding numbers computed for the 1,338 transfers, along with some Δv statistics. There is a lot of information to parse, but a few things are striking. First, that over 1,000 of the 1,388 have $w_e = w_m$. The Δv ranges seem scattered, but compare those pairs (w_e, w_m) where $|w_e - w_m| \leq 1$ to those where $|w_e - w_m| > 1$. We notice the mean Δv's for the first group are lower. In fact, the mean Δv for all transfers where $|w_e - w_m| \leq 1$ is 989.3 m/s, whereas for $|w_e - w_m| > 1$ the mean value is

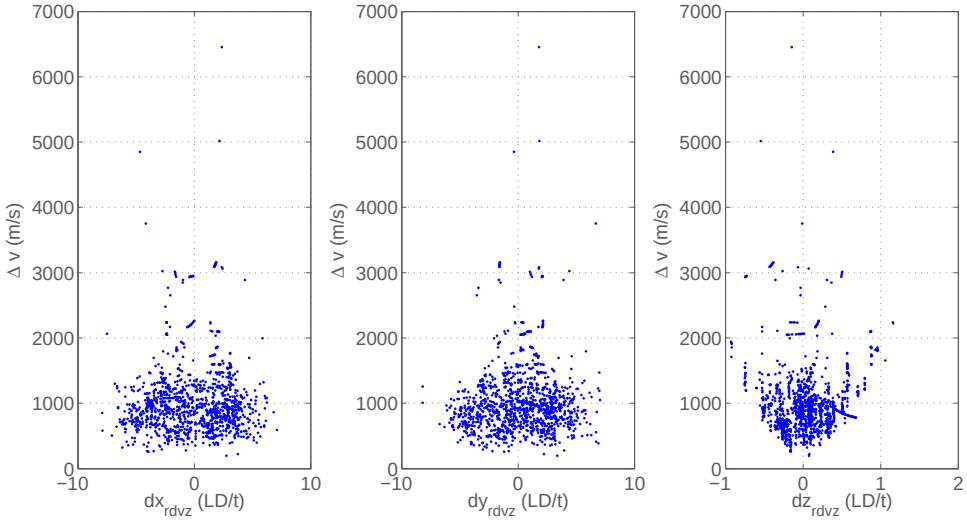

Figure 5.25: Initial results: Velocity components of $\mathbf{q}_{rdvz}$ versus Δv

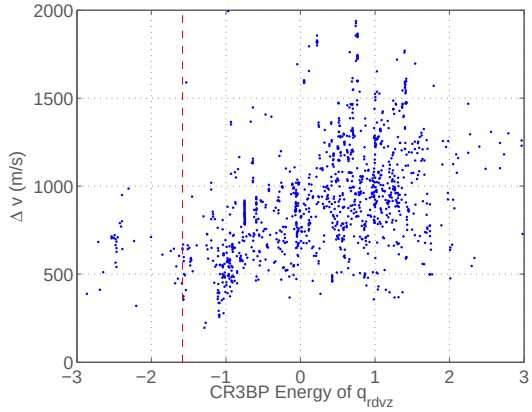

Figure 5.26: Initial results: CR3BP Energy at $\mathbf{q}_{rdvz}$ versus Δv

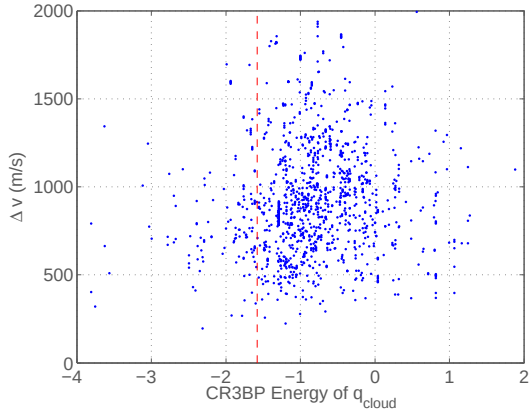

Figure 5.27: Initial results: CR3BP Energy at $\mathbf{q}_{cloud}$ versus resulting Δv

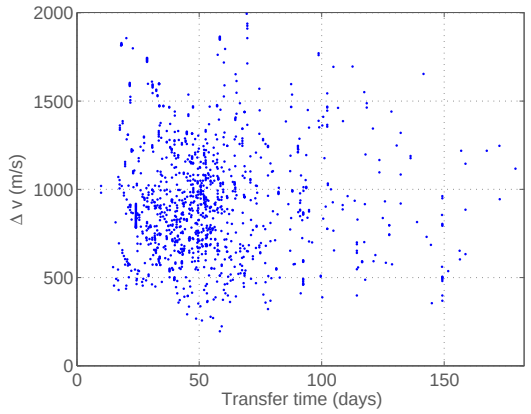

Figure 5.28: Initial results: Transfer times versus Δv

1911.5 m/s – nearly 1,000 m/s higher!

Moreover, by computing the winding numbers for the cloud extremals and comparing them to their paired rendezvous extremals, we see that for 1,275 of the 1,338 continuations the cloud extremal and rendezvous extremal have the same winding number pair. It is not surprisingly actually that the continuation method seems to preserve the structure of the original trajectory. This, combined with the remark above, suggests we may improve our search for low Δv transfers by only using cloud extremals where $|w_e - w_m| \leq 1$.

Figure 5.28 plots the transfer times versus Δv, and we see that a majority of the transfers took between 20 and 60 days, with a small patch of very low Δv values around 50 days. Note that even for transfer times of 150 days transfers were found with $\Delta v < 400$ m/s.

w_e	w_m	count	mean Δv	median Δv	min Δv	max Δv
-1	-1	640	919.6	891.6	255.9	2171.2
-2	-2	241	1003.7	956.5	195.6	4850.1
0	0	78	977.0	889.9	428.9	2241.0
-3	-3	54	1044.9	857.5	354.1	3753.0
1	1	48	1030.3	864.2	782.5	2886.7
-1	0	39	781.4	788.4	269.5	1259.0
-5	-5	28	633.7	502.5	368.6	959.9
-2	-1	24	919.3	893.7	387.8	1468.1
-4	-4	22	1478.8	1000.8	397.1	2947.7
0	1	22	1891.7	2059.4	898.6	2480.2
-2	-3	21	1034.6	937.0	410.3	2033.3
-1	-2	18	1042.9	987.1	409.4	1855.2
-4	-3	15	1579.3	1460.0	775.5	2767.9
0	-1	13	1018.2	1019.4	462.9	1524.1
2	0	13	2788.0	3113.7	683.6	3160.3
-4	-5	10	2207.8	2201.8	2163.5	2264.7
-5	-4	6	851.0	795.7	740.2	1116.2
-3	-4	6	1361.4	1474.7	574.1	1695.3
-3	-2	5	1163.4	1361.2	388.0	1438.9
-2	2	4	906.0	900.5	846.6	976.4
-6	-4	3	886.8	883.0	632.3	1145.0
-3	-1	3	1924.5	1926.2	1909.6	1937.6
-1	1	3	898.1	753.7	641.6	1298.9
3	1	3	1363.8	1363.8	1363.8	1363.8
-18	2	2	3072.1	3072.1	3063.3	3081.0
-1	-3	2	1723.9	1723.9	1653.3	1794.5
2	-1	2	902.9	902.9	559.6	1246.2
2	1	2	1089.8	1089.8	1048.6	1131.0
3	0	2	1090.1	1090.1	813.0	1367.1
11	2	2	5735.4	5735.4	5015.0	6455.7
-5	-3	1	700.9	700.9	700.9	700.9
-4	-2	1	857.7	857.7	857.7	857.7
-2	0	1	710.7	710.7	710.7	710.7
4	3	1	1447.7	1447.7	1447.7	1447.7
6	1	1	1351.3	1351.3	1351.3	1351.3
7	1	1	1165.2	1165.2	1165.2	1165.2
8	1	1	1095.6	1095.6	1095.6	1095.6

Table 5.5: Initial results: Winding number pairs and corresponding Δv statistics for 1,338 transfers.

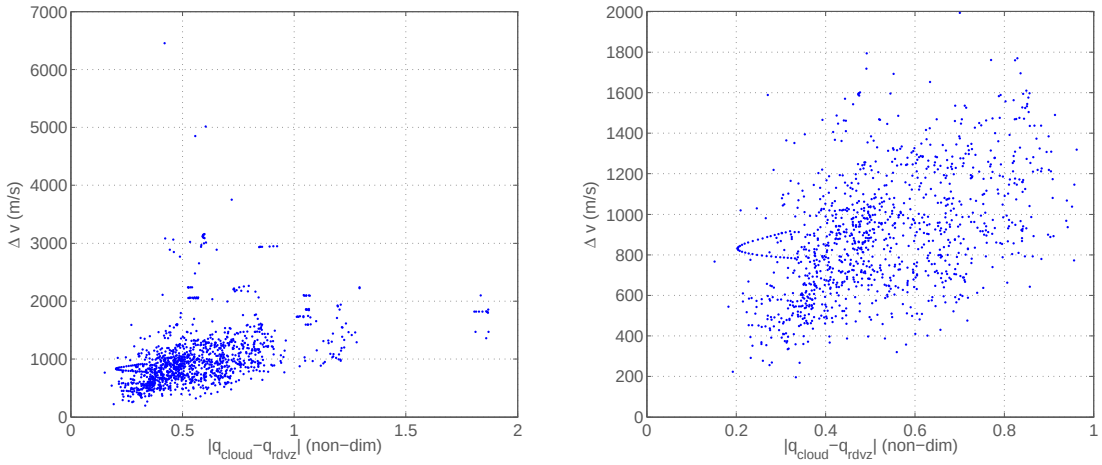

Figure 5.29: Initial results: Continuation distance versus Δv

Figure 5.29 shows that the norm $\|\mathbf{q}_{cloud} - \mathbf{q}_{rdvz}\|$ was correlated to the Δv of the resulting rendezvous extremal. Figure 5.30 shows also a slight preference for continuation pairs where $|\theta_{cloud} - \theta_{rdvz}|$ is small – the lower clusters near 0 and $\pm\pi$ can actually be identified together since the CR4BP uncontrolled dynamics are π-periodic.

5.4.2 Large scale results

From the above analysis, the following characteristics of $\mathbf{q}_{rdvz}$, $\mathbf{q}_{cloud}$ and the of the pair seem to be the best indicators of a successful continuation to a low Δv transfer:

- $|z_{rdvz}| < 0.5$ and $|\dot{z}_{rdvz}| < 0.5$
- Cloud extremal winding numbers (w_e, w_m) such that $|w_e - w_m| \leq 1$
- $\|\mathbf{q}_{cloud} - \mathbf{q}_{rdvz}\| < 0.7$ and $|\theta_{cloud} - \theta_{rdvz}| < 0.05$

We now run continuations on a larger sample of minimoons. Based on the criteria above, for each minimoon we only consider rendezvous points $\mathbf{q}_{rdvz}$ where $|z_{rdvz}| < 0.5$ and $|\dot{z}_{rdvz}| < 0.5$. Note that 2,238 of the minimoons have *no* points that satisfy this criteria. We also restrict our cloud to only use those extremals where $|w_e - w_m| \leq 1$, which leaves 10,687 of the original 12,558 cloud extremals. Finally, for each minimoon we select the 10 pairs $(\mathbf{q}_{rdvz}, \mathbf{q}_{cloud})$ with smallest distance $\|\mathbf{q}_{cloud} - \mathbf{q}_{rdvz}\|$ while simultaneously requiring $|\theta_{cloud} - \theta_{rdvz}| < 0.05$. The Sun restriction is chosen because the continuation runs significantly faster for very close θ_{cloud} and θ_{rdvz}. Note, that there are

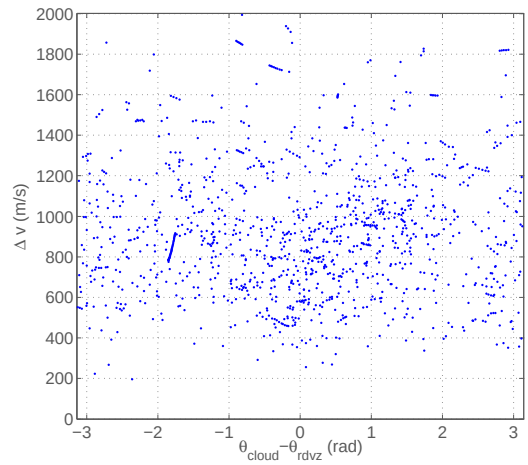

Figure 5.30: Initial results: Continuation final Sun true anomaly difference versus Δv

enough cloud extremals so that the Sun restriction does not eliminate any more of the minimoons from consideration. We randomly select 3,000 minimoons for our continuations, based solely on limited computational time. Future work will include analysis of the entire database.

Continuations are attempted starting with the closest pair. If a solution is found for any of the pairs before the tenth, the algorithm moves on to the next minimoon. This allows the computer to get through more minimoons in less time, while still providing first results for each minimoon. Note if none of the top 10 continuations succeed the algorithm also moves on to the next minimoon.

For each of the 3,000 attemped minimoons a transfer was found. The distribution of delta-v values is given in Figure 5.31. The mean and median Δv values were 724.5 and 680 m/s, respectively. The lowest Δv was 88.4 m/s for minimoon #9,046, with a transfer time of 41.4 days. The transfer is shown in Figure 5.32. The greatest Δv was 4,825.8 m/s for minimoon #16,844, with a transfer time of 99.6 days. The transfer is shown in Figure 5.33.

5.4.3 Refinement

Recall that the results discussed above are solutions to the restricted problem where the control structure is fixed, and the transfer time and Halo departure are not optimized. To approximate how much better solutions to the unrestricted problem could do, in terms of Δv, we refine the initial results for the original 93 minimoons we computed transfers to. For each, we take the extremal with the lowest Δv and initialize continuations methods on t_f, $\mathbf{q}_{dprt}$ and $\mathbf{q}_{rdvz}$. The refinement algorithm

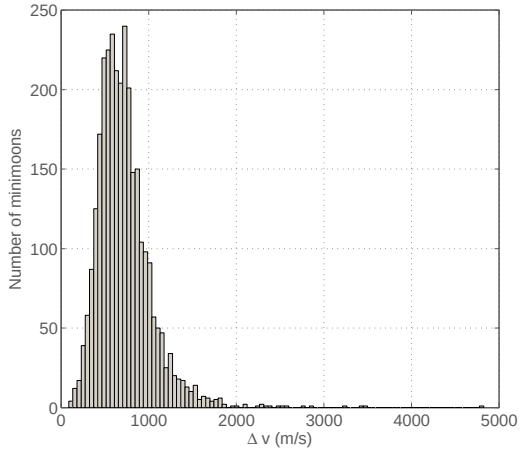

Figure 5.31: Large scale results: Distribution of Δv for the 3,000 minimoons.

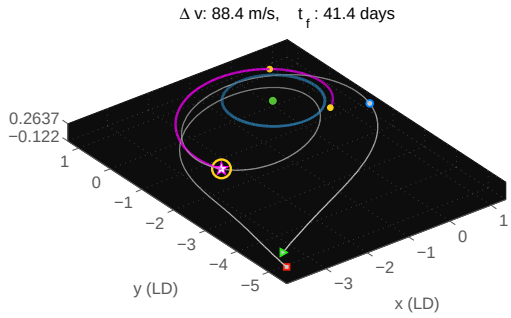

Figure 5.32: Large scale results: Rendezvous with minimoon #9,046

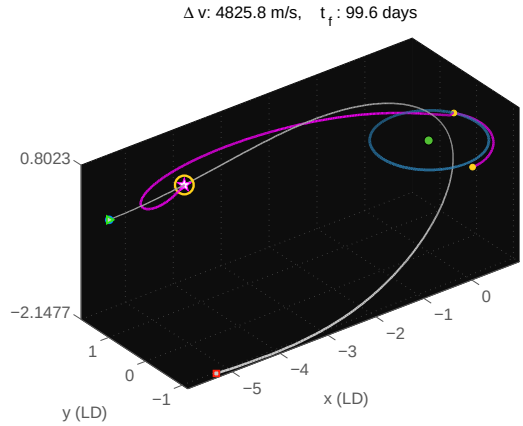

Figure 5.33: Large scale results: Rendezvous with minimoon #16,844

is designed as follows:

(i) Start with a solution to $(\star)_D$ where $D = (t_f,\ \mathbf{q}^i_{dprt},\ \mathbf{q}^j_{rdvz},\ \theta^j_{rdvz})$

(ii) Use a continuation to attempt to solve $(\star)_{D_n}$ for $n = 1, ..., 6$, where the D_n are defined as follows:

$$
\begin{aligned}
D_1 &= (\quad t_f - 3 \text{ hours}, \quad \mathbf{q}^i_{dprt}, \quad \mathbf{q}^j_{rdvz}, \quad \theta^j_{rdvz} \quad) \\
D_2 &= (\quad t_f + 3 \text{ hours}, \quad \mathbf{q}^i_{dprt}, \quad \mathbf{q}^j_{rdvz}, \quad \theta^j_{rdvz} \quad) \\
D_3 &= (\quad t_f, \quad \mathbf{q}^{i-1}_{dprt}, \quad \mathbf{q}^j_{rdvz}, \quad \theta^j_{rdvz} \quad) \\
D_4 &= (\quad t_f, \quad \mathbf{q}^{i+1}_{dprt}, \quad \mathbf{q}^j_{rdvz}, \quad \theta^j_{rdvz} \quad) \\
D_5 &= (\quad t_f, \quad \mathbf{q}^i_{dprt}, \quad \mathbf{q}^{j-1}_{rdvz}, \quad \theta^{j-1}_{rdvz} \quad) \\
D_6 &= (\quad t_f, \quad \mathbf{q}^i_{dprt}, \quad \mathbf{q}^{j+1}_{rdvz}, \quad \theta^{j+1}_{rdvz} \quad)
\end{aligned}
$$

where $\mathbf{q}^{i\pm1}_{dprt}$ represents the next/previous discretized halo departure point, and $(\mathbf{q}^{j\pm1}_{rdvz}, \theta^{j\pm1}_{rdvz})$ is the next/previous minimoon rendezvous point (with exceptional cases when we at the first or last rendezvous point for the minimoon).

(iii) If any of the new delta-v values Δv_i are better than the original, choose the problem $(\star)_{D_i}$ with lowest Δv_i, and repeat. If all Δv_i are greater than the original Δv, the algorithm terminates.

Although this algorithm does not verify any transversality conditions, it provides a crude estimations of locally optimum t_f, $\mathbf{q}_{dprt}$ and $\mathbf{q}_{rdvz}$.

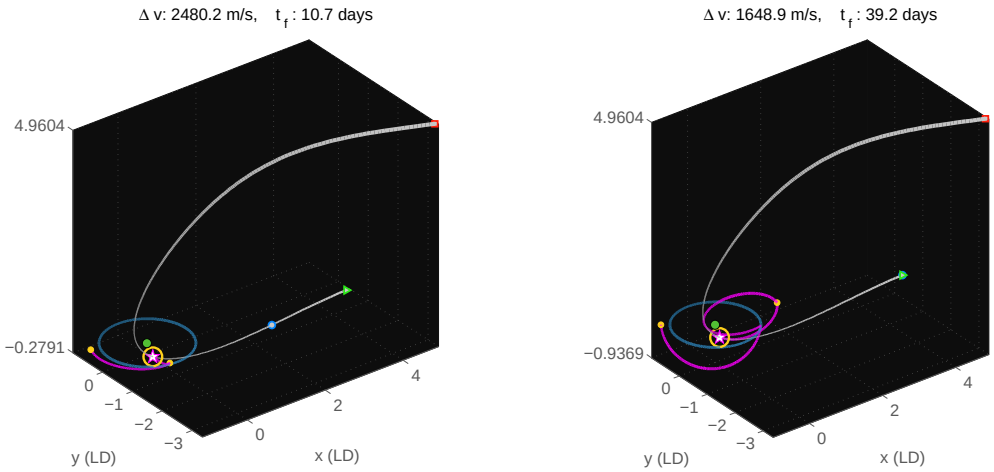

Figure 5.34: Original (left) and refined (right) rendezvous with minimoon #5

The mean and median improvements for the 93 minimoons was 104.25 and 70.769 m/s Δv, respectively. The smallest improvement was 2.22 m/s Δv for minimoon #20, which originally had a Δv of 459.21 m/s. The greatest improvement was 831.35 m/s Δv for minimoon #5, which originally had a Δv of 2,480.2 m/s. Figure 5.34 shows the original and refined transfers to minimoon #5. Figure 5.35 shows the distribution of Δv improvements for the 93 minimoons.

An example that showed good improvement without having very large initial Δv was minimoon #40 – which improved by 473.42 m/s from 1055.5 m/s to 582.04 m/s. The original and refined transfers are shown in Figure 5.36.

Finally, we take the best transfer found in the large scale results, for minimoon #9,046 shown in Figure 5.32 and apply the refinement algorithm. The resulting transfer has a Δv of and a transfer time of days. Both the original and refined transfers are shown in Figure 5.37 for comparison.

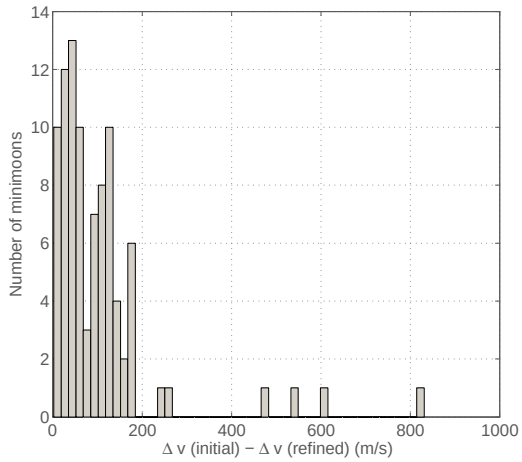

Figure 5.35: Refined results: distribution of Δv improvement for 93 minimoons

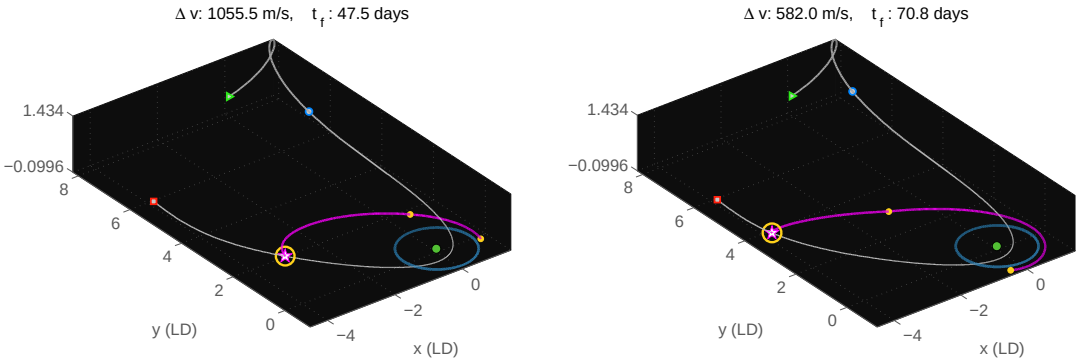

Figure 5.36: Original (left) and refined (right) rendezvous with minimoon #40

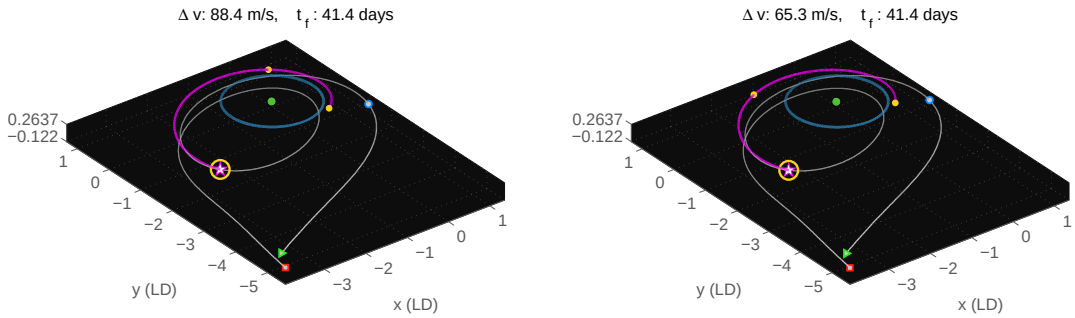

Figure 5.37: Original (left) and refined (right) rendezvous with minimoon #9,046

CHAPTER 6
CONCLUSION AND FURTHER WORK

In this dissertation a new method for overcoming the initialization difficulty associated with indirect methods is proposed and applied to time-minimal and fuel-minimal spacecraft trajectory optimization problems. The methods are able to efficiently initialize the algorithm and compute locally optimal rendezvous transfers for an enormous set of targets – namely, the simluated minimoons. These results are the first to assess the feasibility for a spacecraft to rendezvous with the new population of near Earth asteroids known as minimoons. Our application is unique and ill-suited for existing trajectory optimization techniques since we compute transfers to so many different locations and therefore computational efficiency was critical. Moreover, the rapidly evolving orbits of the minimoons are not associated with invariant manifolds nor are they planar or elliptic, presenting new challenges for trajectory optimization techniques.

A description of the target population is given in Chapter 2, and an overview of the geometric tools and methods used for the computation of solutions in Chapter 3.

In Chapter 4, solutions to the time-minimization problem were computed in order to get an approximate lower bound for the rendezvous transfer times. Continuation techniques that relied on knowledge of an existing solutions were used to overcome the major difficulty of algorithm initialization. The results showed that indeed minimoon rendezvous are feasible with transfer times on the order of one month or less. In Chapter 5, solutions to the fuel-minimization problem were computed while simultaneously considering short transfer times. An improved model was used which made the initialization of the algorithm even more sensitive; so, a continuation-based cloud technique was developed to once again overcome this major difficulty. The results suggested that indeed minimoon rendezvous are feasible with delta-v values of less than 500 meters per second. Moreover, we can envision applying the cloud methodology to other applications of optimal control, where no *a priori* knowledge of solutions exists, in order to initialize the sensitive indirect methods for a large space of problem parameters.

From an application standpoint, the work presented in this dissertation strongly suggests that further investigation of minimoons would be worthwhile. They are a potentially rich population of asteroids which come close to Earth in abundance, and moreover, this work suggests that they are accessible via spacecraft for low-cost.

Future work on minimoon rendezvous missions can proceed in several directions:

- It has been suggested that parking the spacecraft on a periodic orbit about one of the Earth-Sun Lagrange points may be more suitable for a rendezvous mission. In general, other parking orbits should be investigated.

- In order to initialize the indirect algorithm, the selection of the "best" element from a collection of known solutions is not well understood. Sometimes known solutions with parameter values very similar to the desired problem do not lead to convergence, and others with parameter values much different do converge.

- Applying the cloud technique to a different mission scenario, or even a completely different problem, would give insight into how useful this technique can be in general.

BIBLIOGRAPHY

[1] M. Granvik, J. Vaubaillon, and R. Jedicke. The population of natural earth satellites. *Icarus*, 218:262–277, 2011.

[2] J. Betts. A survey of numerical methods for trajectory optimization. *Journal of Guidance, Control, and Dynamics*, 21:193–207, 1998.

[3] J.E. Marsden and S.D. Ross. New methods in celestial mechanics and mission design. *Bull. Amer. Math. Soc. (N.S.)*, 43:43–73, 2006.

[4] V. Szebehely. Theory of orbits: The restricted problem of three bodies. *Academic Press*, 1967.

[5] I. Newton. Principes mathématiques de la philosophie naturelle. tome i,ii (french). traduction de la marquise du chastellet, augmentée des commentaires de clairaut. *Librairie scientifique et technique Albert Blanchard, Paris*, 1966.

[6] D.A. Vallado. Fundamentals of astrodynamics and applications. *Springer*, 2001.

[7] E. Belbruno. Fly me to the moon: an insider's guide to the new science of space travel. *Princeton University Press*, 2007.

[8] E. Belbruno and J. Miller. Sun-perturbed earth-to-moon transfers with ballistic capture. *Journal of Guidance, Control, and Dynamics*, 16:770–775, 1993.

[9] E. Belbruno. Capture dynamics and chaotic motion in celestial mechanics: with applications to the construction of low energy transfers. *Princeton University Press*, 2004.

[10] E. Belbruno and F. Topputo. Computation of weak stability boundaries: Sun-jupiter system. *Celestial Mechanics and Dynamical Astronomy*, 105:3–17, 2009.

[11] E. Belbruno, M. Gidea, and F. Topputo. Weak stability boundary and invariant manifolds. *SIAM Journal on Applied Dynamical Systems*, 9:1061–1089, 2010.

[12] E. Belbruno, M. Gidea, and F. Topputo. Geometry of weak stability boundaries. *Qualitative Theory of Dynamical Systems*, 12:53–66, 2013.

[13] E. Belbruno and F. Topputo. Earth-mars transfers with ballistic capture. *arXiv*, 2014.

[14] G. Gomez, W.S. Koon, M.W. Lo, J.E. Marsden, J. Masdemont, and S.D. Ross. Invariant manifolds, the spatial three-body problem and space mission design. *Adv. Astronaut Sci.*, 109:3–22, 2001.

[15] G. Gomez, A. Jorba, J. Mardesmont, and C. Simo. Dynamics and mission design near libration points. *World Scientific Publishing Co. Pte. Ltd.*, 6, 2001.

[16] G. Gomez, W.S. Koon, M.W. Lo, J.E. Marsden, J. Masdemont, and S.D. Ross. Connecting orbits and invariant manifolds in the spatial three-body problem. *Nonlinearity*, 17:1571–1606, 2004.

[17] W.S. Koon, M.W. Lo, J.E. Marsden, and S.D. Ross. Heteroclinic connections between periodic orbits and resonance transitions in celestial mechanics. *Chaos*, 10:427–469, 2000.

[18] W.S. Koon, M.W. Lo, J.E. Marsden, and S.D. Ross. Dynamical systems, the three-body problem, and space mission design. *Springer*, 2007.

[19] NASA. Copernicus. *http://www.nasa.gov/centers/johnson/copernicus/*.

[20] B.A. Conway. A survey of methods available for the numerical optimization of continuous dynamical systems. *J Optim Theory Appl*, 152:271–306, 2012.

[21] J.T. Betts. Practical methods for optimal control using nonlinear programming. *Society for Industrial and Applied Mathematics*, 2001.

[22] G. Mingotti, F. Toputto, and F. Bernelli-Zazzera. Optimal low-thrust invariant manifold trajectories via attainable sets. *Journal of Guidance Control and Dynamics*, 34, 2011.

[23] G. Mingotti and P. Gurfil. Mixed low-thrust invariant-manifold transfers to distant prograde orbits around mars. *Journal of Guidance, Control, and Dynamics*, 33, 2010.

[24] L. S. Pontryagin, V. G. Boltyanskii, R. V. Gamkrelidze, and E. F. Mishchenko. The mathematical theory of optimal processes. *John Wiley & Sons, New York*, 1962.

[25] M. Ozimek and K. Howell. Low-thrust transfers in the earth-moon system including applications to libration point orbits. *Journal of Guidance, Control, and Dynamics*, 33, 2010.

[26] C. A. Kluever. Using edelbaum's method to compute low-thrust transfers with earth-shadow eclipses. *Journal of Guidance, Control, and Dynamics*, 34, 2011.

[27] M. Pontani and B. A. Conway. Optimal finite-thrust rendezvous trajectories found via particle swarm algorithm. *Journal of Spacecraft and Rockets*, 50, 2013.

[28] J.T. Betts and S.O. Erb. Optimal low thrust trajectories to the moon. *SIAM J. Appl. Dyn. Syst.*, 2:144–170, 2003.

[29] B. Bonnard, J.B. Caillau, and G. Picot. Geometric and numerical techniques in optimal control of the two and three-body problems. *Commun. Inf. Syst.*, 10:239–278, 2010.

[30] J. B. Caillau, B. Daoud, and J. Gergaud. Minimum fuel control of the planar circular restricted three-body problem. *Celestial Mech. Dynam. Astronom.*, 114:137–150, 2012.

[31] J. Gergaud and T. Haberkorn. Homotopy method for minimum consumption orbit transfer problem. *ESAIM Control Optim. Calc. Var.*, 12:294–310, 2006.

[32] A. Moore. Discrete mechanics and optimal control for space trajectory design. *PhD Thesis, California Institute of Technology*, 2011.

[33] G. Picot. Shooting and numerical continuation method for computing time-minimal and energy-minimal trajectories in the earth-moon system using low-propulsion. *Discrete Cont. Dyn. Syst. Ser. B*, 17:245–269, 2012.

[34] J. Gergaud, T. Haberkorn, and P. Martinon. Low thrust minimum-fuel orbital transfer: a homotopic appoach. *Journal of Guidance, Control and Dynamics*, 27:1046–1060, 2004.

[35] J. B. Caillau, O. Cots, and J. Gergaud. Differential continuation for regular optimal control problems. *Optimization Methods and Software*, 27:177–196, 2012.

[36] A. Dervieux, L. Hascoet, and V. Pascal. Tapenade. *http://www-sop.inria.fr/tropics/tapenade.html.*

[37] E. Hairer and G. Wanner. Dopri5. *http://www.unige.ch/ hairer/prog/nonstiff/dopri5.f.*

[38] B. Bonnard, J.B. Caillau, and E. Trelat. Cotcot: short reference manual. *IRIT*, 2005.

[39] E.L. Allgower and K. Georg. Numerical continuation methods, an introduction. *Springer, Berlin*, 1990.

[40] E. Hairer, S.P. Norsett, and G. Wanner. Solving ordinary differential equations 1, nonstiff problems. *Springer Verlag*, 8, 1993.

[41] P. Martinon and J. Gergaud. Using switching detection and variational equations for the shooting method. *Optimal Control Applications and methods*, 2007.

[42] H. Maurer. Numerical solutions of singular control problems using multiple shooting techniques. *Journal of optimization theory and applications*, 1976.

[43] E. Trelat. Optimal control. *Mathematiques Concretes*, 2005.

[44] B. Bolin, R. Jedicke, M. Granvik, P. Brown, E. Howell, M. Nolan, M. Chyba, G. Patterson, and R. Wainscoat. Detecting earth's temporarily captured natural irregular satellites - minimoons. *Icarus*, 241:280–297, May 2014.

[45] H. Urrutzua, D. J. Scheeres, C. Bombardelli, J. L. Gonzalo, and J. Pelaez. What does it take to capture an asteroid? a case study on capturing asteroid 2006 $\mathrm{rh}_1 20$. *American Astronomical Society*, 14, 2014.

[46] E. Bryson and Y.C. Ho. Applied optimal control. optimization, estimation and control. revised printing. *Hemisphere Publishing Corp*, 1975.

[47] H. Maurer. First and second order sufficient optimality conditions in mathematical programming and optimal control. *Mathematical Programming at Oberwolfach*, 14:163–177, 1981.

[48] V. Zeidan. First and second order sufficient conditions for optimal control and the calculus of variations. *Appl. Math. and Optim.*, 11:209–226, 1984.

[49] A.A. Agrachev and A.V. Sarychev. On abnormal extremals for lagrange variational problems. *J. Math. Systems. Estim. Control*, 1:87–118, 1998.

[50] Bonnard B., J.B. Caillau, and E Trélat. Second order optimality conditions in the smooth case and applications in optimal control. *ESAIM Control Optim. and Calc. Var.*

[51] B. Bonnard and I. Kupka. Théorie des singularités de l'application entrée/sortie et optimalité des trajectoires singulières dans le problème du temps minimal (french)[theory of the singularities of the input/output mapping and optimality of singular trajectories in the minimal-time problem]. *Forum Math.*, 2:111–159, 1998.

[52] A.V. Sarychev. Index of second variation of a control system. *Mat. Sb. (N.S.)*, 113:464–486, 1980.

[53] B. Bonnard, L. Faubourg, and E. Trélat. Mécanique céleste et contrôle des véhicules spatiaux. *Springer-Verlag, Berlin*, 2006.

[54] Bonnard B., J.B. Caillau, and E Trélat. Geometric optimal control of elliptic keplerian orbits. *Discrete Cont. Dyn. Syst. Ser. B.*

[55] V. Angelopoulos. The artemis mission. *IGPP/ESS UCLA*, 2008.

[56] F. Topputo. On optimal two-impulse earth-moon transfers in a four-body model. *Celest Mech Dyn Astr*, 117:279–313, 2013.

[57] G. Mingotti, F. Topputo, and F. Bernelli-Zazzera. A method to design sun-perturbed earth-to-moon low-thrust transfers with ballistic capture. *AIDAA*, 2007.

[58] D. Scheeres. The restricted hill four-body problem with applications to the earth-moon-sun system. *Celestial Mechanics and Dynamical Astronomy*, 70:75–98, 1998.

[59] A.V. Dmitruk and A.M. Kaganovich. The hybrid maximum principle is a consequence of the pontryagin maximum principle. *Systems Control Lett.*, 57:964–970, 2008.